FACULTAD DE MEDICINA
PONTIFICIA UNIVERSIDAD
CATÓLICA DE CHILE

DIRECCION DE INVESTIGACION Y DOCTORADO
PROGRAMA DE DOCTORADO EN CIENCIAS MEDICAS
ESCUELA DE MEDICINA

IDENTIFICATION OF LONG NONCODING RNAS IN COMPETING ENDOGENOUS RNA NETWORKS THROUGHOUT THE GASTRIC PRECANCEROUS CASCADE

por

IGNACIO ALBERTO WICHMANN PÉREZ

Tesis presentada a la Escuela de Medicina de la Pontificia Universidad Católica de Chile,

para optar al título de Doctor en Ciencias Médicas

Profesores guía:

ALEJANDRO H. CORVALÁN
Profesor Asociado, Pontificia Universidad Católica de Chile
acorvalan@uc.cl

ELMER A. FERNÁNDEZ
Profesor Titular, Universidad Católica de Córdoba
efernandez@cidie.ucc.edu.ar

Julio, 2020
Santiago, Chile

AUTORIZACIÓN PARA LA REPRODUCCIÓN DE LA TESIS

(SELECCIONE UNA OPCIÓN)

a) Ninguna parte de esta tesis puede reproducirse o transmitirse bajo Ninguna forma o por ningún medio o procedimiento, sin permiso por Escrito del(os) autor(es).

FECHA

21 de agosto de 2020

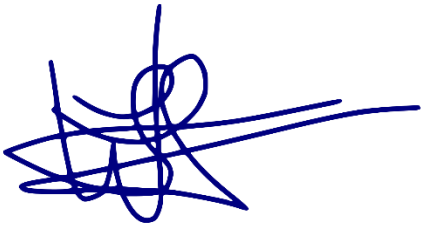

Ignacio Alberto Wichmann Pérez

RUT 16.011.721-4

b) Se autoriza la reproducción total o parcial, con fines académicos, por cualquier medio o procedimiento, incluyendo la cita bibliográfica que acredita al trabajo y a su autor.

Fecha

Firma

Este trabajo va dedicado a todos quienes me han apoyado durante estos años. En especial a mis tutores Alejandro y Elmer, quienes me impulsaron por el camino de la investigación y han tenido un impacto inconmensurable sobre mi desarrollo profesional y personal; y a mi esposa Lorena quien, con su apoyo incondicional y paciencia, me acompañó e inspiró en este camino.

AGRADECIMIENTOS

El desarrollo de esta tesis doctoral en su forma actual no hubiese sido posible sin el apoyo de muchas personas. De manera particular quisiera agradecer a:

Lorena, mi esposa. Por su paciencia sin fin, apoyo constante y ternura.

Mis padres Pola y Pablo. Por su sabiduría y ejemplo de vida. A ustedes les debo quien soy.

Mis abuelos Tita y Álvaro, Nené y Carlos. Espero hacerlos sentir orgullosos. Gracias por el tiempo que alcanzaron a compartir conmigo.

Mis hermanos Cristina, Pablo y Constanza, y mis cuñados Rodrigo, Josefa y Juan Pablo. Por compartir conmigo en esta vida y regalarme 7 maravillosos sobrinos.

Mis suegros Graciela y Osvaldo. Por recibirme en su casa y hacerme sentir como un hijo más.

Mis cuñado Ignacio y Carito. Por recibirme en su familia.

A mis amigos de "La Vieja Loca": Matute, Edu, Waldo, Juane y Pol. Por ser cable a tierra y válvula de escape. Por estar siempre.

A mi amigo sabio Daniel. Por su sensatez y amistad.

A mis compañeros de laboratorio actuales y con quienes tuve la oportunidad de compartir: Iva, Keila, Wilda, Andrés, Graciela, Pablo, Carolina, Héctor, María José, Alejandra, Tita, Natalia, Victor, Álvaro, James, Tomás y Sofía. Por todo lo que me enseñaron durante estos años.

Al Dr. Gonzalo Carrasco-Aviño, por su ayuda en la discusión de resultados, harmonización de datos y por proveer figuras relevantes para el desarrollo de esta tesis.

A Allan Peñaloza-Otarola, Thais Ratis-Ramos y Raúl Arias-Carrasco; por su aporte al desarrollo de esta tesis.

A mis colegas Bárbara, Jonathan, Eric, Felipe, Fabián y Sergio. Por las infinitas conversaciones sobre ciencia y sobre la vida. Por todas las veces que compartimos durante este proceso formativo.

A la Vicerrectoría de Investigación UC y a la Escuela de Medicina UC, por su apoyo económico estos años.

A los jefes de programa que he tenido: por haberme aceptado en el Programa de Doctorado en Ciencias Médicas y por la oportunidad de completar este proceso de aprendizaje. Dr. Jaime

Pereira, Dra. Claudia Sáez, Dra. Silvana Zanlungo, Dr. Jorge Carvajal, Dra. Andrea Leiva, Dra. Carolina Bizama.

A mi comisión evaluadora, Dra. Carolina Bizama y Dr. Vinicius Maracaja-Coutinho, por su ayuda desinteresada durante la elaboración y maduración de este proyecto.

En especial, a mis tutores Alejandro y Elmer, quienes creyeron en mí desde un principio y me empujaron a seguir este camino. Han tenido un rol clave en mi desarrollo profesional y personal y han dejado una huella imborrable en mi vida.

Por último, a mis amigos del colegio, de la vida y familia.

Gracias a todos.

TABLE OF CONTENTS

LIST OF TABLES

LIST OF FIGURES

ABSTRACT

Background: Gastric cancer (GC) is the third leading cause of cancer death worldwide. Intestinal type GC is the most common form of GC and develops as the last step in a sequential series of preneoplastic lesions known as Correa's gastric precancerous cascade. This process encompasses i) non-atrophic gastritis, ii) multifocal atrophic gastritis, iii) intestinal metaplasia (IM), iv) dysplasia and v) GC. It has been proposed that long-lived resident gastric stem cells can acquire molecular alterations driving the progression of this cascade, at least in part through activation of intestinal transcriptional programs in IM, leading to trans-differentiation of gastric into intestinal-like cells. KLF5 is a key player in this phenotype shift that also promotes cell proliferation in many different cancers and transcriptionally regulates the expression of long noncoding RNAs (lncRNAs). lncRNAs are a subtype of non-protein coding transcripts spanning >200 nucleotides in length, some of which have the capacity to bind and sequester miRNAs in a plethora of cell types and conditions including GC. By binding to multiple miRNAs, lncRNAs can inhibit the role of miRNAs as translational repressors. This mechanism, termed the competing endogenous RNA (ceRNA) hypothesis, involves both coding and non-coding RNAs that share common miRNAs. Aberrant activation of transcriptional programs cognate to gastric stem cell biology and trans-differentiation of gastric cells has not, to our knowledge, been evaluated in terms of its effects on the expression levels of lncRNAs. Such an approach may provide valuable mechanistic insights into the origins of dysregulation of ceRNA networks in the context of Correa's gastric precancerous cascade. **Hypothesis:** "*KLF5 is progressively expressed in Correa's gastric precancerous cascade, resulting in the aberrant expression of lncRNAs which hamper miRNA-induced silencing of pro-oncogenic mRNAs through competing endogenous RNA networks*". **Aim:** The general aim of this study was to describe novel ceRNA networks dysregulated by aberrant expression of KLF5-dependent lncRNAs throughout Correa's gastric precancerous cascade and in gastric cancer. **Methods:** Publicly available human gene expression datasets from representative steps of the gastric precancerous cascade and GC were downloaded from Gene Expression Omnibus (GEO) and the stomach adenocarcinoma (STAD) dataset from The Cancer Genome Atlas (TCGA) repositories. Probe annotations were updated. Co-expression analyses were performed

for an agnostic set of genes associated with gastric stem cell biology or progression of Correa's cascade. Differential expression analyses between different steps of the cascade were performed and results were integrated using a random effects model meta-analysis approach. KLF5 chromatin immunoprecipitation followed by sequencing data coupled to expression profiling by microarray data in KLF5 knockdown and control conditions were downloaded from GEO and re-aligned to reference genome hg38. To construct ceRNA networks in GC, a global catalog of miRNA:target interactions was used in conjunction with miRNA and RNA sequencing data from STAD TCGA. lncRNAs participating in significant ceRNA interactions from the network were cross queried against lncRNAs downregulated upon KLF5 knockdown. Subnetworks were constructed using these selected lncRNAs and related mRNAs and miRNAs from the main network. Functional enrichment analyses were performed using genes from the generated networks and visualized as network layouts in Cytoscape. **Results:** Seven lncRNAs downstream from KLF5 were identified in significant ceRNA interactions in GC: MAPKAPK5-AS1, SNHG1, SNHG3, SNHG7, SNHG15, SNHG17 and MIRLET7BHG. ChIP-seq analysis results strongly suggest that only MAPKAPK5-AS1 is transcriptionally regulated by KLF5. MAPKAPK5-AS1, SNHG1, SNHG3 and SNHG17 increase significantly in GC. SNHG1 and SNHG3 increase significantly in at least one preneoplastic stage. MIRLET7BHG decreases significantly in non-atrophic gastritis and remains downregulated throughout the rest of the cascade. Overrepresentation analysis of the individual MAPKAPK5-AS1 ceRNA network showed that this lncRNA acts as a miRNA sponge for let7i, miR-34a and miR-429. These miRNAs regulate the expression of genes involved in the DNA damage response and cell cycle. These GO terms were also enriched in the integrated ceRNA network of the 7 lncRNAs downstream from KLF5 (including MAPKAPK5-AS1); where the two main clusters of biological processes were DNA repair and mitotic cell cycle. **Conclusion:** Our results show that lncRNAs regulated by KLF5 most likely contribute to the development and progression of GC by acting as novel ceRNAs that promote cell proliferation and alter the DNA damage response. Future efforts must be made in the future to validate of our results in clinical samples and *in vitro*, to provide mechanistic evidence supporting the functionality of the proposed ceRNA interactions in gastric cells.

INTRODUCTION

Section 1: Overview of gastric cancer, Correa's gastric precancerous cascade and risk factors

I. **The global burden of gastric cancer.** Gastric cancer (GC) is the third leading cause of cancer death and fourth most common cancer worldwide[1,2]. GC age-standardized mortality rates range from 2.8 to 28.1 per 100,000 inhabitants in men and from 1.5 to 2.8 per 100,000 in women[3]. The highest estimated mortality rates are found in eastern Asia, central and eastern Europe and South America; while the lowest mortality rates are found in North America and Australia[3–6]. In 2018, GC was responsible for 782,685 deaths worldwide (8.2% of all cancer deaths), with 1,033,701 new cases (5.7% of new cancer cases). In Chile, GC was the fourth most common malignancy, representing 5,162 (9.7%) of all new cancers cases; and ranked second in mortality, with 3,478 (12.2%) deaths[1,2].

In recent years, there has been a global decline in GC incidence and mortality. Observed annual percent change in mortality has been approximately -4% in European countries, Korea and Australia. Meanwhile, the GC annual percent change in Chile has been lower at around -1.6%[3,4]. In fact, the most recent GLOBOCAN data shows a steady number of total GC deaths in Chile since 2009 (3,350 GC deaths in 2009[7] vs 3,478 deaths in 2018[1]). A possible explanation for the slow decrease in mortality rates in Chile is the lack of effective screening strategies and misdiagnosis of the disease at initial stages. The delay in diagnosis contributes to the development of more advanced lesions, at which point curative treatment is no longer an option[8]. In this sense, it is relevant to obtain a better understanding of the physiopathology underlying the disease. This knowledge may set the basis for the development of novel approaches to aid in the timely diagnosis of early GC or populations at high-risk for developing this neoplasm.

II. **Gastric cancer classification.** Gastric neoplasms are highly heterogeneous and have been classified into various subtypes according to the histological or molecular characteristics of the tumors[9]. Laurén's classification[10] is the most common approach in research and

clinical practice[11] and comprises 2 main histological subtypes: intestinal and diffuse type GC, along with a third mixed subtype. Intestinal type GC is the most frequent type of GC, with a relative frequency of approximately 55%, and is characterized by the presence of large glandular lumina and papillary fold formations. Diffuse type GC is characterized by scattered solitary tumor cells or small cellular clusters and represents approximately 30% of gastric tumors. Roughly 15% of the cases belong to the mixed subtype[10,11].

Despite the widespread use of this classification system, the heterogeneity of GC poses a major challenge for histopathological classifications in terms of offering accurate preventive, diagnostic and therapeutic interventions for GC patients; therefore, it is recommended that GC classifications consider molecular characteristics of the tumors as well. In this sense, new technologies may aid in constructing a GC classification system that combines molecular and genetic findings with histopathological characteristics[11,12]. Consequently, an approach by The Cancer Genome Atlas initiative has divided GC into 4 molecular subtypes: Epstein-Barr virus-positive tumors (EBV), which display hypermethylation and PIK3CA mutations; microsatellite unstable tumors (MSI), which show high mutation rates; genome stable tumors (GS), which are enriched for diffuse type adenocarcinomas and RhoA mutations; and tumors with chromosomal instability (CIN), characterized by aneuploidy and receptor tyrosine kinase amplifications[13]. This recent classification is based on analysis of molecular information from high-throughput platforms that has been deposited in an open-access repository, setting the basis for *in-silico* molecular profiling of GC and other tumors.

III. **Correa's gastric precancerous cascade.** Intestinal-type GC follows a series of well-established histopathological sequential lesions triggered by chronic infection by *Helicobacter pylori* (*H. pylori*), known as the multistep cascade of GC or Correa's gastric precancerous cascade[14] (Fig 1). This sequence encompasses i) non-atrophic gastritis, ii) multifocal atrophic gastritis, iii) intestinal metaplasia and iv) dysplasia. Ultimately, these preneoplastic stages lead to the onset of invasive gastric adenocarcinoma.

Correa's cascade begins with the colonization of normal gastric mucosa by *H. pylori,* leading to accumulation of inflammatory infiltrates without loss of glands (non-atrophic gastritis or NAG). This initial inflammatory state is followed by the onset of multiple atrophic patches at the antrum and corpus (multifocal atrophic gastritis or MAG). Atrophy is defined by loss of glands, either by shrinkage and replacement by fibrous tissue and/or replacement by pseudopyloric metaplasia or intestinal metaplasia (IM) (Fig 1B and 1C)[15]. Metaplasia can be defined as a "change of cells to a form that does not normally occur in the tissue in which it is found"[16]. Therefore, gastric IM corresponds to growth of intestinal-like epithelium within the stomach; and can be further subclassified as complete (CIM) or incomplete (IIM) IM. CIM is characterized by the growth of differentiated intestinal cells resembling a small bowel phenotype which includes Paneth, goblet and epithelial cells with a well-defined brush border and exclusive expression of sialomucins (Fig 1D-1d and 1E-1e). This step is succeeded by IIM, in which goblet cells predominate along with loss of the brush border, co-expression of sialo- and sulfomucins, as well as loss of expression of digestive enzymes (Fig 1D-1d and 1F-1f)[17]. Metaplastic lesions progress to dysplasia and, next, to GC. Progression rates to GC increase ten-fold from 0.6% (CI95% 0-1.7%) to 6.1% (CI95% 1.9-10.1%) when comparing CIM to IIM[18]. Therefore, IM seems to be the turning point of gastric precancerous lesions. Considering the rapid turnover of mucous-secreting cells from the foveolar and surface epithelium, it is most likely that long-lived gastric cells acquire molecular alterations driving the progression of this cascade[19,20].

IV. **Risk factors for gastric cancer.** GC is a multifactorial disease that results from a complex interaction between host genetic and environmental factors including dietary habits, smoking, obesity, salt consumption, socioeconomic status and infection by *H. pylori* or Epstein-Barr virus (EBV)[21–24].

Host genetic factors include hereditary GC, which is rare: 10% of all GC cases aggregate within families and only 1-3% of total GC burden can be attributed to hereditary germline mutations[25]. Sporadic GC makes up the remaining cases.

The principal risk factor for sporadic GC is chronic infection by *H. pylori*, a gram-negative bacterium that colonizes the stomach of roughly half of the world population[3]. *H. pylori* is a well-established carcinogenic agent and is responsible for 89% of non-cardiac GC as well as 29% of cardiac GC[26]. Co-evolution between *H. pylori* and humans during the last 100.000 years has led to mutual adaptation between the host and pathogen, in which the bacterium has become less virulent over time[21,27]. In this sense, gastric precancerous lesions are more frequent in presence of mismatching host ancestry and infecting *H. pylori* strains[28,29].

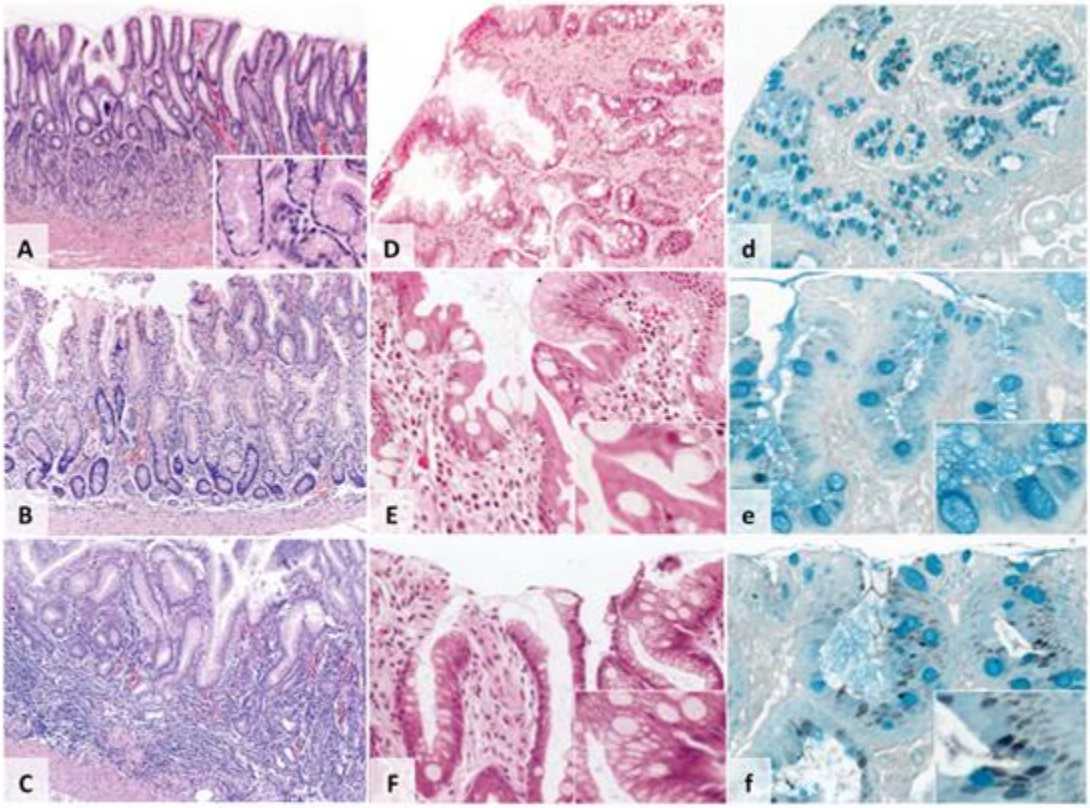

Figure 1. Atrophy and intestinal metaplasia in Correa's gastric precancerous cascade. A Normal antral gastric mucosa (HE, 40x). Inset shows normal antral mucous gland. **B** and **C** Extensive atrophy either by replacement of normal glands by intestinal metaplasia (**B**) or loss of glandular units (**C**) (HE, 40x). **D** (HE, 100x) and "**d**" (High Iron Diamine-Alcian Blue, HID-AB, 100x) sample showing regions with both complete (positive only for sialomucins – regions stained blue by HID-AB) and incomplete intestinal metaplasia (positive for sialomucins (blue) and sulfomucins – regions stained brown/black by HID-AB). **E** (HE, 100x) and "**e**" (HID-AB, 100x) complete IM, characterized by well-defined and equal in size/shape goblet cells, presence of brush border and only sialomucins (blue in "**e**"); insets 400x. **F** (HE, 100x) and "**f**" (HID-AB, 100x) extensive incomplete intestinal metaplasia, characterized by poorly formed, different in shape and size goblet cells, absence of brush border and positive staining for sialomucins and sulfomucins (blue and brown/black in "**f**", respectively); insets 400x. (Courtesy of Gonzalo Carrasco-Aviño, M.D.)

V. ***Helicobacter pylori* in gastric carcinogenesis.** To withstand the acidic nature of the stomach, *H. pylori* colonizes a narrow 25 μm niche adjacent to the gastric epithelial lining,

where alkaline mucous secretions protect it from the hydrochloric acid present in the stomach lumen[21]. The proximity between the bacterium and host cells allows for the interaction between bacterial virulence factors and gastric epithelial cells. Among these, four major virulence factors have been identified: outer membrane proteins (OMPs), vacuolating cytotoxin (VacA), cag-pathogenicity island (cagPAI) and cytotoxin associated gene A (CagA)[24]. OMPs are associated with gastric inflammation and are necessary for bacterial adhesion to the gastric epithelium[30]. VacA is a bacterial toxin, which causes host cell vacuolization, increases apoptosis and inhibits cell proliferation[31]. *H. pylori* cagPAI is a 40 Kb region of the bacterial genome which encodes for over 30 proteins, including a type IV secretion system (T4SS) that serves as a syringe-like membrane-bound scaffold essential for the injection of CagA and peptidoglycan, as well as NFκB activation[32]. CagA is encoded within the cagPAI and plays a key role in carcinogenesis, inducing neoplastic lesions even in absence of inflammation[33,34]. Infecting cagPAI$^+$ and CagA$^+$ *H. pylori* strains have increased oncogenic potential[32]. Once delivered upon host cells, CagA forms a complex signaling hub that increases cell proliferation through activation of mitotic signaling pathways including WNT/β-Catenin, mitogen-activated protein kinase (MAPK) and phosphoinositide 3-kinase (PI3K-AKT); as well as activation of pro-inflammatory pathways (i.e. NFκB) and inhibition of apoptosis via degradation of p53[35,36]. Additionally, CagA$^+$ *H. pylori* strains have been shown to directly colonize the gastric glands and expand subpopulations of resident stem cells at the gland base[37]. Moreover, CagA$^+$ strains have also been reported to induce DNA damage in stem cells[38]. Taken together, a growing body of evidence suggests that *H. pylori* infection may favor gastric carcinogenesis directly by expanding and damaging the gastric stem cell compartment.

Section 2: Tissue regeneration, stem cells and the gastric stem cell niche

I. **Functional organization of the stomach.** The stomach is an endoderm-derived exocrine organ which internal wall is coated with a surface epithelium of columnar mucous-secreting cells that protect the organ from its acidic contents[39]. The gastric surface

epithelium invaginates into the funnel-shaped gastric pits or foveolae that form a continuum with the gastric glands[20], which are the functional units of the stomach. Gastric glands are, in turn, subdivided into 3 segments: isthmus, neck and base. Gastric stem cell populations reside within the isthmus and base and actively proliferate to maintain epithelial turnover[40]. There exist 4 main types of adult differentiated gastric cells: pit, parietal, neck and zymogenic cells[32].

Three major anatomical regions can be recognized within the stomach: i) the fundus, ii) the corpus or body and iii) the pyloric antrum[20,40,41] (Fig 2A). The cellular composition of the gastric glands differs between these anatomic regions: glands from the proximal portion of the stomach, that encompasses the fundus and corpus, are composed primarily by acid-secreting parietal cells and zymogenic chief cells (Fig 2B). On the other hand, pyloric antrum glands are largely devoid of parietal and chief cells and are more abundantly composed by mucous-secreting cells and specialized G cells that secrete gastrin[20] (Fig 2C). Many different populations of gastric stem cells residing within antral or corpus glands have been described, and express distinct proteins that serve as stem cell markers.

II. **Gastric stem cells.** The homeostatic turnover of the gastric glands and epithelium is fueled by stem cell populations residing within a stem cell niche at the gland isthmus and base (Fig 2B-C). To date, several specific gastric stem cell markers have been discovered by the use of lineage tracing experiments[41].

   a. **Villin (VIL1).** Villin is an actin-binding protein expressed at the brush border of intestinal absorptive cells[32]. A $VIL1^+$ gastric stem cell population was first described in antrum glands by Braunstein et al.[42] in mice bearing lacZ β-galactosidase inserted at the Villin locus. Qiao and collaborators[43] used transgenic mice harboring Villin-controlled expression of lacZ or GFP, and demonstrated that this small population of stem cells located at the lower third of the antrum glands is capable of multi-lineage replenishment in response to exogenous administration of IFN-γ. Interestingly, this stem cell population does not replicate in absence of IFN-γ.

b. **SOX2.** Sex determining region Y-box 2 (SOX2) marks another relevant gastric stem cell population present in the antrum and corpus[44]. $SOX2^{+}$ stem cells mark mutually exclusive cells with $LGR5^{+}$ stem cells and are capable of differentiating into all main gastric lineages. Selective ablation of SOX2 cells results in impaired tissue turnover homeostasis and lethality in mice.

c. **CCKBR (CCK2R).** Cholecystokinin B receptor (CCKBR) is a gastrin receptor which labels actively cycling stem cells that express low levels of LGR5 ($Lgr5^{low}$). Although these cells typically don't respond to gastrin, stimulation with progastrin (a pro-peptide which represents 10% of the protein product) in transgenic mice increases proliferation, gland fission and interconversion of $LGR5^{low}$ $CCKBR^{+}$ cells into $LGR5^{+}$ cells in the antrum[45].

   Interestingly, a series of experiments by Tomkova et. al[46] showed that expression gastrin is induced by p73 in gastric cells; moreover, gastrin and p73 levels are correlated in gastric cancer. A subsequent study by our group[47] showed that p73 expression increases throughout the gastric precancerous cascade and serves as a potential biomarker for high-grade gastritis. Collectively, these data open the question whether p73 may result in the interconversion of CCKBR $LGR5^{low}$ slow-dividing stem cells into $LGR5^{high}$ fast-dividing stem cells and contribute to gastric carcinogenesis.

d. **LGR5 (GPR49).** Leucine-rich repeat containing G-protein coupled receptor (LGR5, also known as GPR49) is a G-protein coupled receptor, which amplifies WNT signals[48]. Briefly, LGR5 acts as a decoy substrate to prevent ubiquitination and proteasomal degradation of WNT receptor FZD. $LGR5^{+}$ cells can be found at the base of both antrum[49] and corpus[50] glands, as well as the isthmus of corpus glands[51].

e. **MIST1 (BHLHA15).** Karam and Leblond first proposed that gastric stem cells were located at the gland isthmus through a series of five papers using microscopic autoradiographic experiments. These researchers proposed the existence of a population of small self-renewing undifferentiated granule-free cells located in the isthmus of the corpus glands as the cell-of-origin of all gastric lineages, but were

unable to convincingly prove the latter claim[52]. It was not until recently that a study by Hayakawa et al. proposed that these poorly differentiated cells at the corpus gland isthmus correspond to a population of Mist1^{+} quiescent gastric stem cells[51,53] that are distinct from MIST1^{+} adult chief cells. They further demonstrated that these cells are capable of replenishing complete gastric glands and differentiate into all gastric cell lineages and can give rise to both intestinal and diffuse gastric cancer under specific conditions.

f. RUNX1. Matsuo et al[54] observed that a RUNX1 enhancer element marked an active stem cell group located at the isthmus, as well as a small fraction of committed chief cells at the gland base.

g. TROY (TNFRSF19). Recently, in 2013, Hans Clevers' group described an additional population of fully differentiated TROY^{+} (tumor necrosis factor receptor superfamily member 19 or TNFRSF19) chief cells residing at the base of the corpus glands which act as slowly dividing reserve stem cells upon cytotoxic tissue damage. These cells were shown to express LGR5 by microarray analysis and RT-qPCR[55]. It was later confirmed that these cells also express WNT agonist LGR5[50].

III. **The gastric stem cell niche.** Gastric stem cells reside in a specific niche that is crucial to regulate their fate into self-renewing stem cells or differentiate into one of the 4 main lineages of gastric cells[53]. This stem cell niche offers limited space for stem cells. Dividing stem cells undergo symmetric division and compete for their residence within this niche. Cells "forced out" of this niche commit to a differentiated lineage[56].

Sonic hedgehog (SHH) seems to play a preponderant role in the maintenance of this niche, as it regulates signaling by BMP, NOTCH and FGF10[41]. Parietal cells located in the proximal third of the gland base secrete SHH to the mesenchyme, which responds by secreting BMP[57] (Fig 2). Loss of parietal cells leads to loss of this BMP gradient and is accompanied

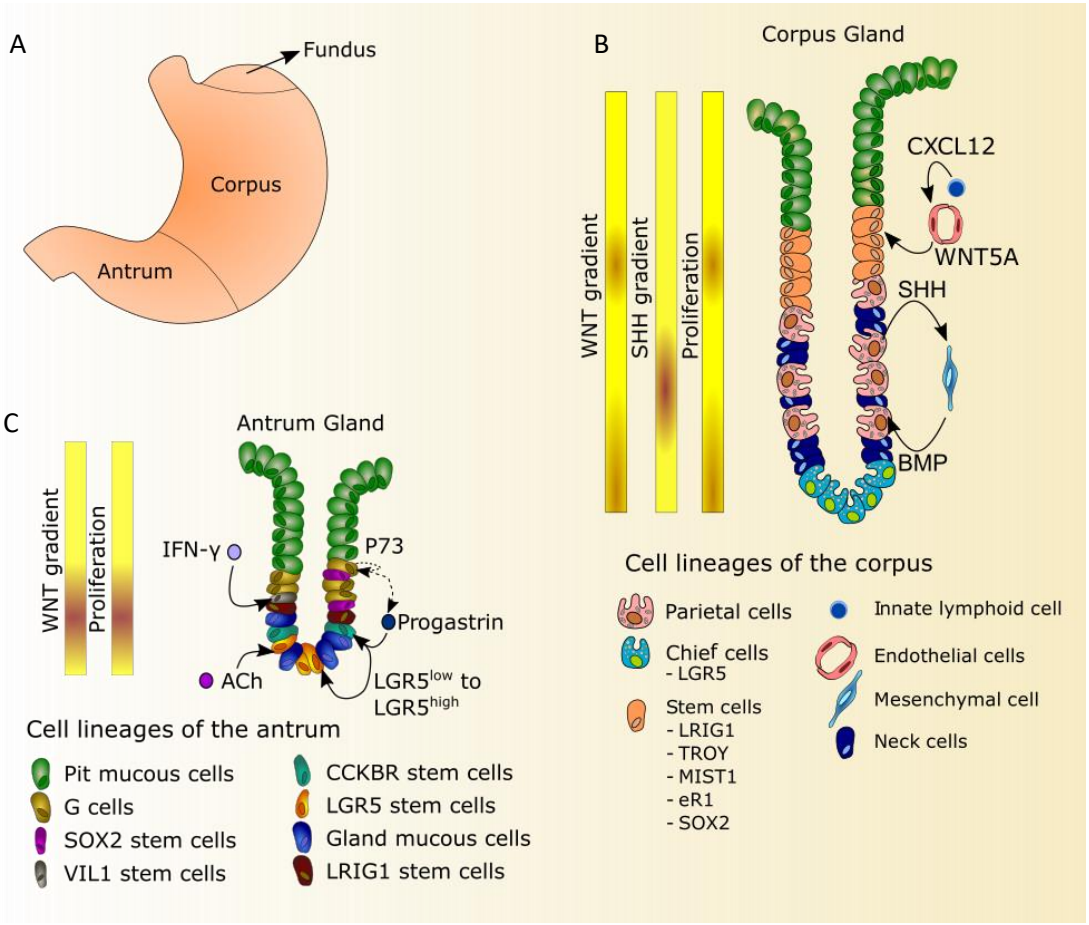

Figure 2. Gastric glands and stem cells of the corpus and antrum. A Anatomical regions of the stomach. **B** Main cell types in corpus glands are oxyntic parietal cells and chief cells. Distinct resident stem cell populations exist within the isthmus and base of these glands and are maintained by a specialized niche, represented as yellow bars adjacent to the gland diagram. Relevant soluble ligands for the maintenance of these gradients are shown to the right of the diagram. **C** Cellular composition of antral glands. Resident stem cells are located at the base of the glands. Gradients and relevant soluble ligands are shown as in **B**. It is unknown whether P73 expressed in G cells may favor interconversion from CCKBR to LGR5 stem cells by stimulating secretion of progastrin (dashed line).

by de-differentiation of chief cells into mucous neck cells (chief cell precursors)[19]. SHH also exerts a main role by antagonizing NOTCH signaling, which is specifically active at the gland isthmus region[58,59]. A high NOTCH signal shifts cellular phenotype into an absorptive, intestinal type. On the other hand, low NOTCH signaling produces secretory lineages[41]. Therefore, loss of SHH may be an interesting molecular switch for the development of intestinal metaplasia upon the occurrence of MAG. Another known function of SHH within the stomach is the suppression of fibroblast growth factor 10 (FGF10) during development. FGF10 is expressed in the mesenchyme during gastric

development, though its role in adult stomach is unknown[41]. It remains interesting that oncogenic activation of RAS together with loss of APC, can induce the onset of neoplastic lesions of the stomach in mice[51].

WNT signaling also plays a preponderant role in gastric stem cell homeostasis (Fig 2). During gastrointestinal development, the stomach develops following inhibition of WNT by BARX1. Loss of BARX1 during development leads to expression of an intestinal program in the stomach[60]. In the adult stomach, genes controlled by WNT transcriptional programs, such as TROY and LGR5, are expressed by resident stem cells within the gland base at the corpus and antrum[49,50]. Additionally, a perivascular niche maintains MIST1^{+} stem cells residing at the isthmus of corpus glands. Within this niche, innate lymphoid cells secrete soluble CXCL12 that activates CXCR4^{+} endothelial cells. These cells respond by secreting WNT5A ligand that stimulates proliferation of MIST1^{+} stem cells[51]. Constitutive activation of Wnt signaling can lead to the development of neoplastic lesions in mice[41].

Section 3: Wnt, CDX and KLF5 in Correa's gastric precancerous cascade and gastric cancer

A recent 16-year follow-up prospective study reported that prolonged *H. pylori* infection is associated with progression of precancerous lesions, especially in patients with MAG[18]; and that patients with incomplete IM have increased risk of developing GC compared to patients with complete IM (OR, 11.3; 95% CI 1.4 to 91.4). Therefore, IM seems to be the turning point of for the development of intestinal type GC. The underlying mechanisms driving the progression of IM to dysplasia and GC are not yet fully understood.

The rise of intestinal metaplasia from gastric stem cells requires a coordinated dysfunction between cellular signals and their surrounding environment. One of the phenomena that occur in MAG is the loss of oxyntic cells in the gastric corpus. Oxyntic cells maintain a morphogenic gradient of SHH and BMP in the region located between the gland isthmus and base[19,57], which is essential both for the patterning of the stomach during embryonic development[61] and for the differentiation of chief precursor cells in gland homeostasis[62]. Loss of these cells leads to loss of

this morphogenic gradient and de-differentiation of chief cells into chief precursor cells[19]. In turn, either de-differentiated cells or resident gastric stem cells – this is a highly debated topic – may act as the cell-of-origin for the establishment of gastric IM[63–68].

Several transcriptional programs that contribute to the trans-differentiation process from gastric-to-intestinal cells have been described; among which are the *caudal* homeobox genes CDX1 and CDX2[16]. Both of these transcription factors are key players in the development, maintenance and differentiation of enterocytes[69]. In fact, a murine model study reported that long-term partial loss of CDX2 results in loss of all differentiated intestinal cell types and interconversion from intestinal to gastric-like epithelium in the small intestine. Meanwhile, the combined loss of both CDX1 and CDX2 leads to an epithelial switch from intestinal to cecum-like cells in the colon[70]. Conversely, transgenic expression of CDX2 genes determines the apparition of differentiated intestinal cells in the mouse stomach[71,72]. Similarly, CDX1 promotes differentiation of intestinal lineages within the gastric epithelium[73,74].

Ectopic expression of CDX1 and CDX2 has been observed in gastric intestinal metaplasia and intestinal type GC[75]. Interestingly, expression of CDX2 antecedes expression of CDX1 and the onset of gastric intestinal metaplasia[76]. Moreover, CDX1 is a direct transcriptional target of CDX2[77], suggesting that the first step towards metaplastic changes is the upregulation of CDX2 that subsequently activates expression of CDX1.

CDX2 expression is induced by NFκB signaling[78,79], which is activated by *H. pylori* infection in early stages of the gastric precancerous cascade[32,80,81]. On the other hand, expression of CDX1 is controlled both by CDX2[77] and by Wnt[82–84] signaling cascades. Expression of WNT5A, the soluble Wnt ligand that maintains the perivascular niche of gastric stem cells is the corpus[51,53], is known to increase in primary gastric tumors[85–87]. Therefore, the Wnt pathway may take a more preponderant role in the regulation of CDX1 at later stages of the transformation process.

Despite the clear involvement of CDX1 and CDX2 in the development of intestinal metaplasia and the increased risk of malignant transformation upon establishment of IM compared to previous stages of the gastric precancerous cascade, the oncogenic potential of this epithelial alteration remains a controversial topic. A recent review article even goes as far as to state that IM does not progress to GC. Instead, the authors state that IM has been falsely accused based on guilt by

association considering that development of gastric cancer is a result from increased genetic instability of gastric stem cells and not a direct transition from metaplasia to cancer, as has been suggested by many animal models[88]. This claim poses a very interesting view of the events leading to GC development that cannot be reduced to a sequence of lesions, but rather builds upon this knowledge by considering additional events that must take place for the disease to develop. In line with this theory, a recent study by Patrick Tan's group in Singapore showed that intestinal metaplasia is a reversible state that is influenced by persistent *H. pylori* infection[89]. More importantly, the authors of this study stated that transition of IM to GC is likely not a direct lineal process, but requires mutations in key tumor-suppressor genes including p53 (which clonal mutations occur in GC and not in IM) and genomic alterations favoring cell immortality and genomic instability, such as telomere elongation and intragenic DNA hypomethylation. In a nutshell, these papers point out the need for additional alterations capable of explaining the transformation of stem cells on the verge of malignization into fully malignant immortal cancer cells.

As one of the key modulators of IM, critical questions surge regarding the oncogenic potential of CDX1 and its downstream genes. Krüppel-like factor 5 (KLF5) is a zinc-finger transcription factor which expression is regulated by CDX1[73]. KLF5 promotes pluripotency during embryonic development and is essential for the maintenance of an undifferentiated embryonic stem cell phenotype[90,91]. In fact, KLF5 acts together with KLF4 and KLF2 to upregulate the expression of OCT4, NANOG and SOX2 in an intricate pluripotency core circuitry[92,93]; although, to this effect, its impact is less potent compared with the other members of the KLF family[94].

Expression of KLF5 is related both to intestinal-like differentiation of gastric cells and to the expression of stem cell marker LGR5[73]. Moreover, KLF5 is frequently amplified in GC tissues and is a relevant transcriptional regulator of genes related to GC progression[95]. One of the most relevant cellular processes regulated by KLF5 is cell proliferation[96,97]. In gastrointestinal carcinomas, KLF5 has been shown to be one the master regulators governing the expression of HNF4, promoting cellular proliferation[98]. Similarly, KLF5 has been shown to inhibit the expression of p21/WAF and has been associated to poor prognosis and advanced TNM staging in GC[99].

Section 4: KLF5, long noncoding RNAs and competing endogenous RNA networks

It is currently known that while 2% of the genome corresponds to protein-coding genes, over 75% of the genome is actively transcribed[100] into small noncoding RNAs (< 200 nucleotides in length) and long noncoding (lnc) RNAs (> 200 nucleotides in length)[101]. A specific type of small noncoding RNAs, termed microRNAs (miRNAs), regulate gene expression at a post-transcriptional level through complementary binding of a miRNA seed region with the 3'-UTR of target mRNAs. Binding between a miRNA and a mRNA leads to translational repression or mRNA decay of the target gene[102]. Recent evidence has shown that expression of the target gene can be de-repressed by concomitant expression of different types of coding and noncoding RNAs which share a common miRNA target sequence, here onward referred to as miRNA response element (mRE). This crosstalk between a miRNA and its targets is known as a competing endogenous RNA (ceRNA) network, where RNAs sharing mREs compete for a determined pool of available miRNAs[100]. This regulatory circuit affects many cellular processes including differentiation, development, pluripotency and cancer[103,104]. Two papers recently proved that ceRNA networks are sensitive to up-regulation of transcription factors, demonstrating that transcription factor and ceRNA networks are closely intertwined[105,106]. Consistently, it has also been shown that several lncRNAs are induced during reprogramming of induced pluripotent stem cells[107] or are normally expressed in human embryonic stem cells[108]. In this line, Kim and col.[109] performed single-cell RNA-sequencing of mouse induced pluripotent stem cells (iPSCs) at different stages of pluripotency induction. Their results show that early iPSCs express various pluripotency factors including Oct4, Sox2 and Nanog, in a gene cluster which gene ontology functional annotation returned "unannotated''. Notably, 285 genes from this cluster were noncoding genes of unknown function and included 29 lncRNAs and 27 uncharacterized genes also classified as lncRNAs by Ensembl[110]. Additionally, a study by Mohamed et al.[111] showed that Oct4 can regulate the expression of 4 evolutionarily-conserved lncRNAs in mice. In turn, knockdown or overexpression of 2 of these lncRNAs led to altered Oct4 expression and modulated commitment to specific cell lineages. These data strongly serve as the basis to state that functional characterization of noncoding genes is needed, and that many of them may serve a functional role regulating the

cellular response to embryonic transcription factors. Furthermore, lncRNAs such as long intergenic noncoding RNA regulator of reprogramming (linc-ROR) functions as a ceRNA regulating the expression of pluripotency transcription factors Oct4, Sox2 and Nanog by sponging miR-145, therefore hampering mRNA degradation of these targets[112]. linc-ROR is upregulated and acts as a ceRNA in pancreatic[113], colon[114], prostate[115] and gastric cancer cells[113].

Taken together, these data support the claim that overexpression of pluripotency factors in gastric cells may induce the expression of lncRNAs which act as ceRNA involved in the progression of Correa's gastric precancerous cascade and GC. Such knowledge would provide valuable mechanistic insights into the origins of dysregulation of ceRNA networks in the context of Correa's gastric precancerous cascade. Specifically, besides being a relevant gene in stem cell biology, KLF5 has been shown to regulate the expression of several lncRNAs acting as ceRNAs in cancer tissues[116,117], but its role as a regulator of lncRNAs in the gastric precancerous cascade has, to our knowledge, not been evaluated.

We herein describe a pipeline for the evaluation of KLF5 as a relevant transcription factor in gastric preneoplasia and GC in the context of specific gastric intestinal metaplasia and stem cell markers. Next, we evaluate transcriptional regulation of lncRNAs by KLF5 in GC cells. Finally, we use the TCGA database to construct GC-specific ceRNA networks influenced by KLF5-dependent lncRNAs.

HYPOTHESIS

KLF5 is progressively expressed in Correa's gastric precancerous cascade, resulting in the aberrant expression of lncRNAs which hamper miRNA-induced silencing of pro-oncogenic mRNAs through competing endogenous RNA networks.

GENERAL AIM

To describe novel ceRNA networks dysregulated by aberrant expression of KLF5-dependent lncRNAs throughout Correa's gastric precancerous cascade and in gastric cancer.

SPECIFIC AIMS

1. To evaluate the expression patterns of KLF5 in conjunction with markers cognate to gastric stem cell biology and progression of the gastric precancerous cascade.

2. To identify lncRNAs regulated by KLF5 and determine their expression profiles in the gastric precancerous cascade and gastric cancer.

3. To identify significant KLF5-dependent lncRNA ceRNA interactions in gastric cancer.

METHODS

1. **To evaluate the expression patterns of KLF5 in conjunction with markers cognate to gastric stem cell biology and progression of the gastric precancerous cascade.**

This aim was divided into the following activities:

1.1. Selection and preprocessing of expression data

1.2. Generation of co-expression matrices and correlograms

1.3. Graphical representation of expression changes throughout the gastric precancerous cascade

1.4. Differential expression analysis

1.5. Integration of differential expression results from independent experiments by meta-analysis

1.1. Selection and preprocessing of expression data:

A comprehensive search on Gene Expression Omnibus (GEO[118]) was performed using the search terms "gastritis" and "intestinal metaplasia"; the results were filtered to include only GEO series comprising human samples. Additionally, gene expression data from the Asian Cancer Research Group (ACRG[119]) and gastric adenocarcinoma TCGA[13] studies were downloaded. Accession number, publication date and number of samples per dataset are shown in Table 1.

- **GEO microarray data:** Expression data from GEO were downloaded using getGEO() function from R package GEOquery[120]. Data were loaded into R. Expression matrices, phenotype data and platform annotations were retrieved using exprs(), pData() and fData() functions from the GEOquery package. We identified stable gene annotations from the annotation data frame obtained by fData() and mapped each probe to current HGNC symbols using the function mapIDs() from the org.Hs.eg.db R package[121] using the stable gene identifier as reference. No annotation data was associated with its corresponding platform for dataset GSE11762 (Platform GPL15314), which was therefore discarded. Dataset GSE2444 was also dropped from

further analysis due to sample mislabeling which impeded group selection for differential expression analysis. Outdated annotations were filtered out from the original dataset along with the respective expression data and saved as R objects intended for manual curation in the future. Dataset GSE66229 was split into 2 separate cohorts: a 98 NTAM / 98 Tumor paired sample cohort and a 100 NTAM / 202 Tumor unpaired sample cohort. After updating the annotations, expression matrices were log2-transformed and quantile-normalized using normalizeQuantiles() function from the limma R package[122]. Only for the GSE66229 cohorts, log10-transformed data had to be linearized and subsequently log2-transformed to keep the scaling factor consistent across datasets. Probe level signals were averaged to obtain gene-level signals using avereps() function from the limma R package. Principal components analysis (PCA) was performed and visualized using ggplot2 R package[123] to filter out any potential outliers. To avoid unwanted variance introduced by removed samples, raw data was reprocessed as needed, following the steps indicated above.

Table 1. Selected datasets

									IM					
Accession	**Country**	**Year**	**Technology**	**Platform**	**Citation**	**Normal**	**NAG**	**MAG**	**CIM**	**IIM**	**Dys**	**NTAM**	**Tumor**	**Paired**
GSE2669	Singapore	2005	Microarray	GPL2048	NA	10	0	26	22		0	0	64	0
GSE27411	Sweden	2014	Microarray	GPL6255	24119614	3	3	3	0		0	0	0	0
GSE55696	China	2017	Microarray	GPL6480	25548486	0	0	19	0		39	0	19	0
GSE106656	Mexico	2017	Microarray	GPL6244	NA	0	7	7	7		0	0	0	0
GSE78523	Spain	2017	Microarray	GPL18990	28441455	15	0	0	17	13	0	0	0	0
GSE60662	Japan	2014	Microarray	GPL13497	25069978	4	4	4	4		0	0	0	0
GSE60427	Bhutan/D. Republic	2015	Microarray	GPL17077	25977263	7	8	8	8		0	0	0	0
GSE66229	S. Korea	2015	Microarray	GPL570	29725014	0	0	0	0		0	100	300	98
STAD TCGA	Multiple	2014	RNAseq	HiSeq2000	25079317	0	0	0	0		0	35	415	32
					Total	**39**	**22**	**67**	**71**		**39**	**135**	**798**	**130**

NAG: Non-atrophic gastritis; MAG: Multifocal atrophic gastritis; IM: Intestinal metaplasia; CIM: Complete intestinal metaplasia; IIM: Incomplete intestinal metaplasia; Dys: Dysplasia; NTAM: Non-tumor adjacent mucosa; Paired: Number of paired NTAM / Tumor samples (applicable only to TCGA and GSE66229); STAD: Stomach Adenocarcinoma; TCGA: The Cancer Genome Atlas. Note: Functioning hyperlinks are embedded within the table. Click to go to selected dataset, platform or reference under column "Citation", which contains PMIDs.

- **TCGA RNA-seq data:** RNA-seq V2 data from the stomach adenocarcinoma (STAD) TCGA study[13] were downloaded and preprocessed using DownloadRNASeqData() and ProcessRNASeqData() functions from Module_A and Module_B from TCGA-Assembler R package[124,125], respectively. Clinical data were downloaded from the same database using the DownloadClinicalData() function from the same R package. Country or city of procurement data were manually curated by retrieving these clinical tracks from cBioPortal[126,127]. Entrez IDs from the annotation object generated by the ProcessRNASeqData() function were used as stable gene identifier to update HGNC symbols to the latest version. Outdated entries were manually imputed into de NCBI Gene Database for retrieval of updated Entrez ID and HGNC symbol. STAD TCGA data were split into 2 separate cohorts as described for the GSE66229 dataset (32 paired NTAM / Tumor samples and 35 NTAM / 262 Tumor samples). Genes with expression <1 count per million (CPM) in, at least, 32 samples (number of NTAM) were dropped from further analyses. These filtered counts were re-normalized by TMM as implemented in edgeR R package[128]. To filter out any outlier samples, TMM-normalized log2 data were visualized in interactive multi-dimension scaling (MDS) plots generated using Glimma R package[129]. Although no samples were removed from further analyses, we observed a strong batch effect which resulted in strong grouping of NTAM samples collected in South Korea and United States.

1.2. Generation of co-expression matrices and correlograms:

A list of 24 interest genes was generated based on their potential use as markers of either i) intestinal metaplasia or ii) gastric stem cells (Table 2). Pearson correlation matrices were generated between gene pairs from the list for each individual dataset (Figure 3a), using the cor() function from R package corrplot[130]. Correlations with *P-val* < 0.01 were considered as 0 (no correlation – Figure 3b-c). Individual correlograms for each dataset comprising correlations between pairs of interest genes were generated using the function corrplot() from the same package. To generate an average correlation matrix (Figure 4), we created a list containing all correlation matrices. We summed the correlation coefficients between each pair of interest

Table 2. Interest genes

HGNC Symbol	Role
KLF5	Intestinal TF. Increases in IM. Is regulated by CDX1 and contributes to cancer progression[73,95,117]
LGR5	Gastric stem cell marker[49,50]
TP73	Putative oncogenic isoforms arising from splicing events or alternative promoters. Improves stem cell induction[131,132]
POU5F1 (OCT4)	Embryonic TF. Expressed in adult gastric stem cells. Upregulated in preneoplastic lesions and GC. Regulates lncRNAs[133–135]
SOX2	Gastric stem cell marker. Stem cell induction (Yamanaka factor)[44,136]
RUNX1	Gastric stem cell marker[54]
AXIN2	Gastric stem cell marker[137]
VIL1	Gastric stem cell marker. Population of stem cells stimulated by IFN-γ[42,43,138]
BHLHA15 (MIST1)	Gastric stem cell marker[51]
TNFRSF19 (TROY)	Gastric stem cell marker[50,55]
CCKBR	Gastric stem cell marker. Progastrin induces interconversion to LGR5$^+$ cells[45]
LRIG1	Gastric stem cell marker. Associated with KLF5 in gastritis. Decreases in intestinal metaplasia[139–141]
GAST	Induces preneoplastic lesions by a proliferative effect on epithelial cells[142–144]
TFF2	Increases in preneoplastic lesions, intestinal metaplasia marker[145]
TFF3	Increases in preneoplastic lesions, putative SPEM marker[146]
CDX1	Intestinal TF, increases in IM and regulates KLF5[16,73]
CDX2	Intestinal TF, increases in IM[16]
CFTR	Chloride channel, increases in IM[147]
OLFM4	Notch-dependent immune response mudulator. Increases in IM[148]
IFNG	Pro-inflammatory cytokine. Promotes proliferation of VIL1 gastric stem cells[42,43]
LGR4	Wnt agonist, similar to LGR5. Regulates stem cells through SOX2[149]
LGR6	Wnt agonist, similar to LGR5. Stem cell marker in other tissues[150]
SOX9	TF, induces formation of columnar-like epithelium in Barrett's esophagus[151]
CTNNB1	TF, canonical Wnt pathway. Increased in *H. pylori*-positive tissues[152]

TF: Transcription factor; GC: Gastric cancer; SPEM: Spasmolitic polypeptide-expressing metaplasia; IM: Intestinal metaplasia

genes of all correlation matrices included in the list to obtain a "sum of correlation coefficients matrix". Considering that not all datasets evaluated all of the interest genes due to differences in the microarray platform or the RNA-seq experiment from TCGA, we generated a "meter matrix", in which each pair of genes summed 1 if the gene pair was evaluated in a given dataset or 0 if the pair of genes was missing in a particular dataset. This approach enabled us to keep track of how many times the correlation between the gene pairs was calculated across all queried correlation matrices. To obtain an "average correlation coefficient matrix", the "sum of correlation coefficients matrix" was divided by the "meter matrix". In a final step, we calculated the

correlation distance (CorDist) as a scaling factor ranging from 0 (perfect correlation) to 1 (perfect anti-correlation) for each gene pair by the formula $CorDist = \frac{1-cor}{2}$; and a new correlogram was generated with heatmap.2() function from package gplots.

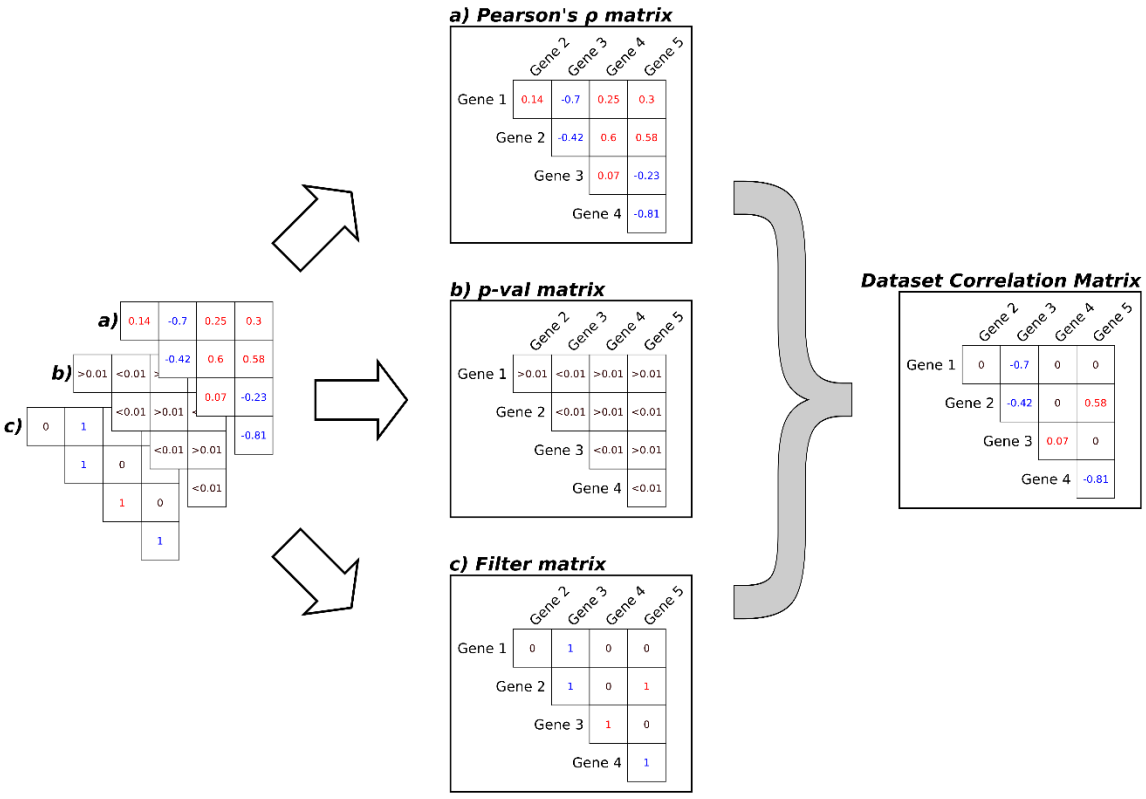

Figure 3. Generation of correlation matrices by dataset. Pearson correlation coefficients between pairs of genes from the interest gene table were calculated (a) for each individual dataset, along with p-values (b) from each correlation. A filter matrix was generated (c), assigning either 1 or 0 as multiplication factors for each of the observed correlation coefficients from the Pearson's correlation matrix based on the significance level of the correlations (1 for *P-val* < 0.01 and 0 for *P-val* > 0.01). This approach enabled us to retain only significant correlations (Dataset correlation matrix).

1.3. Graphical representation of expression changes throughout the gastric precancerous cascade:

Mean expression values of the control condition for each dataset – defined as the least malignant condition for each experiment – were calculated and subtracted from the normalized expression matrices. The transposed expression matrices were converted into data frames and a "Condition" column was added as a grouping variable. The expression data frame was transformed to "long" format using the melt() function from R package reshape2[153]. A "GEO_accession" column was

added to the data frame with the corresponding accession number for each dataset; and rbind() function from R base was used to merge all individual data frames into a global data frame. The split() function from R base was used to split the merged data set into a list of individual data sets by gene as a splitting variable. The facet_wrap() ggplot2 – embedded within a loop structure – was added to make graphical representations of each gene by dataset, grouped by condition.

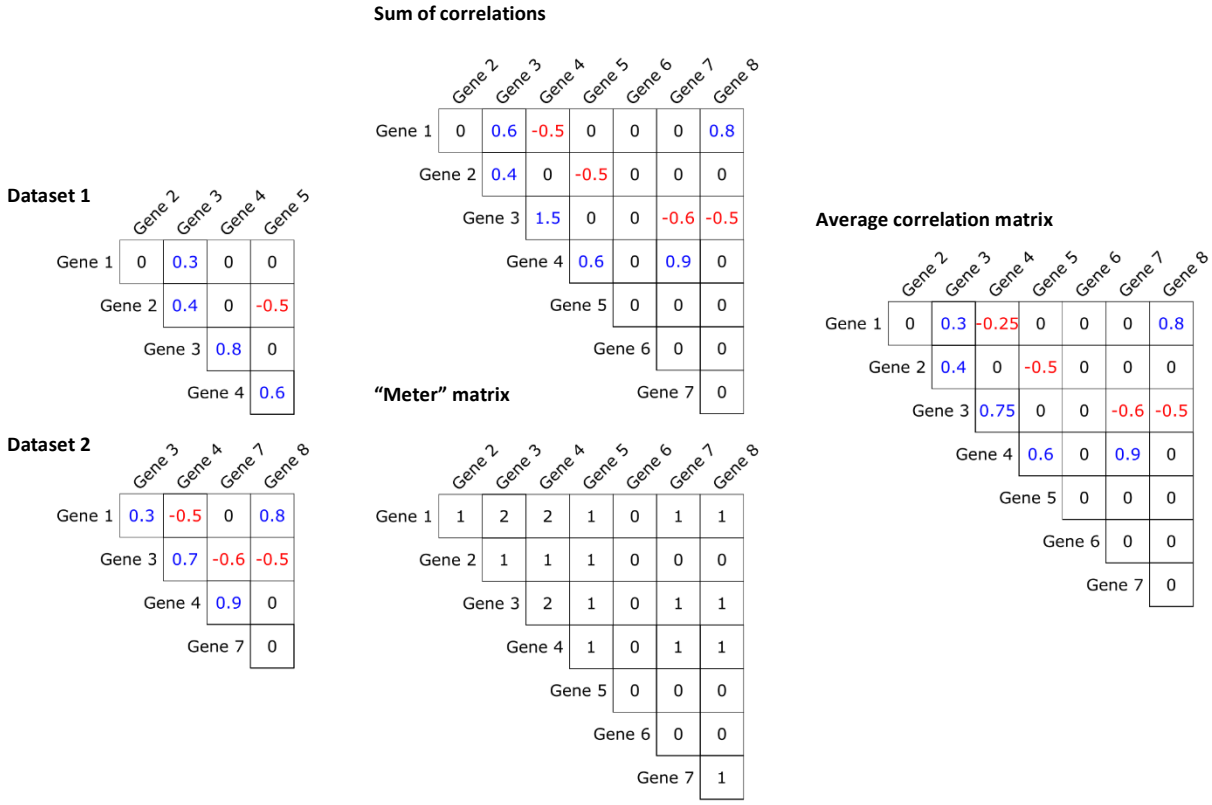

Figure 4. Generation of average correlation matrix. Correlation coefficients between pairs of genes as obtained for different datasets (i.e. Dataset 1 and Dataset2 from the diagram, left panels) were summed to obtain a "sum of correlations" matrix (upper-mid panel. The number of times a gene pair correlation was evaluated across datasets was imputed into a "Meter" matrix (lower-mid panel). An average correlation matrix was obtained by dividing the sum of correlations matrix by the meter matrix (right panel).

1.4. Differential expression analysis:

Differential expression analyses were performed using limma for microarray experiments and limma-voom method for STAD TCGA RNA-seq data. Additionally, for paired sample experiments (ACRG - GSE66229 and STAD TCGA), we used condition + subject as blocking variable. For TCGA unpaired differential expression analysis, we used condition + country to account for the

previously described batch effect. For all individual dataset analyses, a $\log_2$ fold-change cutoff was set at 0.5 at an adjusted *P-value* < 0.05 (BH method[154]). Heatmaps for differentially expressed genes from each dataset were generated using heatmap.2() function from R package gplots[155], using both Euclidean and Spearman correlation distances. For the meta-analysis, differential expression results without $\log_2$ fold-change cutoff (eBayes method) were exported and used as input for MetaVolcanoR (see following method).

1.5. Integration of differential expression results from independent experiments by meta-analysis:

To integrate the results obtained by differential expression analyses, a random effects model meta-analysis was performed using the results obtained for all datasets at a $\log_2$ fold-change cutoff set at 0 (limma eBayes method). Complete differential expression results for each contrast generated for every dataset were retrieved using `topTable()` function from limma R package and integrated into a random effects model meta-analysis using function `rem_mv()` from R package MetaVolcanoR[156]. Genes from our list of interest genes were interrogated in the results from the meta-analysis and forest plots were generated using `draw_forest()` function from the mentioned R package. Results for the meta-analysis were retrieved using `meta_table()` function from the same package.

2. **To identify lncRNAs regulated by KLF5 and determine their expression profiles in the gastric precancerous cascade and gastric cancer.**

This aim was divided into the following activities:

2.1. Discovery of KLF5 peaks in promoter regions of lncRNAs in GC cells by ChIP-seq analysis

2.2. Identification of lncRNAs downstream from KLF5 by microarray expression profiling in GC cells in control and KLF5 siRNA experimental conditions

2.3. Expression profiling of selected lncRNAs throughout the gastric precancerous cascade and gastric cancer using results from specific aim 1

2.1. Discovery of KLF5 peaks in promoter regions of lncRNAs in GC cells by ChIP-seq analysis**:**

ChIP-seq data acquisition: R package GEOquery[120] was used to download KLF5 ChIP-seq BED files from AGS, KATOIII and YCC3 gastric cancer cell lines (GEO accession number GSE51705[95]). Genomic sites occupied by KLF5 (peaks from the BED files) were re-mapped from genome build hg19 to hg38 by Thais Ratis-Ramos from Dr. Vinicius Maracaja-Coutinho's lab using `LiftOver`, a tool used to convert genome coordinates and genome annotation files between assemblies. Genomic positions for novel lncRNAs identified in a recent publication by their group were also included[157]. The BED file was processed using `closest` function from BEDTools[158], which reports the least genomic distance from the peak to the nearest genomic feature (in this case, transcript). This distance was used to filter overlapping transcripts (distance reported as 0) and absence of peaks (reported as -1). Peaks mapping between -1 and -10000 bp from TSS of lncRNAs were used to generate BED files that were uploaded as custom tracks to the UCSC genome browser[159].

2.2. Identification of lncRNAs downstream from KLF5 by microarray expression profiling in GC cells in control and KLF5 siRNA experimental conditions:

Expression data from AGS, KATOIII and YCC3 gastric cancer cell lines in siControl, siKLF5, siGATA4 and siGATA6 conditions were downloaded from GEO as described above (GEO accession number GSE51704). Affymetrix Human Genome U133 Plus 2.0 Array (platform accession number GPL570)

probes were re-annotated by Dr. Raúl Arias-Carrasco, from Dr. Vinicius Maracaja-Coutinho's group. Briefly, probe sequences were re-aligned to the human genome (build hg38) using BLAT[160]. Feature annotations were reassigned using BEDTools[158]. Probes aligning to more than one feature were discarded. For more details, see supplementary material in De Lima *et al*[161]. The probe-level expression matrix was quantile-normalized using `normalizeQuantiles()` and averaged to gene-level signal using `avereps()` functions from LIMMA[122] R package. Principal components analysis was carried out to confirm global differences between experimental groups (siControl, siGATA4, siGATA6 and siKLF5). Differential expression analysis was performed between each contrast with LIMMA, using `eBayes()` without fold-change cutoff for significance. Differentially expressed genes from all contrasts were plotted using Spearman correlation distance and hierarchical clustering at default settings (complete linkage) from `heatmap.2()` function, R package gplots[162]. Differential expression results from siKLF5 vs siControl conditions in the 3 GC cell lines from the experiment (AGS, KATOIII and YCC3) were integrated using the random effect model from MetaVolcanoR[156] R package.

2.3. Expression profiling of selected lncRNAs throughout the gastric precancerous cascade and gastric cancer using results from specific aim 1:

- **Meta-analysis in NAG, MAG and IM vs Normal:** Expression profiles of KLF5 and selected lncRNAs were recovered from the meta-analysis in NAG, MAG and IM vs Normal contrasts.
- **Meta-analysis in Tumor vs NTAM:** Expression profiles of KLF5 and selected lncRNAs were recovered from the meta-analysis results performed between the ACRG (GSE66229) and STAD TCGA studies.

3. To identify significant KLF5-dependent lncRNA ceRNA interactions in gastric cancer.

Competing endogenous RNA networks in GC were constructed using SPONGE R package[163]. In contrast with other existing methods, SPONGE defines a 'multiple miRNAs sensitivity correlation', that corresponds to the contribution of multiple miRNAs binding to the computed correlation between a ceRNA gene pair. Thus, the workflow implemented by this analysis pipeline has several advantages over alternative approaches that are based only on correlations between ceRNA pairs and absence/presence of a shared miRNA response element. First of all, this algorithm takes into account the expression levels of ceRNA pairs, as well as those of shared miRNAs between the ceRNAs. Secondly, they use a probabilistic approach to estimate a distribution under a null hypothesis, which serves to compute and adjust computed *P-values* between potential ceRNA pairs. Additionally, SPONGE is built upon a correlation approach, which allows for fast *P-value* calculations.

Since SPONGE uses miRNA and mRNA/lncRNA expression levels as input for computation of correlations, partial correlations and multiple miRNA sensitivity correlations; the user must provide the miRNA and mRNA/lncRNA expression matrices in a format compatible with the algorithm. Additionally, one can provide a miRNA-target interaction matrix to determine correlation values in miRNA-target pairs. Although this step is optional, providing this interaction matrix will reduce computation time and improve the overall results from the pipeline.

Competing endogenous RNA networks were constructed using TCGA RNA-seq and miRNA-seq expression data. A miRNA-target interaction matrix was also provided. An elastic net regression filter was used to discard miRNA-target pairs with no significant interactions or partial correlation coefficients < 0.05 (default value for the program). The *P-value* of ceRNA interactions were adjusted by FDR. A more detailed summary of the workflow is described below, presented as 5 activities:

3.1. Generation of a miRNA-target interaction matrix

3.2. TCGA miRNA-seq and RNA-seq expression matrices

3.3. Elastic net regression

3.4. Significance analysis of potential competing endogenous RNAs by computing null distributions of multiple sensitivity correlations

3.5. Visualization of the ceRNA networks and over-representation analysis

3.1. Generation of a miRNA-target interaction matrix:

A catalog of miRNA-target interactions was constructed by Allan Peñaloza-Otarola from Vinicius Maracaja-Coutinho's group, by integration of multiple databases using reference miRNA annotations from miRBase v22.1[164] and reference gene annotations from GENCODE[165]. miRNA-mRNA interactions were retrieved from TargetMiner[166], miRDB[167], TargetScanHuman[168] and TarBase v8[169]. Experimentally validated miRNA-mRNA interactions were considered as valid, and computationally predicted interactions were considered as such only if present in 3 of the 4 databases.

A miRNA-lncRNA catalog was generated similarly by integrating data from LncBase[170] and starBase[171]. This miRNA-target interaction catalog was converted to a binary matrix with miRNA IDs as columns and target IDs as rows, where presence of an interaction between a miRNA and its target was summarized as 0 if absent or 1 if present (Figure 5). The original interaction matrix included 944 mature miRNAs and 26275 targets. This matrix was standardized to include miRNAs as annotated in the TCGA miRNA-seq and RNA-seq expression datasets. To this end, values for miRNA -3p and -5p strands were summed to global miRNA interaction values, taking values as either 0 (no strands interact with target RNA), 1 (only 1 strand interacts with target RNA) or 2 (both strands interact with target RNA). miRBase version was checked using miRBaseConverter R package[172]. Target RNA IDs were converted to HGNC symbols using biomaRt[173,174] and Homo.sapiens[175] packages. This updated interaction matrix was filtered to match gene and miRNA IDs present in TCGA RNA-seq and miRNA-seq expression matrices. The final re-annotated interaction matrix comprised 445 miRNAs and 18081 target RNAs (Figure 6), resulting in a loss of 8194 targets and their miRNA interactions.

3.2. TCGA miRNA-seq and RNA-seq expression matrices:

These were downloaded, normalized by TMM and converted to logCPM as described above. Samples were filtered to include only tumor samples for which both miRNA-seq and RNA-seq expression data were available (368 tumor samples total). Of note, RNA-seq expression matrix included mRNAs, lncRNAs and pseudogenes. Only transcripts matching with interaction matrix rows were retained (18081 transcripts). Only miRNAs matching with interaction matrix columns were retained (445 miRNAs).

	hsa-let-7a-2-3p	hsa-let-7a-3p	hsa-let-7a-5p	hsa-let-7b-3p
AC004383.4	0	1	1	0
AC005152.2	0	0	0	0
AC006445.8	1	0	0	0
AC007255.7	0	0	0	0

Figure 5. Binary interaction matrix (before re-annotation of transcript IDs). miRNA-target pair interactions are represented as 0 (absent) or as 1 (present).

	hsa-let-7a-2	hsa-let-7a	hsa-let-7b	hsa-let-7c
ATGB1	0	2	0	1
PROM1	0	0	0	0
AP3M1	1	0	0	0
XIAPP1	0	0	0	1

Figure 6. Binary interaction matrix (after re-annotation of transcript IDs). Interactions are represented as 0 (absent), 1 (only 1 miRNA strand interacts with the transcript) or 2 (both miRNA strands interact with the transcript).

3.3. Elastic net regression:

An elastic net regularization method was performed as part of the SPONGE algorithm, using the miRNA and RNA-seq expression matrices to select and keep only miRNA-target pairs with negative correlation between them. This regression assumes the occurrence of a negative correlation between the transcripts due to the convention that miRNAs bind target mRNAs and hinder their translation into proteins[176]. If the match between the miRNA seed sequence is perfect, this leads to mRNA cleavage. Thus, miRNA binding may decrease the overall expression levels of their targets. Fitting this regression model to the miRNA-target interactions acts as a filter to reduce the amount of false positive ceRNA pairs.

3.4. Significance analysis of potential competing endogenous RNAs by computing null distributions of multiple sensitivity correlations:

The combinatorial effects of multiple miRNAs on the expression levels of ceRNA pairs was defined as multiple miRNAs sensitivity correlation (mscor) by List *et al*[163]. The mscor estimates the contribution of multiple shared miRNAs in a given ceRNA interaction between two genes, and is computed internally within the SPONGE algorithm by calling R package ppcor[177]. Briefly, the mscor value can be defined as the result of subtracting the partial correlation (Partial cor) between the target genes of shared miRNAs from the correlation (Cor) of the gene pair. A similar multiple miRNA sensitivity correlation may be observed in miRNA-target pairs by chance in a scenario in which i) no interaction takes place between the miRNAs and the gene pair and ii) the correlation between the gene pairs varies. To correct for this confounder, a null distribution model is computed by calculating mscor values between miRNA-mRNA pairs in which no interactions occur. After generating the null distribution, the mscor calculated for "real" miRNA-target pairs (with interactions) is fit to this null distribution and a *P-value* is calculated. As a result, the amount of false interactions decreases dramatically. For the analyses presented in this work, null distribution models were generated using 10^5 iterations and a sample size equivalent to the real expression dataset (368 samples, 445 miRNAs and 18081 mRNAs).

3.5. Visualization of the ceRNA networks and over-representation analysis:

A small ceRNA subnetwork was generated for lncRNA MAPKAPK5-AS1, that is most likely transcriptionally regulated by KLF5. This subnetwork was visualized using Cytoscape[178]. Nodes representing genes from the network were filled according to the GC vs NTAM meta-analysis results using a continuous color palette ranging from green to red (green for downregulated genes and red for upregulated genes; scale limits -2.11 to 2.11). Non-differentially expressed gene nodes were colored in yellow. Gene ontology (GO, biological process) over-representation analysis (ORA) was performed with Cytoscape plugin BiNGO[179] using all genes from this subnetwork. BiNGO results were converted to a network view using Cytoscape plugin Enrichment Map[180]. Default values of Jaccard + Overlaps metrics were used.

Additionally, a larger ceRNA subnetwork was constructed using MAPKAPK5-AS1 together with 6 lncRNAs that were indirectly regulated by KLF5 that also act as significant ceRNAs in GC (*P-adj* < 0.05). This subnetwork was visualized using `sponge_plot_network()` function from SPONGE. ORA was performed and results were converted to a network view as described for the previous subnetwork. To avoid overlap between highly redundant GO terms from this analysis, only GO terms with extreme statistical significance values (*P-adj* < 5E-10) were selected. Clustering and annotation of GO terms were performed using Enrichment Map[180] (as described above) followed by MCL clustering by similarity coefficient as implemented in AutoAnnotate[181] Cytoscape plugin.

RESULTS

1. **To evaluate the expression patterns of KLF5 in conjunction with markers cognate to gastric stem cell biology and progression of the gastric precancerous cascade.**

1.1. Dataset selection:

We performed a comprehensive query on GEO using "intestinal metaplasia" or "gastritis" as search terms, that yielded a total of 27 expression profiling experiments in human samples, including whole-transcriptome RNA-sequencing and whole-transcriptome microarrays, as well as smaller panels such as targeted RNA-seq experiments. After an initial filtering step (see methods section), a total of 8 expression microarray datasets were selected for further analyses, to which we added the STAD TCGA RNA-seq dataset which was downloaded separately. These datasets included studies from over 9 different countries, publication years and microarray platforms. All steps of the gastric precancerous cascade were successfully covered by, at least, one microarray experiment. Accession numbers, publication year, citation (PMID), number of samples per condition, platform, etc.; are available as active hyperlinks in Table 1 (methods section).

1.2. Integrated average correlation analysis reveals a potent co-expression signature between gastric stem cell marker VIL1, *Caudal* homeobox genes CDX1 and CDX2, pluripotency factor KLF5, Wnt pathway transcription factor β-catenin and intestinal metaplasia markers OLFM4, CFTR and TFF3:

We performed an integrative correlation analysis of a panel of 24 stem cell and intestinal metaplasia markers (Table 2) across all datasets (note: ACRG - GSE66229 and TCGA were split into 2 datasets each – paired and unpaired cohorts). Co-expression analyses between gene pairs on the global average co-expression matrix shows 3 distinct gene clusters (Figure 7). Cluster 1 comprises VIL1, CDX1, CDX2, KLF5, CTNNB1, OLFM4, CFTR and TFF3. This gene set is notoriously anti-correlated with a second cluster encompassing 4 gastric stem cell markers: BHLHA15, LRIG1, SOX2 and CCKBR. The third cluster is not as defined.

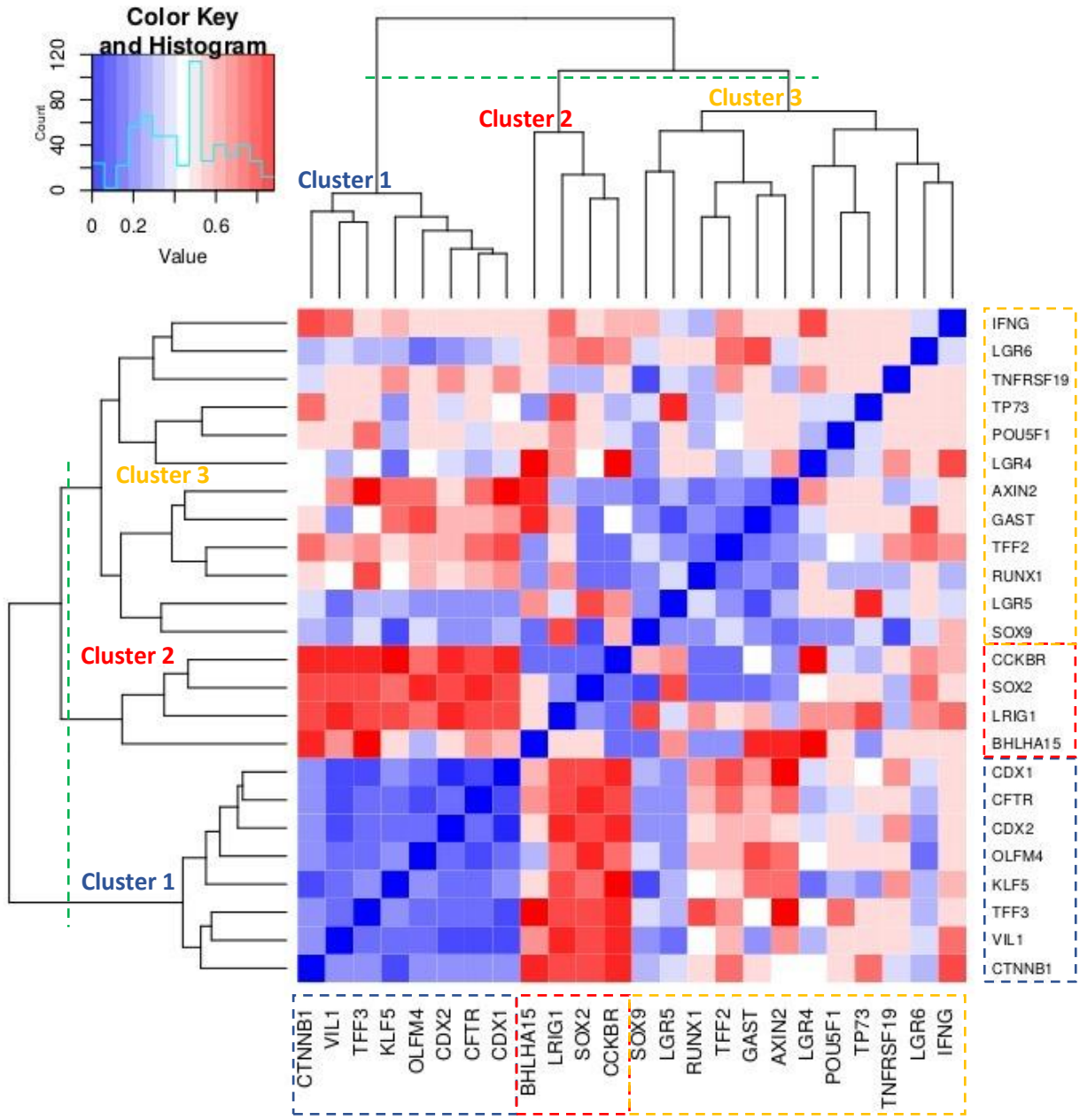

Figure 7. Correlation analysis of gastric stem cell and gastric intestinal metaplasia markers. Correlation distances between gene pairs. Correlation distance heatmap shows 3 distinct gene clusters: cluster 1 (blue) is the strongest gene cluster, enriched for intestinal metaplasia markers and intestinal transcription factors such as CDX1, CDX2 and KLF5, along with gastric stem cell marker VIL1. Cluster 2 (red) is inversely correlated with cluster 1 and is enriched for gastric stem cell markers. Cluster 3 does not show any strong correlations between gene pairs. Green line represents the point at which clusters diverge on the dendrogram.

1.3. <u>Genes from the cluster 1 show an increasing trend during the progression of the gastric precancerous cascade, that is especially notorious in intestinal metaplasia compared to normal gastric tissues</u>:

We generated visual representations of all genes from our interest gene panel, that are shown as log2 fold-change (LFC) compared to the control condition of each dataset. Samples were

grouped by condition and dataset. Examination of these results showed that the 8 genes comprised in cluster 1 from our global average correlation analysis show an increasing trend during the gastric carcinogenic process (Figures 8 and 9), while genes from cluster 2 show a decreasing trend (data in supplementary material). Though some of the genes from cluster 3 such as gastric stem cell marker LGR5 and intestinal transcription factor SOX9 behaved similar to genes from cluster 1 during the progression of the gastric precancerous cascade (see supplementary material), they did not group in well-defined clusters of co-expressed or mutually exclusive genes (as seen in Figure 2). Interestingly, the most notorious changes occurred in IM compared with lesions from previous stages (normal, NAG and MAG).

1.4. KLF5 increases significantly in intestinal metaplasia together with VIL1, CDX1 and CTNNB1, TFF3 and OLFM4:

Considering our previous results, expression changes in genes from Cluster 1 were integrated into a meta-analysis comparing intestinal metaplasia with normal gastric tissues, contrast present in 4 datasets representing a total of 71 IM samples and 39 normal samples (GSE2669, GSE78523, GSE60662 and GSE60427; Table 1). Six out of eight genes from Cluster 1 ranked among the top 3% of differentially expressed genes from the meta-analysis; including KLF5, VIL1, CDX1, CTNNB1, TFF3 and OLFM4 (Table 3). Forest plots for these 6 genes are shown in Figure 10.

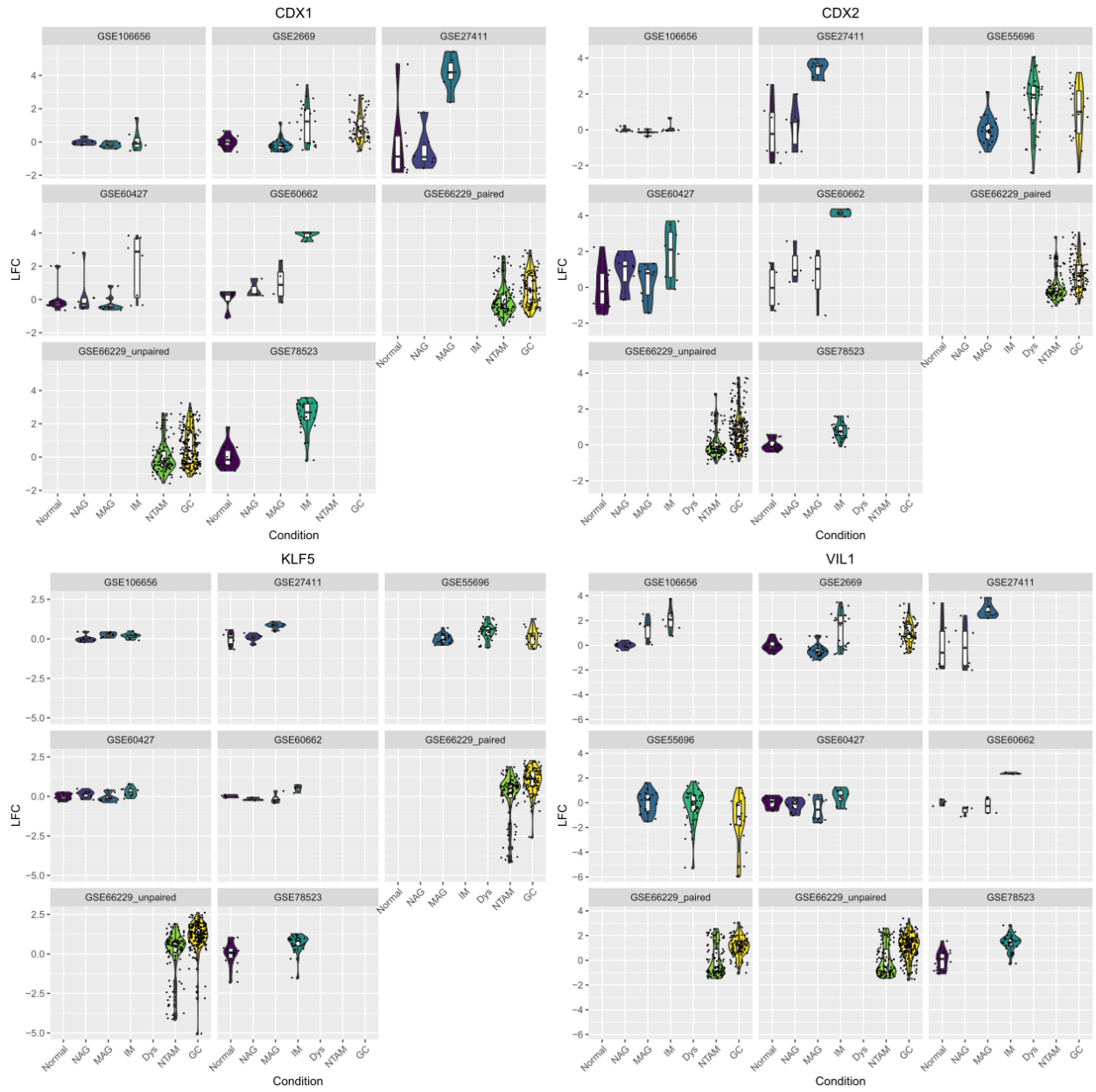

Figure 8. Graphical representation of genes from Cluster 1 throughout the gastric precancerous cascade. Expression changes of CDX1 (top left), CDX2 (top right), KLF5 (bottom left) and VIL1 (bottom right) are shown throughout the progression of preneoplastic lesions of the stomach for each of the individual datasets. Preneoplastic lesions are ordered sequentially. Violin plots are colored by condition. Boxplots represent 1st, 2nd and 3rd quartiles. Points represent individual samples. Note that the scale is adjusted individually for the LFC range of each gene across datasets. LFC: Log_2-fold change. NAG: Non-atrophic gastritis. MAG: Multifocal atrophic gastritis. IM: Intestinal Metaplasia. Dys: Dysplasia. NTAM: Non-tumor adjacent mucosa.

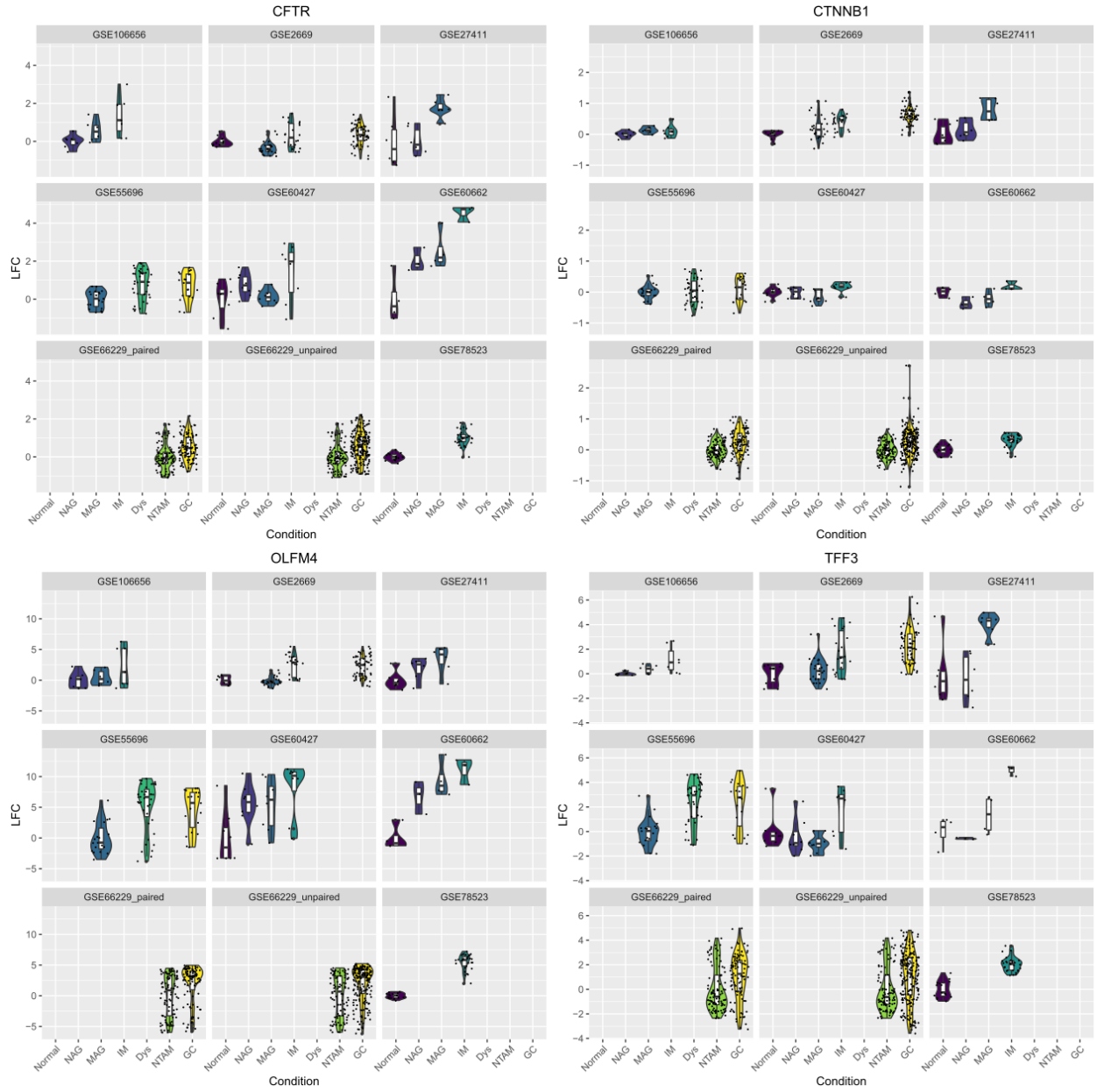

Figure 9. Graphical representation of genes from Cluster 1 throughout the gastric precancerous cascade. Expression changes of CFTR (top left), CTNNB1 (top right), OLFM4 (bottom left) and TFF3 (bottom right) are shown throughout the progression of preneoplastic lesions of the stomach for each of the individual datasets. Preneoplastic lesions are ordered sequentially. Violin plots are colored by condition. Boxplots represent 1st, 2nd and 3rd quartiles. Points represent individual samples. Note that the scale is adjusted individually for the LFC range of each gene across datasets. LFC: Log_2-fold change. NAG: Non-atrophic gastritis. MAG: Multifocal atrophic gastritis. IM: Intestinal Metaplasia. Dys: Dysplasia. NTAM: Non-tumor adjacent mucosa.

Table 3. Meta-analysis results: Cluster 1 - Intestinal metaplasia vs normal gastric tissues.

Gene	Consistency	LFC	CI (lower limit)	CI (upper limit)	p-val	Rank	Percentile
CDX1	4	2.32	1.25	3.39	2.29E-05	79	0.32%
TFF3	4	2.51	1.16	3.87	2.74E-04	206	0.85%
OLFM4	4	6.42	2.85	9.99	4.24E-04	219	0.90%
VIL1	4	1.38	0.65	2.11	2.27E-04	269	1.10%
CTNNB1	4	0.29	0.19	0.39	6.22E-09	344	1.41%
KLF5	3	0.44	0.20	0.69	2.92E-04	653	2.68%
CDX2	3	2.1	0.26	3.93	2.5E-02	3293	13.52%
CFTR	4	1.72	-0.01	3.44	5.12E-02	4728	19.41%

Consistency: LFC sign consistency across queried datasets containing the gene. CI: 95% confidence interval. Rank: Position of the gene in ranked order of the meta-analysis; 24364 genes were queried. LFC: Integrated log2 fold-change.

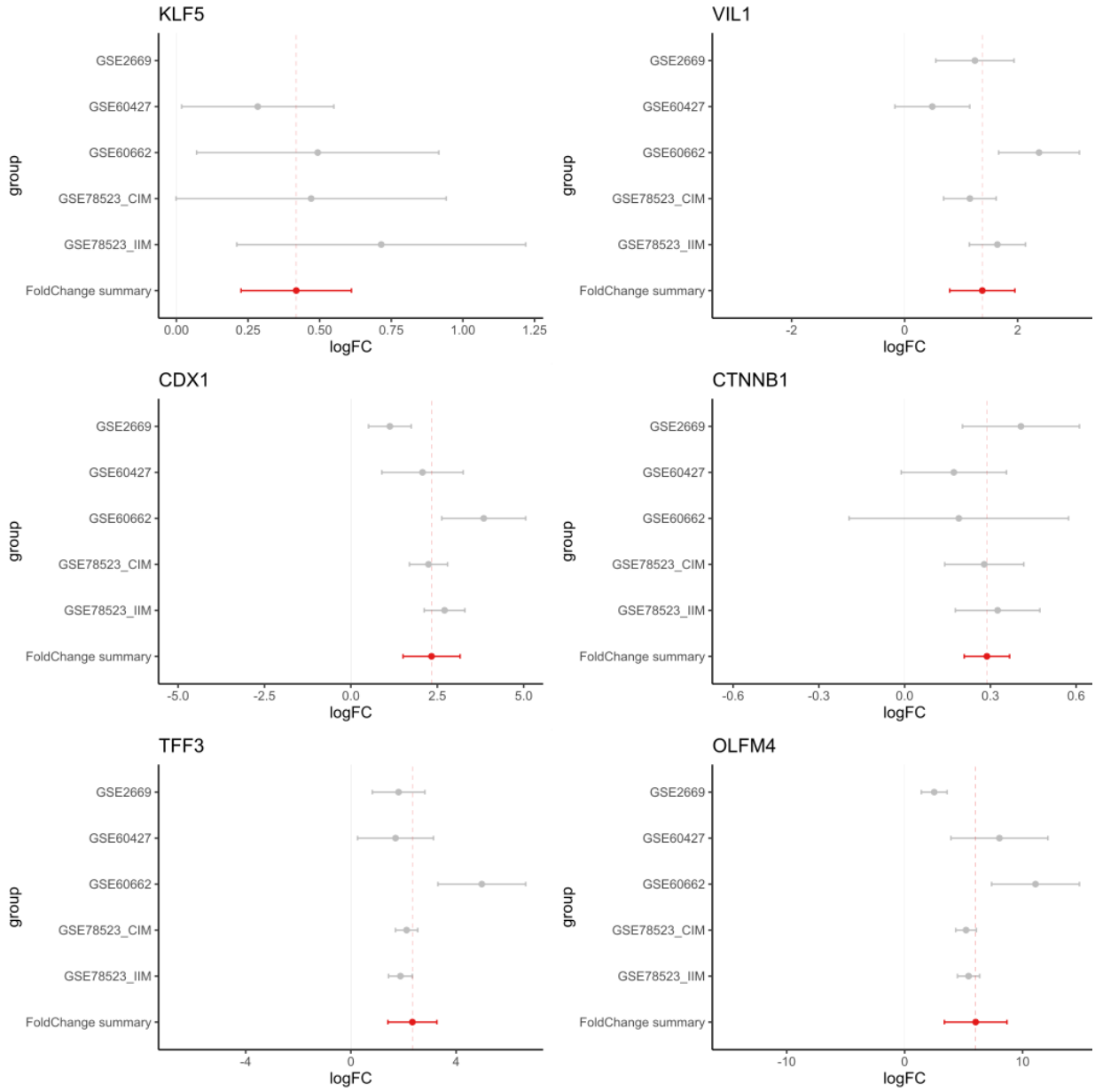

Figure 10. Meta-analysis - Top 6 genes from Cluster 1 in intestinal metaplasia vs normal gastric tissues. Forest plots show mean log_2 fold-change (logFC) and 95% confidence intervals (CI) in individual datasets where differential expression analyses were performed (grey bars) for intestinal metaplasia – normal contrast. Datasets are indicated in the Y axis, labelled as "group". Integrated logFC and 95% CI is indicated in red as FoldChange summary. Note that GSE78523 is depicted as 2 separate datasets, due to the fact that this particular experiment had samples from complete intestinal metaplasia (CIM) and incomplete intestinal metaplasia (IIM).

2. **To identify lncRNAs regulated by KLF5 and determine their expression profiles in the gastric precancerous cascade and gastric cancer.**

2.1. lncRNA MAPKAP5-AS1 is transcriptionally regulated by KLF5:

Having confirmed that KLF5 increases significantly in IM compared with normal tissues and is accompanied by increased expression of gastric stem cell marker VIL1 and well-established IM markers; the next step to discover lncRNAs downstream from KLF5 was to analyze KLF5 peaks using available ChIP-seq data (GSE51705) performed in 3 GC cell lines: AGS, KATO III and YCC3. We found 221 KLF5 peaks within 10 Kb upstream from the TSS of lncRNAs in AGS cells, 742 in KATO III, and 140 in YCC3 GC cells.

To determine which of these lncRNAs were effectively downstream from KLF5, we performed differential expression analysis between control (siControl) and KLF5 knockdown (siKLF5) conditions using public microarray data in the same 3 GC cell lines: AGS, KATO III and YCC3 (GSE51704). Principal components analysis (PCA) showed that KLF5 knockdown had a strong effect on the observed variance in the 3 cell lines (Figure 11 A, C and E). Hierarchical clustering using Spearman correlation distance metrics and complete linkage resulted in clear separation of the 4 experimental conditions from the dataset (siControl, siGATA4, siGATA6 and siKLF5) in the 3 cell lines (Figure 11 B, D and F).

Results for the 3 cell lines were integrated using the same meta-analysis strategy previously described in the methods section. As a control, we first verified that KLF5 was effectively knocked down in siKLF5 condition (Figure 12, left panel; logFC = -1.69, *P-value* = 8.82E-27). We found a total of 78 lncRNAs that were consistently downregulated in the 3 GC cell lines upon KLF5 knockdown. Analyzed in conjunction with KLF5 ChIP-seq data, only 6 known lncRNAs contained KLF5 peaks within 10 Kb of their TSS: MAPKAPK5-AS1, LINC002481, TOB1-AS1, PCOLCE-AS1, LINC00313 and PAX8-AS1. KLF5 peaks were also found in the promoter regions of 2 newly mapped lncRNAs[157]: TCONS_00178516 and TCONS_00039332.

KLF5 peaks mapped consistently only to the promoter region of lncRNA MAPKAPK5-AS1 in the 3 GC cell lines, in a genomic region between -633 and -2143 upstream from the TSS (Figure 13).

Taken together, these data strongly suggest that lncRNA MAPKAPK5-AS1 is transcriptionally regulated by KLF5 in gastric cells (Figure 12, right panel).

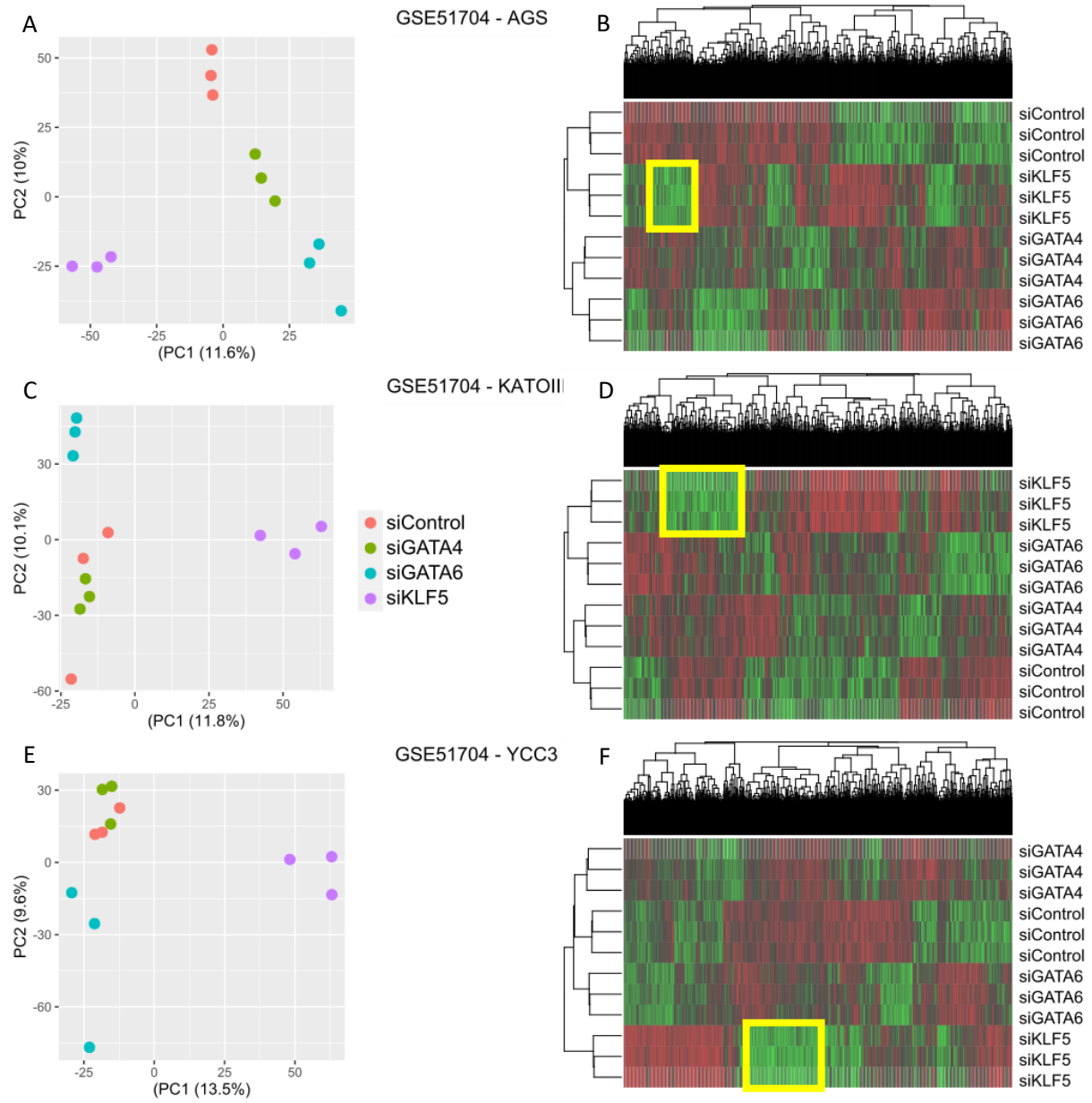

Figure 11. Differential expression analysis for KLF5 knockdown in GC cells. A, C and E show principal components analysis performed in AGS, KATOIII and YCC3 GC cells, respectively in siControl, siGATA4, siGATA6 and siKLF5 experimental conditions (red, green, cyan and purple dots, respectively). KLF5 knockdown has the strongest effect on variance out of all experimental conditions. X axis represents principal component 1 (PC1) with its respective cumulative variance. Y axis represents PC2 with its respective cumulative variance. **B, D and F** hierarchical clustering heatmaps showing differentially expressed genes in AGS, KATOIII and YCC3 GC cells, respectively (Spearman correlation distance, complete linkage). Differentially expressed genes from all contrasts are shown. Yellow bins highlight genes that are exclusively downregulated in siKLF5 condition on each cell line.

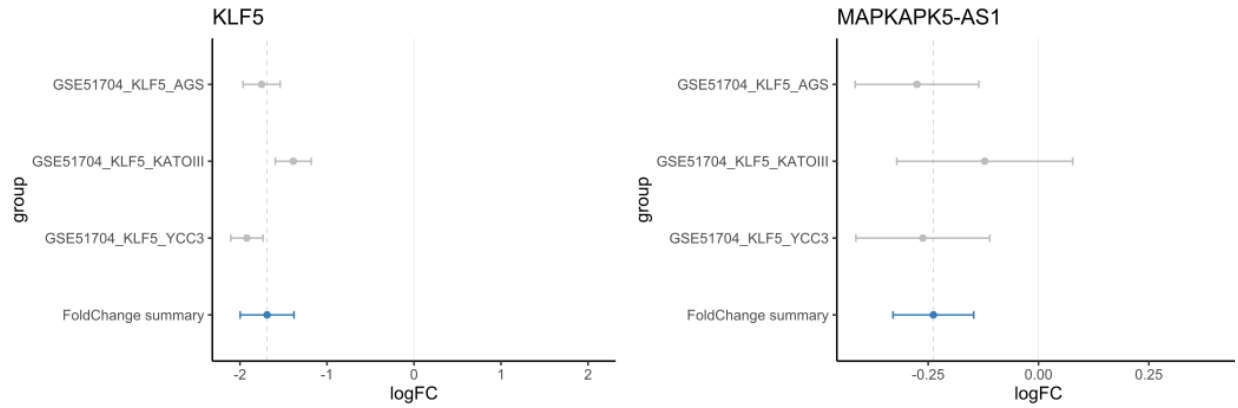

Figure 12. Meta-analysis - KLF5 and MAPKAPK5-AS1 in 3 gastric cancer cell lines upon KLF5 knockdown. Forest plots show mean log2 fold-change (logFC) and 95% confidence intervals (CI) for each individual cell line (grey bars) in siKLF5 – siControl. Datasets and cell lines are indicated in the Y axis, labelled as "group". Integrated logFC and 95% CI is indicated in blue as FoldChange summary. Left panel: KLF5 knockdown was effective in the 3 GC cells (logFC = -1.69, P-value = 8.82E-27) Right panel: Expression of MAPKAPK5-AS1 was consistently reduced in the 3 GC cells upon siKLF5 knockdown (logFC = -0.23, P-value = 4.65E-07).

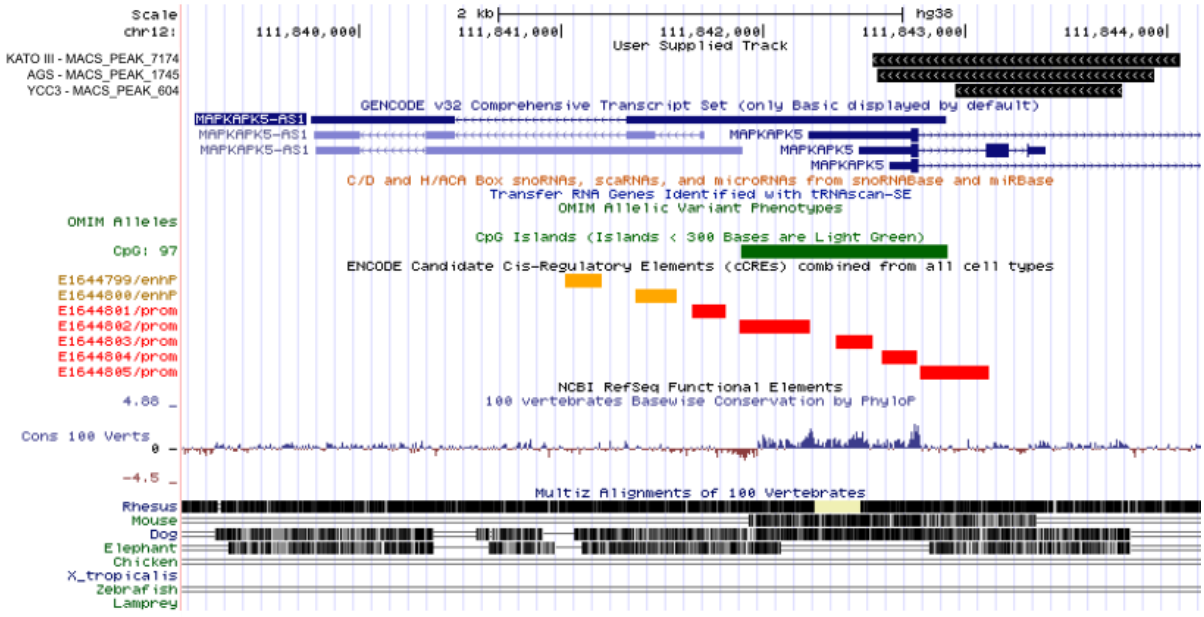

Figure 13. KLF5 peaks map to the MAPKAPK5-AS1 promoter region. KLF5 binding on MAPKAPK5-AS1 genomic promoter in KATO III, AGS and YCC3 GC cells through analyzing GSE51705 database (black bars on top right corner of the diagram). The MAPKAPK5-AS1 gene I shown in blue. A CpG island containing 97 CpG dinucleotides is shown as a green bar. Orange and red bars show genomic regions with proximal enhancer- or promoter-like signatures (ENCODE data as visualized in the UCSC genome browser).

2.2. KLF5 and MAPKAPK5-AS1 are overexpressed in GC:

Since we had previously shown that KLF5 increases mainly in IM (Figure 8 and Figure 10), we next characterized the expression profiles of KLF5 and lncRNA MAPKAPK5-AS1 using the meta-analysis results. KLF5 expression did not vary significantly at early stages of the gastric precancerous cascade (NAG and MAG) but increased significantly in IM compared with normal gastric tissues (Figure 14A; summary logFC 0.42, P-value = 2.07E-05). MAPKAPK5-AS1 expression changes were highly variable across NAG, MAG and IM compared with normal gastric tissues (Figure 14C) and no significant global expression changes were observed in preneoplastic lesions. To determine whether KLF5 and lncRNA MAPKAPK5-AS1 were upregulated in GC, we verified the expression profiles of KLF5 and MAPKAPK5-AS1 in the GC vs NTAM meta-analysis results. Both KLF5 and MAPKAPK5-AS1 increase significantly in GC tissues compared with NTAM (Figure 14B and D; logFC 1.11, *P-value* = 4.54E-52 for KLF5; logFC 0.15, *P-value* = 4.2E-06 for MAPKAPK5-AS1).

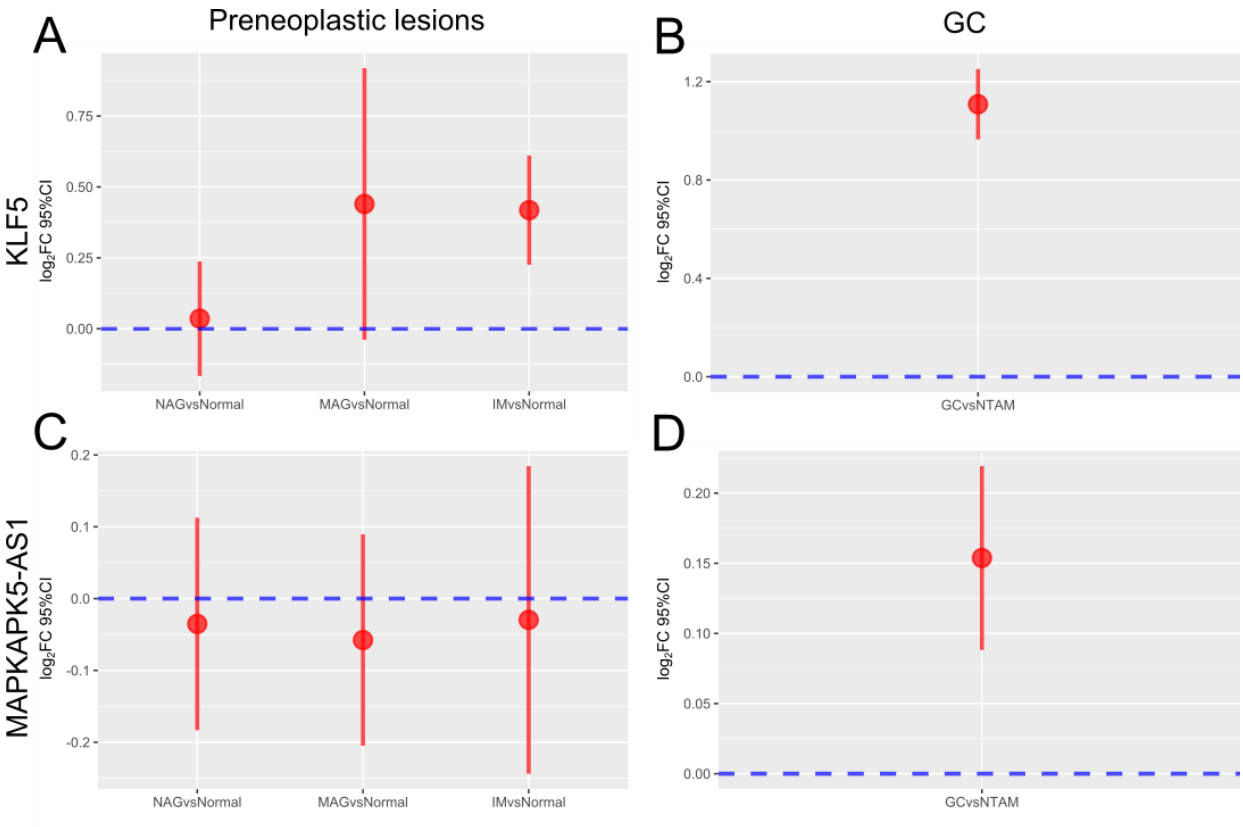

Figure 14. Meta-analysis results: KLF5 and MAPKAPK5-AS1 expression profiles in preneoplastic lesions and gastric cancer. A-B KLF5 increases significantly in IM compared with normal tissues (IMvsNormal contrast; logFC 0.42, *P-value* = 2.07E-05) and in GC compared with non-tumor adjacent mucosa (GCvsNTAM contrast; summary logFC 1.11, *P-value* = 4.54E-52). **C-D** MAPKAPK5-AS1 only increases in GC compared with NTAM (logFC 0.15, *P-value* = 4.22E-6). Blue dashed line indicates the baseline for each contrast.

3. **To identify significant KLF5-dependent lncRNA ceRNA interactions in gastric cancer.**

3.1. MAPKAPK5-AS1 acts as a ceRNA and enhances the expression of genes involved in DNA repair and cellular proliferation by sponging miRNAs miR-34a, let-7i and miR-424 in GC:

To determine the participation of MAPKAPK5-AS1 in ceRNA networks in GC, we generated the complete GC ceRNA network using SPONGE, as described in the methods section. Next, we generated a subnetwork specific to this lncRNA and its cognate miRNAs and ceRNA interactions (Table 4). This subnetwork was visualized in Cytoscape (Figure 15A). MAPKAPK5-AS1 establishes ceRNA interactions with 22 different genes, sharing 3 miRNAs: miR-34a, let7i and miR-424. Twenty of the genes from this ceRNA subnetwork are differentially expressed in GC (Figure 14A and Table 5). We subsequently performed overrepresentation analysis on all genes from this ceRNA using BiNGO and Annotation Map Cytoscape plugins (Figure 15B). Enriched GO terms from this analysis can be subclassified into 2 categories: DNA repair (DNA repair, recombinational repair, double-strand break repair via homologous recombination and response to ionizing radiation) and cell proliferation (cell cycle, cell cycle phase, cell cycle process, chromosome organization and mitotic cell cycle). Taken together, we conclude that MAPKAPK5-AS1, a lncRNA regulated by KLF5, acts as a miRNA sponge to promote cellular division.

3.2. MAPKAPK5-AS1 is part of a larger ceRNA network regulating cell proliferation and DNA repair:

Previous results showed that, aside from MAPKAPK5-AS1, 77 additional lncRNAs were influenced by KLF5 perturbations (these lncRNAs were significantly downregulated in 3 GC cell lines upon KLF5 knockdown). Seven of these lncRNAs may be transcriptionally regulated by KLF5 (peaks within 10 Kb from TSS), 5 of which are currently annotated: LINC002481, TOB1-AS1, PCOLCE-AS1, LINC00313 and PAX8-AS1. None of these lncRNAs act as significant ceRNAs in GC.

To thoroughly examine ceRNA networks that may be influenced by lncRNAs downstream from KLF5, we queried the generated ceRNA network with 77 lncRNAs which promoters were not bound by KLF5 but that were downregulated in siKLF5 condition. We found that six of these

indirectly regulated lncRNAs established significant ceRNA interactions in GC (P-adj < 0.05): SNHG1, SNHG15, SNHG3, SNHG7, SNHG17 and MIRLET7BHG.

The remaining 70 lncRNAs which were not directly regulated by KLF5 binding to their promoter regions were queried in the generated global GC ceRNA network, where we found that 6 additional lncRNAs act as significant ceRNAs: SNHG1, SNHG3, SNHG7, SNHG15, SNHG17 and MIRLET7BHG. Collectively, including MAPKAPK5-AS1, these lncRNAs have the potential to sponge a total of 55 miRNAs regulating 308 mRNAs (Figure 15B). Remarkably, this large network showed a striking functional overlap with the smaller MAPKAPK5-AS1 individual network; as the enriched GO terms resulting from this analysis once again mapped to 2 major clusters: One involved in DNA repair and the other involved in cellular proliferation (Figure 15D).

Table 4. MAPKAPK5-AS1 ceRNA interactions in gastric cancer.

ceRNA pair		shared miRNAs	cor	pcor	mscor	P-val	P-adj
MAPKAPK5-AS1	**CDCA8**	let-7i	0.365	0.248	0.117	0.004	0.042
MAPKAPK5-AS1	**CNOT11**	let-7i	0.357	0.231	0.126	0.002	0.034
MAPKAPK5-AS1	**CMTM8**	let-7i	0.431	0.318	0.112	0.004	0.047
MAPKAPK5-AS1	**BLM**	let-7i, miR-34a	0.239	0.127	0.113	0.002	0.017
MAPKAPK5-AS1	**E2F3**	let-7i, miR-34a	0.148	0.012	0.136	0.000	0.006
MAPKAPK5-AS1	**NR6A1**	let-7i, miR-34a	0.172	0.055	0.118	0.001	0.014
MAPKAPK5-AS1	**PVR**	let-7i, miR-34a	0.111	0.012	0.099	0.004	0.028
MAPKAPK5-AS1	**CUL2**	let-7i, miR-424	0.171	0.076	0.094	0.006	0.032
MAPKAPK5-AS1	**MOCS3**	let-7i, miR-34a	0.132	0.013	0.119	0.001	0.013
MAPKAPK5-AS1	**SBNO1**	let-7i, miR-424	0.202	0.109	0.093	0.006	0.034
MAPKAPK5-AS1	**CHD7**	let-7i, miR-34a	0.211	0.090	0.121	0.001	0.012
MAPKAPK5-AS1	**WNK2**	let-7i, miR-34a	0.143	0.054	0.089	0.008	0.039
MAPKAPK5-AS1	**C17orf100**	let-7i, miR-34a	0.132	0.017	0.115	0.002	0.015
MAPKAPK5-AS1	**MEN1**	let-7i, miR-34a	0.270	0.155	0.115	0.002	0.012
MAPKAPK5-AS1	**AURKA**	let-7i, miR-34a	0.302	0.175	0.127	0.001	0.008
MAPKAPK5-AS1	**TOP2A**	let-7i, miR-34a	0.341	0.212	0.129	0.001	0.007
MAPKAPK5-AS1	**GPSM2**	let-7i, miR-34a	0.283	0.179	0.103	0.004	0.019
MAPKAPK5-AS1	**HSPA14**	let-7i, miR-424	0.321	0.223	0.099	0.005	0.021
MAPKAPK5-AS1	**TRIB3**	let-7i, miR-34a	0.292	0.204	0.088	0.009	0.031
MAPKAPK5-AS1	**SPRYD4**	let-7i, miR-34a	0.307	0.190	0.116	0.002	0.012
MAPKAPK5-AS1	**CENPA**	let-7i, miR-34a	0.357	0.250	0.107	0.002	0.008
MAPKAPK5-AS1	**RAD54B**	let-7i, miR-34a	0.395	0.291	0.104	0.003	0.009

cor: Correlation; pcor: partial correlation; mscor: multiple miRNA sensitivity correlation; P-adj: adjusted *P-value* (FDR).

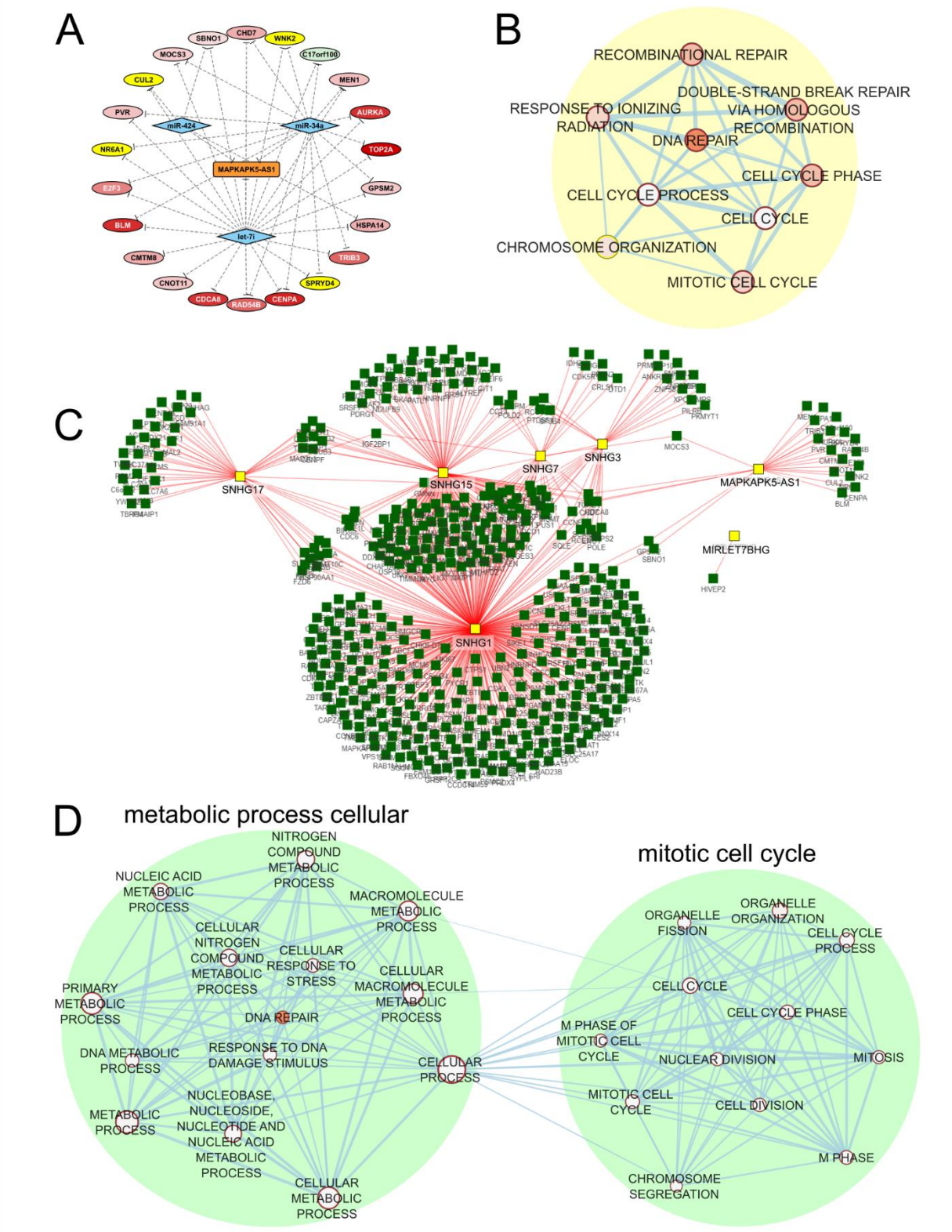

Figure 15. MAPKAPK5-AS1 binds to multiple miRNAs and is part of a ceRNA network regulating DNA repair and cell proliferation. A MAPKAPK5-AS1 significant interactions in GC. mRNAs are shown as ellipses, miRNAs as blue diamonds and MAPKAPK5 as an orange rectangle at the center of the network. Significantly upregulated genes in GC compared to adjacent non-tumor tissues are shown in red; downregulated genes are shown in green; non-differentially expressed genes are shown in yellow. **B** Enriched GO terms from the network in **A** (biological

process). **C** Integrated ceRNA network of 7 lncRNAs downstream from KLF5: MAPKAPK5-AS1, SNHG1, SNHG3, SNHG7, SNHG15, SNHG17 and MIRLET7BHG. lncRNAs are shown in yellow. miRNAs from the network were omitted to simplify the representation. **D** Enriched GO terms from the network in **C** (biological process). All network representations were performed using Cytoscape. Functional enrichments were performed using Cytoscape plugin BiNGO and network visualization of GO terms was performed as implemented in Cytoscape plugins Enrichment Map and AutoAnnotate.

Table 5. Meta-analysis results (gastric cancer vs non-tumor adjacent mucosa) for genes from MAPKAPK5-AS1 ceRNA network.

Gene	LFC	CI (lower limit)	CI (upper limit)	P-val
MAPKAPK5-AS1	0.154	0.088	0.219	4.22E-06
CDCA8	1.684	1.376	1.992	7.52E-27
CNOT11	0.454	0.417	0.490	5.04E-132
CMTM8	0.680	0.451	0.909	5.60E-09
BLM	1.735	1.296	2.175	1.01E-14
E2F3	1.025	0.786	1.264	4.58E-17
NR6A1	0.675	-0.348	1.697	1.96E-01
PVR	0.498	0.198	0.798	1.13E-03
CUL2	0.140	-0.087	0.368	2.27E-01
MOCS3	0.389	0.267	0.511	3.60E-10
SBNO1	0.282	0.089	0.475	4.22E-03
CHD7	0.660	0.302	1.017	3.00E-04
WNK2	-0.159	-0.398	0.079	1.90E-01
C17orf100	-0.362	-0.593	-0.131	2.10E-03
MEN1	0.511	0.478	0.544	7.81E-201
AURKA	1.705	1.319	2.092	5.42E-18
TOP2A	2.105	1.423	2.787	1.46E-09
GPSM2	0.440	0.214	0.665	1.33E-04
HSPA14	0.651	0.545	0.757	2.54E-33
TRIB3	1.263	0.783	1.742	2.48E-07
SPRYD4	-0.014	-0.323	0.294	9.27E-01
CENPA	1.826	1.272	2.380	1.03E-10
RAD54B	1.288	0.569	2.007	4.48E-04

CI: 95% confidence interval. LFC: Integrated log2 fold-change.

3.3. lncRNAs SNHG1, SNHG3, SNHG15 and SNHG17 increase in GC:

As previously mentioned, 6 lncRNAs downstream from KLF5 are significant ceRNAs in GC: SNHG1, SNHG3, SNHG7, SNHG15, SNHG17 and MIRLET7BHG. To evaluate the expression changes of these lncRNAs throughout Correa's gastric precancerous cascade and GC, we interrogated the results from our meta-analysis (Table 6).

Most small nucleolar host genes from this group (SNHG1, SNHG3, SNHG15 and SNHG17) are significantly upregulated in GC tissues compared with non-tumor adjacent mucosa samples

(Figures 16B and 17B). Additionally, 2 of these genes increase significantly in at least one of the preneoplastic stages of the disease: SNHG1 (NAG and MAG vs normal) and SNHG3 (IM vs normal; Table 6 and Figure 16). Although not statistically significant, SNHG17 shows an increasing trend in preneoplastic stages and is significantly increased in GC (Table 6 and Figure 17). Conversely, the expression levels of the let7b miRNA cluster gene (MIRLET7BHG) is consistently downregulated in preneoplastic lesions and in GC (Figure 17B). No significant changes or trends were observed for SNHG7.

Table 6. Expression profiling of SNHG1, SNHG3, SNHG7, SNHG15, SNHG17 and MIRLET7BHG throughout Correa's gastric precancerous cascade and gastric cancer.

	NAG vs Normal		MAG vs Normal		IM vs Normal		GC vs NTAM	
	LFC	**P-val**	**LFC**	**P-val**	**LFC**	**P-val**	**LFC**	**P-val**
SNHG1	***0.423***	***3.71E-03***	***0.298***	***3.80E-02***	0.163	1.74E-01	***0.821***	***3.00E-04***
SNHG3	0.367	2.21E-01	0.426	7.49E-02	***0.478***	***1.05E-03***	**0.727**	**1.59E-07**
SNHG7	0.092	6.39E-01	0.027	8.89E-01	0.101	2.48E-01	0.030	7.63E-01
SNHG15	0.238	3.29E-01	0.377	2.54E-01	0.032	7.76E-01	***0.711***	***6.30E-123***
SNHG17	0.207	2.09E-01	0.090	7.06E-01	0.227	5.65E-02	***0.747***	***1.87E-157***
MIRLET7BHG	***-0.244***	***2.77E-03***	***-0.296***	***2.55E-04***	***-0.391***	***3.46E-03***	***-0.185***	***2.91E-06***

LFC: Integrated log2 fold-change; NAG: Non-atrophic gastritis; MAG: Multifocal atrophic gastritis; IM: Intestinal metaplasia; GC: Gastric cancer; NTAM: Non-tumor adjacent mucosa. Significant results are highlighted in bold italic characters.

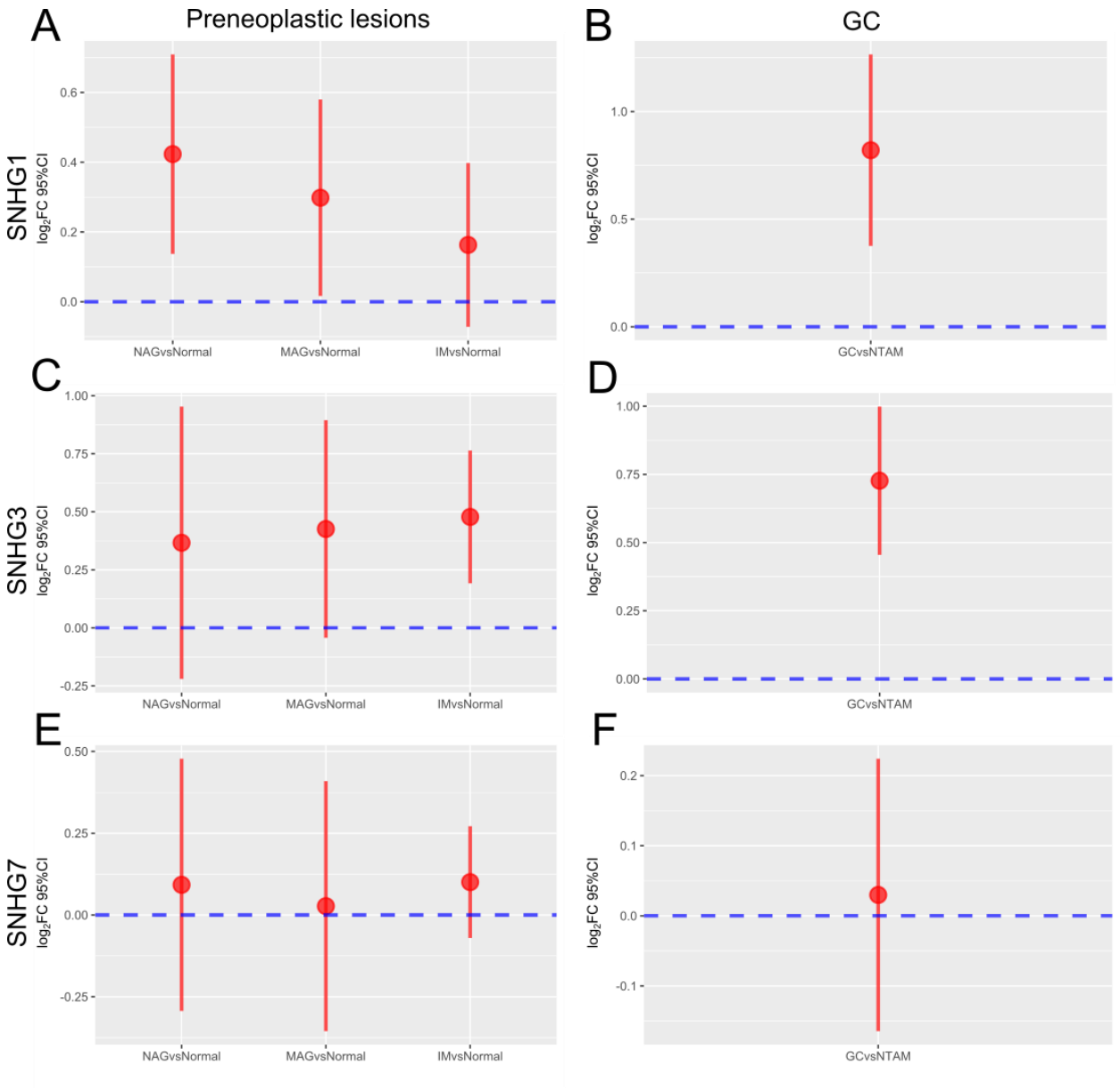

Figure 16. Meta-analysis results: SNHG1, SNHG3 and SNHG7 expression profiles in preneoplastic lesions and gastric cancer. A-B SNHG1 increases significantly in NAG and MAG compared with normal tissues (NAGvsNormal and MAGvsNormal contrasts) and in GC compared with non-tumor adjacent mucosa (GCvsNTAM contrast. **C-D** SNHG3 increases significantly in IM compared with normal gastric tissues (IMvsNormal contrast), as well as in GC compared with NTAM. **E-F** SNHG7 does not change significantly in any of the contrasts. Blue dashed line indicates the baseline for each contrast.

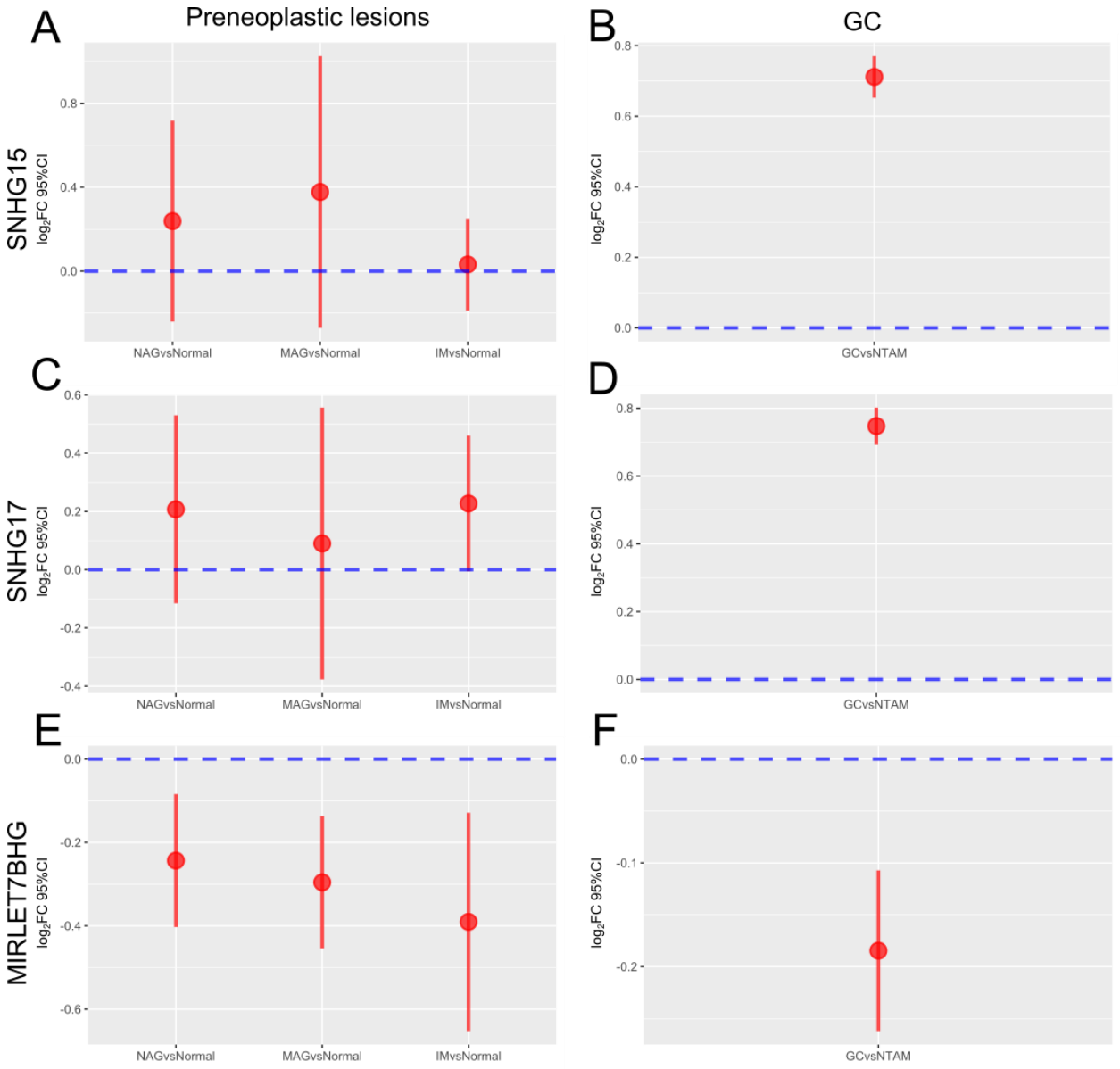

Figure 17. Meta-analysis results: SNHG15, SNHG17 and MIRLET7BHG expression profiles in preneoplastic lesions and gastric cancer. A-D SNHG15 and SNHG17 increase significantly only in GC compared with non-tumor adjacent mucosa (GCvsNTAM contrast). **E-F** MIRLET7BHG is consistently downregulated in all the represented contrasts. Blue dashed line indicates the baseline for each contrast.

DISCUSSION

1. KLF5, gastric stem cells and Correa's gastric precancerous cascade

Multiple cellular processes lead to the malignant transformation of gastric epithelial into malignant tumor cells throughout the progression of Correa's gastric precancerous cascade. There exists general consensus regarding the lack of knowledge fueling the progression of premalignant lesions to invasive cancer[182,183]. To tackle this issue, we integrated multiple expression microarray experiments representing different steps of the gastric precancerous cascade by a random-effects meta-analysis approach, together with co-expression analysis of an agnostic set of genes associated with stem cell biology and progression of premalignant stages.

To our knowledge, ours is the first study to integrate multiple transcriptomic experiments to recapitulate the different steps of Correa's cascade by a meta-analysis approach using only open access data. As a by-product of our work, we have established this meta-analysis as a reference database to search for gene perturbations across the different contrasts generated in gastric preneoplasia. One of the strengths of this new database is that all gene identifiers from each microarray and RNA-sequencing experiment have been updated to the latest version available, thus making the results more reproducible between datasets. Although this approach is a significant improvement compared to the native status of the annotations, there are still some limitations regarding the original mapping quality of the microarray probes. A recent study by De Lima *et al.*[161] showed that many microarray probes have been misannotated by the original manufacturer of the platform or map to multiple genomic regions. Therefore, a more precise approach to this issue would be to re-map the complete platforms using the probe sequences against the reference genome. We plan on updating our reference database by adding this step in the future. This approach may be applicable to other cancers with long-standing preneoplastic processes, as well as diseases with pre-clinical presentations.

Secondly, given as our primary interest was to describe the expression profiles of specific genes in gastric preneoplasia and cancer tissues, we performed co-expression analysis on this particular set of genes instead of generating a consensus network as implemented in weighted gene co-expression network analysis[184]. Results from this co-expression analysis do not, therefore,

constitute different modules *per se*, but rather small sets of co-expressed genes. This issue may be re-addressed in future studies.

Results from our meta-analysis and co-expression analysis strongly suggest that KLF5, a pluripotency factor, increases significantly in IM and in GC together with i) gastric stem cell marker Vil1, ii) intestinal transcription factors CDX1 and CDX2, iii) β-catenin (CTNNB1), and iv) markers of IM such as OLFM4, TFF3 and CFTR. Our findings are consistent with previous reports stating that that KLF5 increases early in the gastric precancerous process following infection by *H. pylori*[140]. Similarly, CDX1, CDX2, VIL1, and CTNNB1 are known to be induced by *H. pylori* by different mechanisms[133,185,186]. Furthermore, CTNNB1 is the canonical Wnt signaling pathway transcription factor that regulates the expression of CDX1[82,83]. In turn, CDX1 regulates the expression of KLF5, favoring gastric to intestinal transdifferentiation in IM[73]. The remaining genes from this transcriptomic signature – VIL1, TFF3 and CFTR – increase at this stage of the preneoplastic process[147,187,188]. Therefore, this gene set associated to KLF5 by co-expression analysis recapitulates previous reports and the natural history of the cascade.

2. KLF5 and lncRNAs

KLF5 is frequently amplified in GC[189–192] and is known to be a relevant transcription factor in the development and progression of the disease[95,98,99]. Recent studies have shown that KLF5 contributes to various human cancers by regulating the expression of lncRNAs that promote cell growth and invasion[116,117,193]. Therefore, we explored lncRNAs downstream from this transcription factor by ChIP-seq coupled to transcriptome expression profiling by microarray in control and KLF5 knockdown condition.

We found that KLF5 directly binds to lncRNA MAPKAPK5-AS1 promoter region and likely regulates its expression in gastric cells. MAPKAPK5-AS1 is a lncRNA that has previously been shown to establish ceRNA interactions in hepatocellular cell carcinoma[194] and lung cancer[195], and is involved in the progression of colorectal cancer by downregulation of tumor suppressor p21[196] and proposed as a prognostic biomarker for glioma[197,198].

Additionally, KLF5 had a significant effect on the expression levels of 6 other lncRNAs: SNHG1, SNHG3, SNHG7, SNHG15, SNHG17 and MIRLET7BHG. These genes are dysregulated in multiple human cancers, including GC. Curiously, all lncRNAs from this set of lncRNAs that belong to the small nucleolar host gene family (SNHG) have been associated to increased cell proliferation, invasion and migration[199–206]. Additionally, a recently published article has shown that SNHG17 is induced by *H. pylori* at early stages of the gastric precancerous cascade and shifts the DNA repair machinery towards non-homologous end joining[207], a process that favors chromosome instability and may promote malignant transformation at later stages. On the other hand, MIRLET7BHG corresponds to the gene cluster that contains miR-let7b. Its role as a lncRNA is unexplored.

KLF5 ChIP-seq analysis in GC cells showed no peaks within 10 Kb upstream from the TSS of these lncRNAs, but a recent study has shown that multiple lncRNAs are regulated by super-enhancers and can be activated by KLF5 binding to these regions using esophageal squamous cell carcinoma as a model[193]. We propose that some of these lncRNAs may be regulated by KLF5 through this mechanism, but further research is warranted to validate this claim.

3. lncRNAs MAPKAPK5-AS1, SNHG1, SNHG3, SNHG7, SNHG15, SNHG17 and MIRLET7BHG in ceRNA interactions in GC

We developed a bioinformatics pipeline that allowed us to discover lncRNAs downstream from KLF5, which served to contextualize and circumscribe lncRNAs within a biological setting associated to gastric stem cell biology and intestinal metaplasia. Next, we generated a ceRNA network in GC. A key step in the generation of this main GC ceRNA network was the establishment of a formal collaboration with Allan Peñaloza (M.Sc.) from Vinicius' lab at Universidad de Chile, who integrated predictive and validated miRNA:target interactions from multiple databases into a reference global miRNA:target interaction catalog that included both coding and noncoding RNAs as targets. These efforts included re-annotation of multiple miRNAs and their targets, removal of redundancy between different databases and retaining only high

confidence computationally predicted interactions that were present in, at least, 3 different datasets. This approach resulted in a global miRNA:target matrix comprising over 100 million miRNA:target interactions that were used to run an elastic net regression as implemented in SPONGE[163].

The SPONGE algorithm identified over 150000 significant ceRNA interactions between genes (both coding and non-coding) sharing at least 1 miRNA in GC (*P-adj* < 0.05, FDR Benjamini-Hochberg method[154]). Subsequently, lncRNAs downstream from KLF5 were used to subset these significant ceRNA interactions. Such an approach resulted in the discovery of a set of 7 lncRNAs that were engaged in significant ceRNA pairs in GC: MAPKAPK5-AS1, SNHG1, SNHG3, SNHG7, SNHG15, SNHG17 and MIRLET7BHG. Only MAPKAPK5-AS1 is transcriptionally regulated by KLF5. To establish the functionality of these ceRNA interactions, we generated 2 subnetworks: the first, specific to MAPKAPK5-AS1; the second included the 7 lncRNAs.

The individual MAPKAPK5-AS1 ceRNA network includes miRNAs miR-34a, let-7i and miR-424, and 22 protein-coding genes; 17 of which are significantly upregulated in GC vs NTAM and only 1 downregulated. The remaining 4 genes are not differentially expressed in this contrast from the meta-analysis. Functional enrichment analysis of the resulting subnetwork showed that MAPKAPK5-AS1 sponges miRNAs regulating genes involved in mitotic cell cycle and the DNA damage response; 2 biological processes that are associated with the cancer stem cell phenotype[208]. In fact, 2 different studies have shown that expression of MAPKAPK5-AS1 is associated with cell proliferation. The first showed that MAPKAPK5-AS1 is directly related with tumor size in lung cancer, and knockdown of this lncRNA not only reduces cell proliferation but also increases apoptosis *in vitro*[196]. The second study showed that knockdown of MAPKAPK5-AS1 in colorectal cancer cells reduces colony formation, suppresses cell proliferation and increases apoptosis *in vitro*[195]. These experiments should also be performed using GC cells in the future.

Strikingly, the small MAPKAPK5-AS1 ceRNA subnetwork shows a remarkable functional overlap with the larger subnetwork generated using ceRNA interactions established by the 7 lncRNAs altogether. MAPKAPK5-AS1, SNHG1, SNHG3, SNHG7, SNHG15, SNHG17 and MIRLET7BHG collectively alter the expression of genes that belong to the DNA damage response and promote

mitotic cell cycle by establishment of a ceRNA network encompassing 477 protein- and nonprotein-coding genes and 43 miRNAs.

Consistent with literature reports on MAPKAPK5-AS1, all SNHG from this group have been found to increase cell proliferation and invasion in GC[199–206]. Additionally, the DNA damage response has some unique features in cancer cells, which are intimately linked to cancer stem cell properties including DNA repair activity and cancer-stem cell survival after exposure to ionizing radiation[208]. In fact, the DNA damage response has become an attractive target in cancer[209]. Therefore, we propose that this ceRNA network not only promotes gastric cancer progression by positively regulating cell proliferation, but also by altering the DNA damage response. In line with the latter claim, a remarkable paper has recently been published in which the authors show that SNHG17, a member of this ceRNA network, is upregulated in response to *H. pylori* infection at early stages of gastric preneoplasia[207]. SNHG17 contributes to genomic instability by shifting the balance of the DNA damage response following double strand break; specifically, by favoring non-homologous end joining. This was shown to occur by 2 distinct mechanisms. The first, by recruiting NONO (also known as P54 or NRB), which is involved in non-homologous end joining[210]. The second mechanism is by acting as a ceRNA that sponges miR-3909, thus favoring translation of its target gene RING1, a ubiquitin ligase that marks RAD51 for proteasomal degradation[211].

4. Strengths, limitations and future perspectives of the study

The work herein presented is, to the best of our knowledge, the first to provide a reference database for the interrogation of transcriptome-wide changes during the progression of Correa's cascade. Heretofore, most studies on lncRNA ceRNA interactions have focused on individual lncRNAs in cancer, in absence of additional biological context. This study presents a comprehensive analysis of KLF5-mediated lncRNAs in ceRNA networks in GC, including the expression profiles of these lncRNAs during precancerous stages. The involvement of these lncRNAs as ceRNAs expands on previous knowledge regarding the role of KLF5 as an oncogene, that act by promoting cell proliferation and affecting DNA repair. Moreover, our study implements state-of-the-art methods to incorporate both miRNA and target expression levels

into the models that predict potential interactions between both types of transcripts, based on a global miRNA:target interaction catalog recently generated by our collaborators.

On the other hand, the limitations of this study must be mentioned. The principal pitfall of this study is the lack of experimental validation of the proposed miRNA:target interactions. Due to the high dimensionality of the networks presented in this work, it becomes unfeasible to perform conventional validation methods (such as luciferase reporter assay) for all the proposed miRNA:target interactions. Instead, we propose that high-throughput *in vitro* approaches should be considered, such as massively parallel reporter assays (MPRA) that have recently proven their use for the characterization of RNA degradation dynamics[212] and miRNA-mediated post-transcriptional regulation of gene expression[213]. Although MPRA is an appealing alternative for validation of multiple miRNA:target interactions, these techniques raise additional difficulties due to the high cost of implementation and lack of expertise in our local setting. A partial solution to this problem would be to perform *in vitro* studies in conditions showing high and low expression levels of lncRNAs MAPKAPK5-AS1, SNHG1, SNHG3, SNHG7, SNHG15, SNHG17 and MIRLET7BHG. Proliferation assays, as well as integrated transcriptomic and proteomic profiling, would provide further proof of the proposed mechanisms. Future studies are also warranted to confirm the effects of these lncRNAs and their cognate ceRNA network on genome stability; including DNA sequencing to detect point mutations and structural rearrangements, and copy number variation assays.

Future perspectives of this study include the generation of an online database for users to perform personalized queries using this database and visualize the results from each contrast. We believe that these findings will provide further mechanistic insights to aid in the discovery of potential biomarkers and therapeutic targets for the timely diagnosis and opportune treatment of this malignancy.

REFERENCES

1. Bray, F. *et al.* Global cancer statistics 2018: GLOBOCAN estimates of incidence and mortality worldwide for 36 cancers in 185 countries. *CA. Cancer J. Clin.* **68**, 394–424 (2018).
2. Ferlay, J. *et al.* Estimating the global cancer incidence and mortality in 2018: GLOBOCAN sources and methods. *Int. J. Cancer* 1–13 (2018) doi:10.1002/ijc.31937.
3. Ang, T. L. & Fock, K. M. Clinical epidemiology of gastric cancer. *Singapore Med. J.* **55**, 621–628 (2014).
4. Ferlay, J. *et al.* Cancer incidence and mortality worldwide: Sources, methods and major patterns in GLOBOCAN 2012. *Int. J. Cancer* **136**, E359–E386 (2015).
5. Torre, L. A. *et al.* Global Cancer Statistics, 2012. *CA a cancer J. Clin.* **65**, 87–108 (2015).
6. Siegel, R. L., Miller, K. D. & Jemal, A. Cancer statistics. *CA Cancer J Clin* **66**, 7–30 (2016).
7. Jimenez De La Jara, J. *et al.* A snapshot of cancer in Chile: Analytical frameworks for developing a cancer policy. *Biol. Res.* **48**, 1–15 (2015).
8. Liu, H. S. & Xiao, H. S. MicroRNAs as potential biomarkers for gastric cancer. *World J. Gastroenterol.* **20**, 12007–12017 (2014).
9. Van Cutsem, E., Sagaert, X., Topal, B., Haustermans, K. & Prenen, H. Gastric cancer. *Lancet* **388**, 2654–2664 (2016).
10. Laurén, P. The two histological main types of gastric carcinoma:diffuse and so-called intestinal-type carcinoma. *Acta path.et microbiol.scandinav* **64**, 31–49 (1965).
11. Berlth, F., Bollschweiler, E., Drebber, U., Hoelscher, A. H. & Moenig, S. Pathohistological classification systems in gastric cancer: Diagnostic relevance and prognostic value. *World J. Gastroenterol.* **20**, 5679–5684 (2014).
12. Hu, B. *et al.* Gastric cancer: Classification, histology and application of molecular pathology. *J. Gastrointest. Oncol.* **3**, 251–261 (2012).
13. Network, T. C. G. A. R. Comprehensive molecular characterization of gastric adenocarcinoma. *Nature* **513**, 202–209 (2014).
14. Correa, P. & Piazuelo, M. B. The gastric precancerous cascade. *J. Dig. Dis.* **13**, 2–9 (2012).

15. Rugge, M., Capelle, L. G. & Fassan, M. Individual risk stratification of gastric cancer: Evolving concepts and their impact on clinical practice. *Best Pract. Res. Clin. Gastroenterol.* **28**, 1043–1053 (2014).
16. Stairs, D. B., Kong, J. & Lynch, J. P. Cdx Genes, Inflammation, and the Pathogenesis of Intestinal Metaplasia. in 231–270 (2010). doi:10.1016/B978-0-12-381280-3.00010-5.
17. Correa, P., Piazuelo, B. M. & Wilson, K. T. Pathology of Gastric Intestinal Metaplasia: Clinical Implications. *Am. J. Gastroenterol.* **105**, 493–498 (2010).
18. Mera, R. M. *et al.* Dynamics of Helicobacter pylori infection as a determinant of progression of gastric precancerous lesions: 16-year follow-up of an eradication trial. *Gut* **67**, 1239–1246 (2018).
19. Mills, J. C. & Sansom, O. J. Reserve stem cells: Differentiated cells reprogram to fuel repair, metaplasia, and neoplasia in the adult gastrointestinal tract. *Sci. Signal.* **8**, 1–15 (2015).
20. Sáenz, J. B. & Mills, J. C. Acid and the basis for cellular plasticity and reprogramming in gastric repair and cancer. *Nat. Rev. Gastroenterol. Hepatol.* **15**, 257–273 (2018).
21. Amieva, M. & Peek, R. M. Pathobiology of Helicobacter pylori-Induced Gastric Cancer. *Gastroenterology* **150**, 64–78 (2016).
22. Berger, H. *et al.* Gastric cancer pathogenesis. *Helicobacter* **21**, 34–38 (2016).
23. Carrasco-Avino, G. *et al.* The conundrum of the Epstein-Barr virus-associated gastric carcinoma in the Americas. *Oncotarget* **8**, 75687–75698 (2017).
24. Polakovicova, I. *et al.* Role of microRNAs and Exosomes in Helicobacter pylori and Epstein-Barr Virus Associated Gastric Cancers. *Front. Microbiol.* **9**, 636 (2018).
25. Oliveira, C., Pinheiro, H., Figueiredo, J., Seruca, R. & Carneiro, F. Familial gastric cancer: Genetic susceptibility, pathology, and implications for management. *Lancet Oncol.* **16**, e60–e70 (2015).
26. Plummer, M. *et al.* Global burden of cancers attributable to infections in 2012: a synthetic analysis. *Lancet Glob. Heal.* **4**, e609–e616 (2016).
27. Moodley, Y. *et al.* Age of the association between Helicobacter pylori and man. *PLoS Pathog.* **8**, (2012).

28. Kodaman, N., Sobota, R. S., Mera, R., Schneider, B. G. & Williams, S. M. Disrupted human-pathogen co-evolution: A model for disease. *Front. Genet.* **5**, 1–12 (2014).
29. Kodaman, N. *et al.* Human and Helicobacter pylori coevolution shapes the risk of gastric disease. *Proc. Natl. Acad. Sci.* **111**, 1455–1460 (2014).
30. Odenbreit, S. *et al.* Outer membrane protein expression profile in Helicobacter pylori clinical isolates. *Infect. Immun.* **77**, 3782–3790 (2009).
31. Radin, J. N., González-Rivera, C., Ivie, S. E., McClain, M. S. & Cover, T. L. Helicobacter pylori VacA induces programmed necrosis in gastric epithelial cells. *Infect. Immun.* **79**, 2535–2543 (2011).
32. Ding, S.-Z. & Zheng, P.-Y. Helicobacter pylori infection induced gastric cancer; advance in gastric stem cell research and the remaining challenges. *Gut Pathog.* **4**, 18 (2012).
33. Neal, J. T., Peterson, T. S., Kent, M. L. & Guillemin, K. H. pylori virulence factor CagA increases intestinal cell proliferation by Wnt pathway activation in a transgenic zebrafish model. *Dis. Model. Mech.* **6**, 802–810 (2013).
34. Ohnishi, N. *et al.* Transgenic expression of Helicobacter pylori CagA induces gastrointestinal and hematopoietic neoplasms in mouse. *Proc. Natl. Acad. Sci.* **105**, 1003–1008 (2008).
35. Gagnaire, A., Nadel, B., Raoult, D., Neefjes, J. & Gorvel, J. P. Collateral damage: Insights into bacterial mechanisms that predispose host cells to cancer. *Nat. Rev. Microbiol.* **15**, 1–20 (2017).
36. Wei, J. *et al.* Bacterial CagA protein induces degradation of p53 protein in a p14ARF-dependent manner. *Gut* **64**, 1040–1048 (2015).
37. Sigal, M. *et al.* Helicobacter pylori activates and expands Lgr5^{+} stem cells through direct colonization of the gastric glands. *Gastroenterology* **148**, 1392-1404.e21 (2015).
38. Uehara, T. *et al.* H. pylori infection is associated with DNA damage of Lgr5-positive epithelial stem cells in the stomach of patients with gastric cancer. *Dig. Dis. Sci.* **58**, 140–149 (2013).
39. Aloia, L., McKie, M. A. & Huch, M. Cellular plasticity in the adult liver and stomach. *J. Physiol.* **594**, 4815–4825 (2016).

40. Zhao, Y., Feng, F. & Zhou, Y.-N. Stem cells in gastric cancer. *World J. Gastroenterol.* **21**, 112 (2015).
41. Bartfeld, S. & Koo, B. K. Adult gastric stem cells and their niches. *Wiley Interdiscip. Rev. Dev. Biol.* **6**, 1–12 (2017).
42. Braunstein, E. M. *et al.* Villin: A marker for development of the epithelial pyloric border. *Dev. Dyn.* **224**, 90–102 (2002).
43. Qiao, X. T. *et al.* Prospective Identification of a Multilineage Progenitor in Murine Stomach Epithelium. *Gastroenterology* **133**, 1989–1998 (2007).
44. Arnold, K. *et al.* Sox2 + adult stem and progenitor cells are important for tissue regeneration and survival of mice. *Cell Stem Cell* **9**, 317–329 (2011).
45. Hayakawa, Y. *et al.* CCK2R identifies and regulates gastric antral stem cell states and carcinogenesis. *Gut* **64**, 544–553 (2015).
46. Tomkova, K. *et al.* The gastrin gene promoter is regulated by p73 isoforms in tumor cells. *Oncogene* **25**, 6032–6036 (2006).
47. Carrasco, G. *et al.* Overexpression of p73 as a tissue marker for high-risk gastritis. *Clin. Cancer Res.* **16**, 3253–3259 (2010).
48. de Lau, W. *et al.* Lgr5 homologues associate with Wnt receptors and mediate R-spondin signalling. *Nature* **476**, 293–7 (2011).
49. Barker, N. *et al.* Lgr5+veStem Cells Drive Self-Renewal in the Stomach and Build Long-Lived Gastric Units In Vitro. *Cell Stem Cell* **6**, 25–36 (2010).
50. Leushacke, M. *et al.* Lgr5-expressing chief cells drive epithelial regeneration and cancer in the oxyntic stomach. *Nat. Cell Biol.* **19**, 774–786 (2017).
51. Hayakawa, Y. *et al.* Mist1 Expressing Gastric Stem Cells Maintain the Normal and Neoplastic Gastric Epithelium and Are Supported by a Perivascular Stem Cell Niche. *Cancer Cell* **28**, 800–814 (2015).
52. Karam, S. M. & Leblond, C. P. Dynamics of epithelial cells in the corpus of the mouse stomach. I. Identification of proliferative cell types and pinpointing of the stem cell. *Anat. Rec.* **236**, 259–79 (1993).
53. Varga, J. & Greten, F. R. Lifting the Mist on Gastric Stem Cells. *Cell Stem Cell* **18**, 7–9

(2016).

54. Matsuo, J. *et al.* Identification of Stem Cells in the Epithelium of the Stomach Corpus and Antrum of Mice. *Gastroenterology* **152**, 218-231.e14 (2017).
55. Stange, D. E. *et al.* Differentiated Troy+ chief cells act as reserve stem cells to generate all lineages of the stomach epithelium. *Cell* **155**, 357–368 (2013).
56. Leushacke, M., Ng, A., Galle, J., Loeffler, M. & Barker, N. Lgr5+Gastric Stem Cells Divide Symmetrically to Effect Epithelial Homeostasis in the Pylorus. *Cell Rep.* **5**, 349–356 (2013).
57. Flanagan, D. J., Austin, C. R., Vincan, E. & Phesse, T. J. Wnt signalling in gastrointestinal epithelial stem cells. *Genes (Basel).* **9**, (2018).
58. Kim, T.-H., Kim, B.-M., Mao, J., Rowan, S. & Shivdasani, R. A. Endodermal Hedgehog signals modulate Notch pathway activity in the developing digestive tract mesenchyme. *Development* **138**, 3225–3233 (2011).
59. Kim, T.-H. & Shivdasani, R. A. Notch signaling in stomach epithelial stem cell homeostasis. *J. Exp. Med.* **208**, 677–688 (2011).
60. Kim, B. M., Buchner, G., Miletich, I., Sharpe, P. T. & Shivdasani, R. A. The stomach mesenchymal transcription factor barx1 specifies gastric epithelial identity through inhibition of transient Wnt signaling. *Dev. Cell* **8**, 611–622 (2005).
61. Ramalho-Santos, M., Melton, D. A. & McMahon, A. P. Hedgehog signals regulate multiple aspects of gastrointestinal development. *Development* **127**, 2763–72 (2000).
62. Van den Brink, G. R. *et al.* Sonic hedgehog expression correlates with fundic gland differentiation in the adult gastrointestinal tract. *Gut* **51**, 628–633 (2002).
63. Nam, K. T. *et al.* Mature chief cells are cryptic progenitors for metaplasia in the stomach. *Gastroenterology* **139**, (2010).
64. Nozaki, K. *et al.* A molecular signature of gastric metaplasia arising in response to acute parietal cell loss. *Gastroenterology* **134**, 511–22 (2008).
65. Weis, V. G. *et al.* Maturity and age influence chief cell ability to transdifferentiate into metaplasia. *Am. J. Physiol. Gastrointest. Liver Physiol.* **312**, G67–G76 (2017).
66. Goldenring, J. R., Nam, K. T. & Mills, J. C. The origin of pre-neoplastic metaplasia in the

stomach: chief cells emerge from the Mist. *Exp. Cell Res.* **317**, 2759–64 (2011).

67. Yuan, D., Ma, Z., Tuo, B., Li, T. & Liu, X. Physiological Significance of Ion Transporters and Channels in the Stomach and Pathophysiological Relevance in Gastric Cancer. *Evid. Based. Complement. Alternat. Med.* **2020**, 2869138 (2020).
68. Burclaff, J., Willet, S. G., Sáenz, J. B. & Mills, J. C. Proliferation and Differentiation of Gastric Mucous Neck and Chief Cells During Homeostasis and Injury-induced Metaplasia. *Gastroenterology* **158**, 598-609.e5 (2020).
69. Silberg, D. G., Swain, G. P., Eun Ran Suh & Traber, P. G. Cdx1 and Cdx2 expression during intestinal development. *Gastroenterology* **119**, 961–971 (2000).
70. Hryniuk, A., Grainger, S., Savory, J. G. A. & Lohnes, D. Cdx function is required for maintenance of intestinal identity in the adult. *Dev. Biol.* **363**, 426–37 (2012).
71. Silberg, D. G. *et al.* Cdx2 ectopic expression induces gastric intestinal metaplasia in transgenic mice. *Gastroenterology* **122**, 689–696 (2002).
72. Mutoh, H. *et al.* Conversion of gastric mucosa to intestinal metaplasia in Cdx2-expressing transgenic mice. *Biochem. Biophys. Res. Commun.* **294**, 470–479 (2002).
73. Fujii, Y. *et al.* CDX1 confers intestinal phenotype on gastric epithelial cells via induction of stemness-associated reprogramming factors SALL4 and KLF5. *Proc. Natl. Acad. Sci. U. S. A.* **109**, 20584–20589 (2012).
74. Mutoh, H. *et al.* Cdx1 induced intestinal metaplasia in the transgenic mouse stomach: comparative study with Cdx2 transgenic mice. *Gut* **53**, 1416–23 (2004).
75. Bai, Y. Q. *et al.* Ectopic expression of homeodomain protein CDX2 in intestinal metaplasia and carcinomas of the stomach. *Cancer Lett.* **176**, 47–55 (2002).
76. Eda, A. *et al.* Expression of homeobox gene CDX2 precedes that of CDX1 during the progression of intestinal metaplasia. *J. Gastroenterol.* **37**, 94–100 (2002).
77. Mutoh, H., Hayakawa, H., Sakamoto, H., Sashikawa, M. & Sugano, K. Transgenic Cdx2 induces endogenous Cdx1 in intestinal metaplasia of Cdx2-transgenic mouse stomach. *FEBS J.* **276**, 5821–31 (2009).
78. Asano, N. *et al.* Cdx2 expression and intestinal metaplasia induced by H. Pylori infection of gastric cells is regulated by NOD1-Mediated innate immune responses. *Cancer Res.* **76**,

1135–1145 (2016).

79. Kim, S. *et al.* PTEN and TNF-α regulation of the intestinal-specific Cdx-2 homeobox gene through a PI3K, PKB/Akt, and NF-κB-dependent pathway. *Gastroenterology* **123**, 1163–1178 (2002).
80. Keates, S., Hitti, Y. S., Upton, M. & Kelly, C. P. Helicobacter pylori infection activates NF-κB in gastric epithelial cells. *Gastroenterology* **113**, 1099–1109 (1997).
81. Lamb, A. *et al. Helicobacter pylori* CagA activates NF-κB by targeting TAK1 for TRAF6-mediated Lys 63 ubiquitination. *EMBO Rep.* **10**, 1242–1249 (2009).
82. Pilon, N., Oh, K., Sylvestre, J.-R., Savory, J. G. A. & Lohnes, D. Wnt signaling is a key mediator of Cdx1 expression in vivo. *Development* **134**, 2315–2323 (2007).
83. Lickert, H. *et al.* Wnt/β-catenin signaling regulates the expression of the homeobox gene Cdx1 in embryonic intestine. *Development* **127**, 3805–3813 (2000).
84. Prinos, P. *et al.* Multiple pathways governing Cdx1 expression during murine development. *Dev. Biol.* **239**, 257–269 (2001).
85. Saitoh, T., Mine, T. & Katoh, M. Frequent up-regulation of WNT5A mRNA in primary gastric cancer. *Int. J. Mol. Med.* **9**, 515–9 (2002).
86. Kurayoshi, M. *et al.* Expression of Wnt-5a is correlated with aggressiveness of gastric cancer by stimulating cell migration and invasion. *Cancer Res.* **66**, 10439–10448 (2006).
87. Astudillo, P. Wnt5a Signaling in Gastric Cancer. *Frontiers in Cell and Developmental Biology* vol. 8 (2020).
88. Graham, D. Y. & Zou, W. Y. Guilt by association: intestinal metaplasia does not progress to gastric cancer. *Curr. Opin. Gastroenterol.* **34**, 458–464 (2018).
89. Huang, K. K. *et al.* Genomic and Epigenomic Profiling of High-Risk Intestinal Metaplasia Reveals Molecular Determinants of Progression to Gastric Cancer. *Cancer Cell* **33**, 137-150.e5 (2018).
90. Ema, M. *et al.* Krüppel-like factor 5 Is Essential for Blastocyst Development and the Normal Self-Renewal of Mouse ESCs. *Cell Stem Cell* **3**, 555–567 (2008).
91. Parisi, S. *et al.* Direct targets of Klf5 transcription factor contribute to the maintenance of mouse embryonic stem cell undifferentiated state. *BMC Biol.* **8**, 128 (2010).

92. Bourillot, P. Y. & Savatier, P. Krüppel-like transcription factors and control of pluripotency. *BMC Biology* vol. 8 (2010).
93. Jiang, J. *et al.* A core Klf circuitry regulates self-renewal of embryonic stem cells. *Nat. Cell Biol.* **10**, 353–360 (2008).
94. Hall, J. *et al.* Oct4 and LIF/Stat3 Additively Induce Krüppel Factors to Sustain Embryonic Stem Cell Self-Renewal. *Cell Stem Cell* **5**, 597–609 (2009).
95. Chia, N. Y. *et al.* Regulatory crosstalk between lineage-survival oncogenes KLF5, GATA4 and GATA6 cooperatively promotes gastric cancer development. *Gut* **64**, 707–719 (2015).
96. Ghaleb, A. M. *et al.* Krüppel-like factors 4 and 5: The yin and yang regulators of cellular proliferation. *Cell Research* vol. 15 92–96 (2005).
97. Dong, J. T. & Chen, C. Essential role of KLF5 transcription factor in cell proliferation and differentiation and its implications for human diseases. *Cellular and Molecular Life Sciences* vol. 66 2691–2706 (2009).
98. Pan, J. *et al.* Lineage-specific epigenomic and genomic activation of oncogene HNF4A promotes gastrointestinal adenocarcinomas. *Cancer Res.* **80**, canres.0390.2020 (2020).
99. Chen, P. *et al.* KLF5 promotes proliferation in gastric cancer via regulating p21 and CDK4. *Eur. Rev. Med. Pharmacol. Sci.* **24**, 4224–4231 (2020).
100. Tay, Y., Rinn, J. & Pandolfi, P. P. The multilayered complexity of ceRNA crosstalk and competition. *Nature* **505**, 344–352 (2014).
101. Zarkou, V., Galaras, A., Giakountis, A. & Hatzis, P. Crosstalk mechanisms between the WNT signaling pathway and long non-coding RNAs. *Non-coding RNA Res.* **3**, 42–53 (2018).
102. Iwakawa, H. oki & Tomari, Y. The Functions of MicroRNAs: mRNA Decay and Translational Repression. *Trends Cell Biol.* **25**, 651–665 (2015).
103. Cesana, M. & Daley, G. Q. Deciphering the rules of ceRNA networks. *Proc. Natl. Acad. Sci.* **110**, 7112–7113 (2013).
104. Fatica, A. & Bozzoni, I. Long non-coding RNAs: New players in cell differentiation and development. *Nat. Rev. Genet.* **15**, 7–21 (2014).
105. Figliuzzi, M., Marinari, E. & De Martino, A. MicroRNAs as a selective channel of

communication between competing RNAs: A steady-state theory. *Biophys. J.* **104**, 1203–1213 (2013).

106. Ala, U. *et al.* Integrated transcriptional and competitive endogenous RNA networks are cross-regulated in permissive molecular environments. *Proc. Natl. Acad. Sci.* **110**, 7154–7159 (2013).
107. Loewer, S. *et al.* Large intergenic non-coding RNA-RoR modulates reprogramming of human induced pluripotent stem cells. *Nat. Genet.* **42**, 1113–1117 (2010).
108. Ng, S. Y., Johnson, R. & Stanton, L. W. Human long non-coding RNAs promote pluripotency and neuronal differentiation by association with chromatin modifiers and transcription factors. *EMBO J.* **31**, 522–533 (2012).
109. Kim, D. H. *et al.* Single-cell transcriptome analysis reveals dynamic changes in lncRNA expression during reprogramming. *Cell Stem Cell* **16**, 88–101 (2015).
110. Cunningham, F. *et al.* Ensembl 2015. *Nucleic Acids Res.* **43**, D662–D669 (2015).
111. Mohamed, J. S. *et al.* Conserved long noncoding RNAs transcriptionally regulated by Oct4 and Nanog modulate pluripotency in mouse embryonic stem cells Conserved long noncoding RNAs transcriptionally regulated by Oct4 and Nanog modulate pluripotency in mouse embryonic stem cells. 324–337 (2010) doi:10.1261/rna.1441510.
112. Wang, Y. *et al.* Endogenous miRNA Sponge lincRNA-RoR Regulates Oct4, Nanog, and Sox2 in Human Embryonic Stem Cell Self-Renewal. *Dev. Cell* **25**, 69–80 (2013).
113. Gao, S. *et al.* ROR functions as a ceRNA to regulate Nanog expression by sponging miR-145 and predicts poor prognosis in pancreatic cancer. *Oncotarget* **7**, (2016).
114. Zhou, P., Sun, L., Liu, D., Liu, C. & Sun, L. Long Non-Coding RNA lincRNA-ROR Promotes the Progression of Colon Cancer and Holds Prognostic Value by Associating with miR-145. *Pathol. Oncol. Res.* **22**, 733–740 (2016).
115. Liu, T. *et al.* Curcumin suppresses proliferation and in vitro invasion of human prostate cancer stem cells by ceRNA effect of miR-145 and lncRNA-ROR. *Gene* **631**, 29–38 (2017).
116. Jia, X. *et al.* KLF5 regulated lncRNA RP1 promotes the growth and metastasis of breast cancer via repressing p27kip1 translation. *Cell Death Dis.* **10**, (2019).
117. Xu, T. *et al.* KLF5 and MYC modulated LINC00346 contributes to gastric cancer

progression through acting as a competing endogeous RNA and indicates poor outcome. *Cell Death Differ.* **26**, 2179–2193 (2019).

118. Clough, E. & Barrett, T. The Gene Expression Omnibus database. in *Methods in Molecular Biology* vol. 1418 93–110 (Humana Press Inc., 2016).
119. Cristescu, R. *et al.* Molecular analysis of gastric cancer identifies subtypes associated with distinct clinical outcomes. *Nat. Med.* **21**, 449–456 (2015).
120. Davis, S. & Meltzer, P. S. GEOquery: A bridge between the Gene Expression Omnibus (GEO) and BioConductor. *Bioinformatics* **23**, 1846–1847 (2007).
121. Carlson, M. org.Hs.eg.db: Genome wide annotation for Human. (2019) doi:10.18129/B9.bioc.org.Hs.eg.db.
122. Ritchie, M. E. *et al.* Limma powers differential expression analyses for RNA-sequencing and microarray studies. *Nucleic Acids Res.* **43**, e47 (2015).
123. Wickham, H. *ggplot2: elegant graphics for data analysis*. (Springer, 2016).
124. Zhu, Y., Qiu, P. & Ji, Y. TCGA-Assembler: open-source software for retrieving and processing TCGA data. *Nat. Methods* **11**, 599–600 (2014).
125. Wei, L. *et al.* TCGA-assembler 2: Software pipeline for retrieval and processing of TCGA/CPTAC data. *Bioinformatics* **34**, 1615–1617 (2018).
126. Cerami, E. *et al.* The cBio Cancer Genomics Portal: An open platform for exploring multidimensional cancer genomics data. *Cancer Discov.* **2**, 401–404 (2012).
127. Gao, J. *et al.* Integrative analysis of complex cancer genomics and clinical profiles using the cBioPortal. *Sci. Signal.* **6**, (2013).
128. Robinson, M. D., McCarthy, D. J. & Smyth, G. K. edgeR: A Bioconductor package for differential expression analysis of digital gene expression data. *Bioinformatics* **26**, 139–140 (2009).
129. Su, S. *et al.* Glimma: Interactive graphics for gene expression analysis. *Bioinformatics* **33**, 2050–2052 (2017).
130. Wei, T. & Simko, V. R package 'corrplot': Visualization of a Correlation Matrix. (2017).
131. Engelmann, D., Meier, C., Alla, V. & Pützer, B. M. A balancing act: Orchestrating amino-truncated and full-length p73 variants as decisive factors in cancer progression.

Oncogene **34**, 4287–4299 (2015).

132. Lin, Y., Cheng, Z., Yang, Z., Zheng, J. & Lin, T. DNp73 improves generation efficiency of human induced pluripotent stem cells. *BMC Cell Biol.* **13**, 9 (2012).
133. Yong, X. *et al.* Helicobacter pylori upregulates Nanog and Oct4 via Wnt/β-catenin signaling pathway to promote cancer stem cell-like properties in human gastric cancer. *Cancer Lett.* **374**, 292–303 (2016).
134. Garcia, M. *et al.* In vitro culture and phenotypic and molecular characterization of gastric stem cells from human stomach. *Helicobacter* **22**, 1–9 (2017).
135. Jen, J. *et al.* Oct4 transcriptionally regulates the expression of long non-coding RNAs NEAT1 and MALAT1 to promote lung cancer progression. *Mol. Cancer* **16**, 1–12 (2017).
136. Takahashi, K. & Yamanaka, S. Induction of Pluripotent Stem Cells from Mouse Embryonic and Adult Fibroblast Cultures by Defined Factors. *Cell* **126**, 663–676 (2006).
137. Sigal, M. *et al.* Stromal R-spondin orchestrates gastric epithelial stem cells and gland homeostasis. *Nature* **548**, 451–455 (2017).
138. Zuo, X. *et al.* PPARD and Interferon Gamma Promote Transformation of Gastric Progenitor Cells and Tumorigenesis in Mice. *Gastroenterology* **157**, 163–178 (2019).
139. Choi, E. *et al.* Lrig1+ gastric isthmal progenitor cells restore normal gastric lineage cells during damage recovery in adult mouse stomach. *Gut* **67**, 1595–1605 (2018).
140. Noto, J. M. *et al.* Helicobacter Pylori Promotes the Expression of Krüppel-Like Factor 5, a Mediator of Carcinogenesis, In Vitro and In Vivo. *PLoS One* **8**, e54344 (2013).
141. Yu, S. *et al.* Expression of LRIG1, a Negative Regulator of EGFR, Is Dynamically Altered during Different Stages of Gastric Carcinogenesis. *Am. J. Pathol.* **188**, 2912–2923 (2018).
142. Ding, L., El Zaatari, M. & Merchant, J. L. Recapitulating Human Gastric Cancer Pathogenesis: Experimental Models of Gastric Cancer. in 441–478 (2016). doi:10.1007/978-3-319-41388-4_22.
143. Smith, J. P., Nadella, S. & Osborne, N. Gastrin and Gastric Cancer. *Cell. Mol. Gastroenterol. Hepatol.* **4**, 75–83 (2017).
144. Waldum, H. L., Sagatun, L. & Mjønes, P. Gastrin and Gastric Cancer. *Front. Endocrinol. (Lausanne).* **8**, (2017).

145. Engevik, A. C. *et al.* The Development of Spasmolytic Polypeptide/TFF2-Expressing Metaplasia (SPEM) During Gastric Repair Is Absent in the Aged Stomach. *Cell. Mol. Gastroenterol. Hepatol.* **2**, 605–624 (2016).
146. Aikou, S. *et al.* Tests for Serum Levels of Trefoil Factor Family Proteins Can Improve Gastric Cancer Screening. *Gastroenterology* **141**, 837-845.e7 (2011).
147. Weis, V. G. *et al.* Heterogeneity in mouse spasmolytic polypeptide-expressing metaplasia lineages identifies markers of metaplastic progression. *Gut* **62**, 1270–1279 (2013).
148. Wang, X.-Y., Chen, S.-H., Zhang, Y.-N. & Xu, C.-F. Olfactomedin-4 in digestive diseases: A mini-review. *World J. Gastroenterol.* **24**, 1881–1887 (2018).
149. Wang, Y. *et al.* Lgr4 regulates mammary gland development and stem cell activity through the pluripotency transcription factor Sox2. *Stem Cells* **31**, 1921–1931 (2013).
150. Barker, N. & Clevers, H. Leucine-Rich Repeat-Containing G-Protein-Coupled Receptors as Markers of Adult Stem Cells. *Gastroenterology* **138**, 1681–1696 (2010).
151. Clemons, N. J. *et al.* Sox9 drives columnar differentiation of esophageal squamous epithelium: a possible role in the pathogenesis of Barrett's esophagus. *Am. J. Physiol. Liver Physiol.* **303**, G1335–G1346 (2012).
152. Fischer, A.-S. & Sigal, M. The Role of Wnt and R-spondin in the Stomach During Health and Disease. *Biomedicines* **7**, 44 (2019).
153. Wickham, H. Reshaping Data with the reshape Package. *J. Stat. Softw.* **21**, 6–17 (2007).
154. Benjamini, Y. & Hochberg, Y. Controlling the false discovery rate: a practical and powerful approach to multiple testing. *J. R. Stat. Soc. Ser. B* **57**, 289–300 (1995).
155. Warnes, G. R. *et al.* gplots: Various R programming tools for plotting data. *R Packag. version* **2**, 1 (2009).
156. Prada, C. & Nakaya, H. I. MetaVolcanoR: Gene expression meta-analysis visualization tool. (2019) doi:10.18129/B9.bioc.MetaVolcanoR.
157. Amaral, P. P. *et al.* Genomic positional conservation identifies topological anchor point RNAs linked to developmental loci. *Genome Biol.* **19**, (2018).
158. Quinlan, A. R. BEDTools: The Swiss-Army tool for genome feature analysis. *Curr. Protoc. Bioinforma.* **2014**, 11.12.1-11.12.34 (2014).

159. The UCSC Genome Browser Database: 2018 Update - PubMed. https://pubmed.ncbi.nlm.nih.gov/29106570/?from_term=ucsc+genome+browser&from_pos=1.
160. Kent, W. J. BLAT---The BLAST-Like Alignment Tool. *Genome Res.* **12**, 656–664 (2002).
161. De Lima, D. S. *et al.* Long noncoding RNAs are involved in multiple immunological pathways in response to vaccination. doi:10.1073/pnas.1822046116.
162. Warnes, G. R. *et al.* gplots: Various R Programming Tools for Plotting Data. (2020).
163. List, M., Dehghani Amirabad, A., Kostka, D. & Schulz, M. H. Large-scale inference of competing endogenous RNA networks with sparse partial correlation. *Bioinformatics* **35**, i596–i604 (2019).
164. Kozomara, A., Birgaoanu, M. & Griffiths-Jones, S. miRBase: from microRNA sequences to function. *Nucleic Acids Res.* **47**, D155–D162 (2019).
165. Frankish, A. *et al.* GENCODE reference annotation for the human and mouse genomes. *Nucleic Acids Res.* **47**, D766–D773 (2019).
166. Bandyopadhyay, S. & Mitra, R. TargetMiner: microRNA target prediction with systematic identification of tissue-specific negative examples. *Bioinformatics* **25**, 2625–31 (2009).
167. Wong, N. & Wang, X. miRDB: an online resource for microRNA target prediction and functional annotations. *Nucleic Acids Res.* **43**, D146–D152 (2015).
168. Agarwal, V., Bell, G. W., Nam, J. W. & Bartel, D. P. Predicting effective microRNA target sites in mammalian mRNAs. *Elife* **4**, (2015).
169. Karagkouni, D. *et al.* DIANA-TarBase v8: a decade-long collection of experimentally supported miRNA-gene interactions. *Nucleic Acids Res.* **46**, D239–D245 (2018).
170. Paraskevopoulou, M. D. *et al.* DIANA-LncBase v2: indexing microRNA targets on non-coding transcripts. *Nucleic Acids Res.* **44**, D231-8 (2016).
171. Li, J.-H., Liu, S., Zhou, H., Qu, L.-H. & Yang, J.-H. starBase v2.0: decoding miRNA-ceRNA, miRNA-ncRNA and protein-RNA interaction networks from large-scale CLIP-Seq data. *Nucleic Acids Res.* **42**, D92-7 (2014).
172. Xu, T. *et al.* miRBaseConverter: An R/Bioconductor package for converting and retrieving miRNA name, accession, sequence and family information in different versions of

miRBase. *BMC Bioinformatics* **19**, (2018).

173. Durinck, S. *et al.* BioMart and Bioconductor: a powerful link between biological databases and microarray data analysis. *Bioinformatics* **21**, 3439–3440 (2005).
174. Durinck, S., Spellman, P. T., Birney, E. & Huber, W. Mapping identifiers for the integration of genomic datasets with the R/ Bioconductor package biomaRt. *Nat. Protoc.* **4**, 1184–1191 (2009).
175. Team, B. C. Homo.sapiens: Annotation package for the Homo.sapiens object. (2015).
176. Muniategui, A. *et al.* Quantification of miRNA-mRNA interactions. *PLoS One* **7**, (2012).
177. Kim, S. ppcor: An R Package for a Fast Calculation to Semi-partial Correlation Coefficients. *Commun. Stat. Appl. Methods* **22**, 665–674 (2015).
178. Shannon, P. Cytoscape: A Software Environment for Integrated Models of Biomolecular Interaction Networks. *Genome Res.* **13**, 2498–2504 (2003).
179. Maere, S., Heymans, K. & Kuiper, M. BiNGO: a Cytoscape plugin to assess overrepresentation of Gene Ontology categories in Biological Networks. *Bioinformatics* **21**, 3448–3449 (2005).
180. Merico, D., Isserlin, R., Stueker, O., Emili, A. & Bader, G. D. Enrichment Map: A Network-Based Method for Gene-Set Enrichment Visualization and Interpretation. *PLoS One* **5**, e13984 (2010).
181. Kucera, M., Isserlin, R., Arkhangorodsky, A. & Bader, G. D. AutoAnnotate: A Cytoscape app for summarizing networks with semantic annotations [version 1; referees: 2 approved]. *F1000Research* **5**, 1717 (2016).
182. Srivastava, S., Ghosh, S., Kagan, J. & Mazurchuk, R. The PreCancer Atlas (PCA). *Trends in Cancer* vol. 4 513–514 (2018).
183. Srivastava, S., Ghosh, S., Kagan, J. & Mazurchuk, R. The Making of a PreCancer Atlas: Promises, Challenges, and Opportunities. *Trends in Cancer* vol. 4 523–536 (2018).
184. Langfelder, P. & Horvath, S. WGCNA: An R package for weighted correlation network analysis. *BMC Bioinformatics* **9**, 559 (2008).
185. Li, Q. *et al.* HpSlyD inducing CDX2 and VIL1 expression mediated through TCTP protein may contribute to intestinal metaplasia in the stomach. *Sci. Rep.* **7**, 1–14 (2017).

186. Sue, S. *et al.* Intestine-specific homeobox (ISX) induces intestinal metaplasia and cell proliferation to contribute to gastric carcinogenesis. *J. Gastroenterol.* **51**, 949–960 (2016).

187. Jang, B. G., Lee, B. L. & Kim, W. H. Olfactomedin-related proteins 4 (OLFM4) expression is involved in early gastric carcinogenesis and of prognostic significance in advanced gastric cancer. *Virchows Arch.* **467**, 285–294 (2015).

188. Leung, W. K. *et al.* Expression of trefoil peptides (TFFI, TFF2, and TFF3) in gastric carcinomas, intestinal metaplasia, and non-neoplastic gastric tissues. *J. Pathol.* **197**, 582–588 (2002).

189. Deng, N. *et al.* A comprehensive survey of genomic alterations in gastric cancer reveals systematic patterns of molecular exclusivity and co-occurrence among distinct therapeutic targets. *Gut* **61**, 673–684 (2012).

190. Soon, M. S. *et al.* Expression of Kruppel-like factor 5 in gastric cancer and its clinical correlation in Taiwan. *Virchows Arch.* **459**, 161–166 (2011).

191. Zhou, C. *et al.* Difference of molecular alterations in HER2-positive and HER2-negative gastric cancers by whole-genome sequencing analysis. *Cancer Manag. Res.* **10**, 3945–3954 (2018).

192. Kwak, M. K. *et al.* Expression of Krüppel-like factor 5 in human gastric carcinomas. *J. Cancer Res. Clin. Oncol.* **134**, 163–167 (2008).

193. Wang, Q. *et al.* Characterization of super-enhancer-associated functional lncRNAs acting as ceRNAs in ESCC. *Mol. Oncol.* (2020) doi:10.1002/1878-0261.12726.

194. Zhang, J., Fan, D., Jian, Z., Chen, G. G. & Lai, P. B. S. Cancer specific long noncoding RNAs show differential expression patterns and competing endogenous RNA potential in hepatocellular carcinoma. *PLoS One* **10**, (2015).

195. Zhang, H., Wang, Y. & Lu, J. Identification of lung-adenocarcinoma-related long non-coding RNAs by random walking on a competing endogenous RNA network. *Ann. Transl. Med.* **7**, 339–339 (2019).

196. Ji, H. *et al.* Long noncoding RNA MAPKAPK5-AS1 promotes colorectal cancer proliferation by partly silencing p21 expression. *Cancer Sci.* **110**, 72–85 (2019).

197. Wang, W. *et al.* An immune-related lncRNA signature for patients with anaplastic gliomas. *J. Neurooncol.* **136**, 263–271 (2018).
198. Luan, F. *et al.* An autophagy-related long non-coding RNA signature for glioma. *FEBS Open Bio* **9**, 653–667 (2019).
199. Hu, Y. *et al.* LncRNA-SNHG1 contributes to gastric cancer cell proliferation by regulating DNMT1. *Biochem. Biophys. Res. Commun.* **491**, 926–931 (2017).
200. Liu, Z. Q. *et al.* LncRNA SNHG1 promotes EMT process in gastric cancer cells through regulation of the miR-15b/DCLK1/Notch1 axis. *BMC Gastroenterol.* **20**, (2020).
201. Xuan, Y. & Wang, Y. Long non-coding RNA SNHG3 promotes progression of gastric cancer by regulating neighboring MED18 gene methylation. *Cell Death Dis.* **10**, (2019).
202. Wang, M.-W. *et al.* LncRNA SNHG7 promotes the proliferation and inhibits apoptosis of gastric cancer cells by repressing the P15 and P16 expression. *Eur. Rev. Med. Pharmacol. Sci.* **21**, 4613–4622 (2017).
203. Zhang, Y. *et al.* SNHG7 accelerates cell migration and invasion through regulating miR-34a-Snail-EMT axis in gastric cancer. *Cell Cycle* **19**, 142–152 (2020).
204. Chen, S. xiu *et al.* Upregulated expression of long noncoding RNA SNHG15 promotes cell proliferation and invasion through regulates MMP2/MMP9 in patients with GC. *Tumor Biol.* **37**, 6801–6812 (2016).
205. Zhang, G. *et al.* LncRNA SNHG17 promotes gastric cancer progression by epigenetically silencing of p15 and p57. *J. Cell. Physiol.* **234**, 5163–5174 (2019).
206. Chen, L. L., He, J., Qiu, X. T., Yu, J. & Wang, Z. M. The prognostic roles of long non-coding RNA SNHG17 in the patients with gastric cancer. *Eur. Rev. Med. Pharmacol. Sci.* **23**, 1063–1068 (2019).
207. Han, T. *et al.* H. pylori infection alters repair of DNA double-strand breaks via SNHG17. *J. Clin. Invest.* **130**, (2020).
208. Lord, C. J. & Ashworth, A. The DNA damage response and cancer therapy. *Nature* vol. 481 287–294 (2012).
209. O'Connor, M. J. Targeting the DNA Damage Response in Cancer. *Molecular Cell* vol. 60 547–560 (2015).

210. Li, S. *et al.* Involvement of p54(nrb), a PSF partner protein, in DNA double-strand break repair and radioresistance. *Nucleic Acids Res.* **37**, 6746–6753 (2009).
211. Ahmed, K. M., Pandita, R. K., Singh, D. K., Hunt, C. R. & Pandita, T. K. β1-Integrin Impacts Rad51 Stability and DNA Double-Strand Break Repair by Homologous Recombination. *Mol. Cell. Biol.* **38**, (2018).
212. Rabani, M., Pieper, L., Chew, G. L. & Schier, A. F. A Massively Parallel Reporter Assay of 3' UTR Sequences Identifies In Vivo Rules for mRNA Degradation. *Mol. Cell* **68**, 1083-1094.e5 (2017).
213. Vainberg Slutskin, I., Weingarten-Gabbay, S., Nir, R., Weinberger, A. & Segal, E. Unraveling the determinants of microRNA mediated regulation using a massively parallel reporter assay. *Nat. Commun.* **9**, (2018).

2.3.3 Anexos

ceRNA1	ceRNA2	Shared miRNAs	cor	pcor	mscor	P-val	P-adj
MAPKAPK5-AS1	C17orf100	2	0.132	0.017	0.115	1.58E-03	1.47E-02
MAPKAPK5-AS1	CDCA8	1	0.365	0.248	0.117	3.51E-03	4.17E-02
MAPKAPK5-AS1	CHD7	2	0.211	0.090	0.121	1.11E-03	1.20E-02
MAPKAPK5-AS1	CMTM8	1	0.431	0.318	0.112	4.37E-03	4.68E-02
MAPKAPK5-AS1	CNOT11	1	0.357	0.231	0.126	2.31E-03	3.43E-02
MAPKAPK5-AS1	AURKA	2	0.302	0.175	0.127	1.12E-03	7.89E-03
MAPKAPK5-AS1	BLM	2	0.239	0.127	0.113	1.90E-03	1.69E-02
MAPKAPK5-AS1	CENPA	2	0.357	0.250	0.107	2.21E-03	8.16E-03
MAPKAPK5-AS1	CUL2	2	0.171	0.076	0.094	5.60E-03	3.25E-02
MAPKAPK5-AS1	E2F3	2	0.148	0.012	0.136	3.80E-04	6.02E-03
MAPKAPK5-AS1	GPSM2	2	0.283	0.179	0.103	4.21E-03	1.89E-02
MAPKAPK5-AS1	HSPA14	2	0.321	0.223	0.099	5.17E-03	2.12E-02
MAPKAPK5-AS1	MEN1	2	0.270	0.155	0.115	2.22E-03	1.24E-02
MAPKAPK5-AS1	MOCS3	2	0.132	0.013	0.119	1.28E-03	1.31E-02
MAPKAPK5-AS1	NR6A1	2	0.172	0.055	0.118	1.38E-03	1.37E-02
MAPKAPK5-AS1	PVR	2	0.111	0.012	0.099	4.34E-03	2.80E-02
MAPKAPK5-AS1	RAD54B	2	0.395	0.291	0.104	2.61E-03	9.16E-03
MAPKAPK5-AS1	TOP2A	2	0.341	0.212	0.129	1.04E-03	7.49E-03
MAPKAPK5-AS1	SBNO1	2	0.202	0.109	0.093	6.02E-03	3.39E-02
MAPKAPK5-AS1	SPRYD4	2	0.307	0.190	0.116	2.11E-03	1.20E-02
MAPKAPK5-AS1	TRIB3	2	0.292	0.204	0.088	9.10E-03	3.07E-02
MAPKAPK5-AS1	WNK2	2	0.143	0.054	0.089	7.54E-03	3.91E-02
MIRLET7BHG	HIVEP2	2	0.123	0.040	0.083	1.05E-02	4.75E-02
SNHG1	ADIPOR2	2	0.160	0.037	0.122	1.06E-03	1.18E-02
SNHG1	AEN	2	0.116	-0.033	0.149	2.00E-04	4.30E-03
SNHG1	ALG14	2	0.266	0.173	0.093	7.17E-03	2.64E-02
SNHG1	ANAPC5	2	0.345	0.254	0.091	7.91E-03	2.80E-02
SNHG1	ANLN	1	0.458	0.368	0.090	8.23E-03	4.75E-02
SNHG1	AP5M1	1	0.252	0.070	0.182	3.40E-04	3.50E-02
SNHG1	ARL5B	2	0.168	0.083	0.085	9.28E-03	4.41E-02
SNHG1	ARL6IP6	2	0.589	0.511	0.078	4.36E-03	9.38E-03
SNHG1	ASF1B	1	0.425	0.281	0.144	9.40E-04	2.20E-02
SNHG1	ASNSD1	2	0.305	0.131	0.174	1.30E-04	2.43E-03
SNHG1	BAMBI	2	0.128	0.024	0.104	3.27E-03	2.37E-02
SNHG1	BRAT1	2	0.258	0.069	0.188	7.00E-05	1.89E-03
SNHG1	BTBD1	2	0.116	-0.016	0.132	5.30E-04	7.59E-03
SNHG1	C19orf48	3	0.426	0.305	0.121	1.20E-03	3.62E-03
SNHG1	C5orf22	2	0.294	0.220	0.074	1.77E-02	4.74E-02
SNHG1	C5orf34	2	0.480	0.328	0.152	2.00E-05	1.32E-04
SNHG1	C6orf136	3	0.427	0.269	0.158	8.00E-05	4.14E-04
SNHG1	CCDC14	1	0.531	0.433	0.098	5.52E-03	3.72E-02

SNHG1	CCDC43	2	0.400	0.334	0.065	2.43E-02	4.85E-02
SNHG1	CCDC59	2	0.439	0.302	0.137	3.20E-04	1.99E-03
SNHG1	CDCA4	3	0.390	0.181	0.208	1.00E-05	8.47E-05
SNHG1	CDCA5	2	0.480	0.328	0.152	2.00E-05	1.32E-04
SNHG1	CDCA8	2	0.443	0.229	0.214	1.00E-05	1.56E-04
SNHG1	CENPW	1	0.486	0.392	0.094	6.91E-03	4.29E-02
SNHG1	CEP128	2	0.271	0.192	0.079	1.39E-02	4.06E-02
SNHG1	CHD7	3	0.440	0.260	0.180	2.00E-05	1.49E-04
SNHG1	CHKB-DT	2	0.164	0.073	0.090	7.12E-03	3.76E-02
SNHG1	CHORDC1	4	0.576	0.383	0.194	1.00E-05	2.27E-05
SNHG1	CHTOP	1	0.477	0.387	0.090	8.25E-03	4.75E-02
SNHG1	CKAP2	1	0.495	0.397	0.098	5.48E-03	3.72E-02
SNHG1	CLN6	2	0.303	0.100	0.203	3.00E-05	1.20E-03
SNHG1	DAZAP1	1	0.401	0.278	0.123	2.72E-03	3.75E-02
SNHG1	DCAF12	2	0.271	0.116	0.155	2.60E-04	3.24E-03
SNHG1	DCUN1D5	1	0.477	0.279	0.198	1.00E-05	6.97E-04
SNHG1	DESI1	2	0.174	0.053	0.121	1.11E-03	1.20E-02
SNHG1	DHRS13	3	0.231	-0.047	0.278	1.00E-05	3.52E-04
SNHG1	DNAAF5	3	0.329	0.216	0.113	5.16E-03	1.84E-02
SNHG1	DSCC1	2	0.564	0.500	0.064	1.17E-02	2.17E-02
SNHG1	E2F7	3	0.439	0.158	0.281	1.00E-05	8.47E-05
SNHG1	ESCO2	3	0.396	0.314	0.082	1.29E-02	2.42E-02
SNHG1	FAM111B	2	0.420	0.354	0.067	2.24E-02	4.56E-02
SNHG1	FAM136A	2	0.555	0.380	0.175	1.00E-05	4.63E-05
SNHG1	FAM49B	2	0.404	0.291	0.113	1.57E-03	6.43E-03
SNHG1	FANCI	1	0.517	0.422	0.095	6.54E-03	4.13E-02
SNHG1	FBXO45	3	0.397	0.044	0.353	1.00E-05	8.47E-05
SNHG1	GEMIN4	2	0.196	0.027	0.169	4.00E-05	1.38E-03
SNHG1	GINS3	1	0.379	0.258	0.120	3.02E-03	3.89E-02
SNHG1	GMNN	3	0.493	0.328	0.165	1.00E-05	4.38E-05
SNHG1	GNL3	1	0.585	0.505	0.079	9.19E-03	4.43E-02
SNHG1	GOLT1B	2	0.280	0.066	0.215	2.00E-05	8.44E-04
SNHG1	GPSM2	2	0.378	0.273	0.106	2.36E-03	8.56E-03
SNHG1	GRPEL2	1	0.337	0.116	0.221	5.00E-05	2.14E-02
SNHG1	HACD3	2	0.280	0.152	0.128	1.05E-03	7.55E-03
SNHG1	HAUS3	1	0.351	0.219	0.132	1.81E-03	3.11E-02
SNHG1	IER3IP1	1	0.327	0.128	0.199	1.90E-04	3.26E-02
SNHG1	INSIG2	2	0.301	0.116	0.185	9.00E-05	2.13E-03
SNHG1	KCMF1	2	0.361	0.149	0.212	1.00E-05	1.56E-04
SNHG1	KMT5A	2	0.275	0.151	0.124	1.33E-03	8.75E-03
SNHG1	LARP4	2	0.324	0.159	0.165	1.70E-04	2.62E-03
SNHG1	LCLAT1	2	0.355	0.234	0.120	1.03E-03	4.77E-03
SNHG1	LIN7C	2	0.355	0.233	0.122	9.30E-04	4.41E-03
SNHG1	LMBR1	2	0.170	-0.037	0.207	1.00E-05	6.53E-04
SNHG1	LMNB2	2	0.310	0.192	0.118	1.90E-03	1.12E-02

SNHG1	LRFN4	2	0.245	0.068	0.177	2.00E-05	8.62E-04
SNHG1	MAIP1	2	0.426	0.293	0.133	4.40E-04	2.55E-03
SNHG1	MAP3K21	2	0.387	0.222	0.165	5.00E-05	5.03E-04
SNHG1	MEX3A	2	0.271	0.152	0.119	1.77E-03	1.07E-02
SNHG1	MRPL20	1	0.418	0.303	0.115	3.85E-03	4.38E-02
SNHG1	MRPL52	2	0.292	0.195	0.097	5.71E-03	2.27E-02
SNHG1	MRPS2	3	0.344	0.233	0.111	5.52E-03	1.92E-02
SNHG1	MRPS26	1	0.358	0.211	0.147	8.00E-04	2.00E-02
SNHG1	MSL3P1	3	0.172	0.086	0.086	1.52E-02	4.97E-02
SNHG1	MTHFD1L	2	0.427	0.327	0.101	3.13E-03	1.05E-02
SNHG1	MZT1	2	0.545	0.455	0.090	4.53E-03	1.17E-02
SNHG1	NAA15	2	0.427	0.303	0.124	8.10E-04	3.99E-03
SNHG1	NAA20	3	0.482	0.295	0.187	1.00E-05	4.38E-05
SNHG1	NAA25	2	0.604	0.499	0.105	5.60E-04	1.69E-03
SNHG1	NAA40	1	0.484	0.287	0.197	1.00E-05	6.97E-04
SNHG1	NARF	1	0.343	0.124	0.220	6.00E-05	2.32E-02
SNHG1	NCAPG	2	0.578	0.522	0.056	2.15E-02	3.69E-02
SNHG1	NELFCD	1	0.379	0.237	0.142	1.09E-03	2.41E-02
SNHG1	NUDCD1	1	0.518	0.428	0.090	8.25E-03	4.75E-02
SNHG1	NUP37	1	0.553	0.449	0.104	2.25E-03	1.70E-02
SNHG1	OSBPL3	2	0.415	0.344	0.071	1.78E-02	3.85E-02
SNHG1	OTUB1	2	0.341	0.267	0.074	1.76E-02	4.72E-02
SNHG1	PAN3	2	0.385	0.305	0.081	1.04E-02	2.57E-02
SNHG1	PARD6B	3	0.369	0.285	0.084	1.17E-02	2.23E-02
SNHG1	PDIK1L	4	0.402	0.323	0.079	1.80E-02	2.93E-02
SNHG1	PERP	1	0.353	0.168	0.185	1.00E-04	7.35E-03
SNHG1	PGAM5	2	0.212	0.016	0.196	1.00E-05	6.53E-04
SNHG1	PGAP2	1	0.438	0.300	0.138	1.31E-03	2.64E-02
SNHG1	PI4K2B	1	0.350	0.103	0.247	1.00E-05	6.80E-03
SNHG1	PLEKHA1	2	0.166	0.048	0.118	1.31E-03	1.33E-02
SNHG1	POLR1B	1	0.509	0.411	0.097	5.59E-03	3.75E-02
SNHG1	PPIL1	2	0.382	0.267	0.115	1.46E-03	6.18E-03
SNHG1	PRPF19	2	0.379	0.250	0.130	5.70E-04	3.11E-03
SNHG1	PRRG4	3	0.252	0.135	0.117	4.06E-03	1.55E-02
SNHG1	PSAT1	2	0.421	0.202	0.219	1.00E-05	1.56E-04
SNHG1	PTGES2	1	0.321	0.114	0.207	1.40E-04	3.07E-02
SNHG1	PTPMT1	1	0.382	0.230	0.151	6.30E-04	1.78E-02
SNHG1	PUS1	1	0.475	0.366	0.109	3.20E-03	2.73E-02
SNHG1	QTRT2	1	0.304	-0.003	0.307	1.00E-05	6.80E-03
SNHG1	RACGAP1	1	0.462	0.335	0.126	1.34E-03	1.65E-02
SNHG1	RCC2	1	0.355	0.223	0.132	1.78E-03	3.09E-02
SNHG1	REPIN1	2	0.132	-0.088	0.221	1.00E-05	6.53E-04
SNHG1	RMND5A	1	0.363	0.182	0.181	1.20E-04	7.59E-03
SNHG1	SAPCD2	1	0.399	0.259	0.140	1.22E-03	2.53E-02
SNHG1	SBNO1	2	0.255	0.114	0.141	4.90E-04	4.50E-03

SNHG1	SEH1L	1	0.405	0.212	0.193	4.00E-05	3.90E-03
SNHG1	SENP2	2	0.166	-0.016	0.182	2.00E-05	8.62E-04
SNHG1	SFXN1	2	0.280	0.193	0.087	9.52E-03	3.16E-02
SNHG1	SGO1	2	0.490	0.423	0.067	1.82E-02	3.49E-02
SNHG1	SGO2	1	0.492	0.390	0.102	4.67E-03	3.41E-02
SNHG1	SIKE1	2	0.297	0.165	0.133	8.20E-04	6.47E-03
SNHG1	SINHCAF	2	0.455	0.369	0.086	5.90E-03	1.45E-02
SNHG1	SLC25A22	2	0.318	0.117	0.201	4.00E-05	1.37E-03
SNHG1	SLC25A39	3	0.343	0.162	0.181	9.00E-05	1.03E-03
SNHG1	SLC26A6	2	0.281	0.045	0.236	1.00E-05	6.58E-04
SNHG1	SLC39A10	3	0.283	0.171	0.112	5.26E-03	1.86E-02
SNHG1	SMIM13	2	0.250	0.121	0.130	9.50E-04	7.01E-03
SNHG1	ABCF2	2	0.181	-0.023	0.204	1.00E-05	6.53E-04
SNHG1	ACP1	2	0.550	0.392	0.157	1.00E-05	6.89E-05
SNHG1	ADORA2B	2	0.155	0.046	0.109	2.43E-03	1.96E-02
SNHG1	AGPS	2	0.243	0.103	0.139	3.50E-04	5.78E-03
SNHG1	AHCY	1	0.393	0.257	0.137	1.48E-03	2.85E-02
SNHG1	AHSA1	1	0.299	0.061	0.238	1.00E-05	6.80E-03
SNHG1	AMD1	2	0.408	0.254	0.154	9.00E-05	7.80E-04
SNHG1	ANP32A	2	0.387	0.279	0.109	1.93E-03	7.36E-03
SNHG1	ATIC	1	0.420	0.310	0.110	4.81E-03	4.86E-02
SNHG1	ATP6V0B	1	0.255	0.072	0.183	3.20E-04	3.38E-02
SNHG1	ATXN2L	2	0.277	0.028	0.249	1.00E-05	6.58E-04
SNHG1	BAZ1A	3	0.353	0.260	0.093	7.01E-03	1.50E-02
SNHG1	BCS1L	1	0.431	0.309	0.122	2.86E-03	3.82E-02
SNHG1	BIRC5	4	0.406	0.054	0.352	1.00E-05	8.50E-05
SNHG1	BRCA2	2	0.406	0.334	0.072	1.67E-02	3.66E-02
SNHG1	BUB1	1	0.457	0.334	0.123	1.58E-03	1.82E-02
SNHG1	BUB1B	1	0.566	0.463	0.103	2.40E-03	1.79E-02
SNHG1	BZW1	1	0.406	0.196	0.210	1.00E-05	1.11E-03
SNHG1	CAPZA1	2	0.374	0.199	0.175	2.00E-05	2.47E-04
SNHG1	CBFB	3	0.366	0.106	0.260	1.00E-05	8.47E-05
SNHG1	CBX3	2	0.550	0.488	0.062	2.51E-02	4.55E-02
SNHG1	CBX4	2	0.186	0.051	0.135	4.20E-04	6.44E-03
SNHG1	CCNB1	2	0.483	0.200	0.283	1.00E-05	6.89E-05
SNHG1	CCNE1	2	0.273	0.111	0.162	1.80E-04	2.62E-03
SNHG1	CCNF	3	0.300	0.166	0.134	1.59E-03	8.09E-03
SNHG1	CCT4	3	0.545	0.470	0.075	1.71E-02	2.79E-02
SNHG1	CCT7	2	0.333	0.184	0.148	3.70E-04	4.00E-03
SNHG1	CDC25A	2	0.477	0.266	0.211	1.00E-05	6.89E-05
SNHG1	CDC6	3	0.379	0.099	0.280	1.00E-05	8.47E-05
SNHG1	CDK1	3	0.604	0.452	0.152	3.00E-05	9.58E-05
SNHG1	CDK16	1	0.215	-0.048	0.263	1.00E-05	3.17E-02
SNHG1	CDK4	2	0.359	0.227	0.132	4.70E-04	2.66E-03
SNHG1	CHAF1A	1	0.409	0.283	0.126	2.31E-03	3.43E-02

SNHG1	CHD1	2	0.269	0.155	0.114	2.30E-03	1.27E-02
SNHG1	CLDN12	2	0.243	0.161	0.082	1.12E-02	4.93E-02
SNHG1	CLNS1A	1	0.527	0.369	0.158	2.40E-04	6.33E-03
SNHG1	CNIH1	3	0.333	0.081	0.251	1.00E-05	1.58E-04
SNHG1	CPSF6	1	0.521	0.349	0.172	8.00E-05	2.94E-03
SNHG1	CSE1L	3	0.524	0.298	0.226	1.00E-05	4.38E-05
SNHG1	CSNK1E	2	0.270	0.190	0.080	1.37E-02	4.02E-02
SNHG1	CTPS1	1	0.376	0.256	0.120	3.04E-03	3.91E-02
SNHG1	CUL1	2	0.173	0.082	0.091	7.02E-03	3.74E-02
SNHG1	DDX39A	1	0.430	0.301	0.129	2.02E-03	3.25E-02
SNHG1	DDX52	2	0.339	0.214	0.124	1.31E-03	8.69E-03
SNHG1	DEK	2	0.505	0.280	0.225	1.00E-05	6.89E-05
SNHG1	DENR	1	0.567	0.383	0.184	2.00E-05	9.29E-04
SNHG1	DHX9	1	0.365	0.251	0.114	3.96E-03	4.42E-02
SNHG1	DLG3	2	0.159	0.075	0.085	9.70E-03	4.52E-02
SNHG1	DNAJC9	2	0.511	0.318	0.193	1.00E-05	6.89E-05
SNHG1	DPM2	2	0.281	0.121	0.160	2.00E-04	2.76E-03
SNHG1	DSP	2	0.231	0.146	0.085	9.31E-03	4.41E-02
SNHG1	DYNLT1	2	0.324	0.221	0.103	4.30E-03	1.91E-02
SNHG1	EIF2B4	1	0.383	0.268	0.114	3.92E-03	4.42E-02
SNHG1	EIF4E	1	0.398	0.190	0.208	1.00E-05	1.11E-03
SNHG1	ELOC	1	0.405	0.260	0.144	9.30E-04	2.18E-02
SNHG1	ENO1	2	0.238	0.114	0.125	9.50E-04	1.12E-02
SNHG1	ENTR1	1	0.453	0.284	0.168	1.10E-04	3.80E-03
SNHG1	EPCAM	2	0.335	0.235	0.100	4.89E-03	2.05E-02
SNHG1	ERG28	2	0.275	0.053	0.222	1.00E-05	6.58E-04
SNHG1	FAM120A	3	0.111	-0.088	0.199	1.00E-05	3.52E-04
SNHG1	FANCA	2	0.426	0.185	0.241	1.00E-05	1.56E-04
SNHG1	FARSB	2	0.444	0.379	0.065	2.47E-02	4.92E-02
SNHG1	FDXR	2	0.132	-0.047	0.179	2.00E-05	8.62E-04
SNHG1	FEN1	1	0.487	0.236	0.251	1.00E-05	6.97E-04
SNHG1	FOXN2	1	0.378	0.184	0.194	3.00E-05	3.06E-03
SNHG1	FZD6	3	0.183	0.088	0.096	9.39E-03	3.65E-02
SNHG1	G3BP1	2	0.297	-0.004	0.302	1.00E-05	6.58E-04
SNHG1	GALNT3	2	0.185	0.094	0.091	7.05E-03	3.74E-02
SNHG1	GLO1	2	0.418	0.200	0.218	1.00E-05	1.56E-04
SNHG1	GRSF1	2	0.345	0.174	0.171	1.50E-04	2.59E-03
SNHG1	GTF3C2	1	0.380	0.268	0.113	4.26E-03	4.61E-02
SNHG1	GTF3C5	2	0.339	0.095	0.243	1.00E-05	6.58E-04
SNHG1	HDGF	1	0.320	0.109	0.210	1.30E-04	3.07E-02
SNHG1	HMBS	1	0.478	0.379	0.099	5.18E-03	3.61E-02
SNHG1	HMGA1	2	0.330	0.170	0.161	1.90E-04	2.67E-03
SNHG1	HMGB3	1	0.455	0.365	0.089	8.46E-03	4.83E-02
SNHG1	HMGCR	3	0.256	-0.028	0.284	1.00E-05	1.58E-04
SNHG1	HNRNPD	1	0.462	0.369	0.093	7.16E-03	4.38E-02

SNHG1	HSP90AA1	1	0.454	0.357	0.096	5.88E-03	3.87E-02
SNHG1	HSPA1B	2	0.223	0.046	0.177	2.00E-05	8.62E-04
SNHG1	HSPA4	3	0.224	0.061	0.162	1.70E-04	2.70E-03
SNHG1	HSPA5	2	0.208	-0.122	0.330	1.00E-05	6.53E-04
SNHG1	HSPA9	1	0.394	0.132	0.262	1.00E-05	1.11E-03
SNHG1	HSPE1	2	0.546	0.341	0.205	1.00E-05	6.89E-05
SNHG1	ILF2	1	0.471	0.344	0.127	1.27E-03	1.58E-02
SNHG1	ILF3	1	0.377	0.254	0.123	2.66E-03	3.70E-02
SNHG1	KIF11	3	0.558	0.416	0.142	7.00E-05	2.06E-04
SNHG1	KIF22	1	0.445	0.240	0.205	1.00E-05	1.11E-03
SNHG1	KIF23	3	0.517	0.230	0.287	1.00E-05	4.38E-05
SNHG1	KIFC1	1	0.369	0.209	0.159	4.20E-04	1.45E-02
SNHG1	KPNA2	3	0.451	0.269	0.182	1.00E-05	4.38E-05
SNHG1	KRT18	2	0.249	0.105	0.144	2.80E-04	5.36E-03
SNHG1	KTN1	2	0.302	0.195	0.107	3.60E-03	1.71E-02
SNHG1	LIG1	2	0.301	0.096	0.204	2.00E-05	8.44E-04
SNHG1	LMNB1	3	0.305	0.114	0.191	4.00E-05	5.57E-04
SNHG1	LRRC8B	2	0.308	0.018	0.291	1.00E-05	6.58E-04
SNHG1	LYPLA1	2	0.515	0.363	0.152	1.00E-05	6.89E-05
SNHG1	MAP3K4	2	0.151	0.044	0.107	2.68E-03	2.09E-02
SNHG1	MAPKAPK5	1	0.498	0.286	0.212	1.00E-05	6.97E-04
SNHG1	MCM4	1	0.385	0.259	0.126	2.29E-03	3.43E-02
SNHG1	MCM6	1	0.351	0.219	0.132	1.78E-03	3.09E-02
SNHG1	MCM7	2	0.320	0.154	0.165	1.70E-04	2.62E-03
SNHG1	MED17	2	0.438	0.306	0.132	4.70E-04	2.66E-03
SNHG1	MKI67	2	0.403	0.213	0.190	1.00E-05	1.56E-04
SNHG1	MTHFD1	1	0.265	0.097	0.168	7.30E-04	4.99E-02
SNHG1	MTHFD2	3	0.528	0.200	0.328	1.00E-05	4.38E-05
SNHG1	MYC	5	0.246	0.109	0.137	2.35E-03	1.42E-02
SNHG1	MYO6	2	0.322	0.218	0.104	4.05E-03	1.84E-02
SNHG1	NCAPD2	2	0.311	0.130	0.181	1.00E-04	2.20E-03
SNHG1	NCL	2	0.475	0.290	0.185	1.00E-05	6.89E-05
SNHG1	NDUFV1	2	0.203	0.107	0.096	5.20E-03	3.13E-02
SNHG1	NFYA	1	0.267	0.091	0.177	4.70E-04	4.16E-02
SNHG1	NME1	1	0.468	0.369	0.099	5.24E-03	3.62E-02
SNHG1	NOLC1	2	0.435	0.337	0.097	3.83E-03	1.22E-02
SNHG1	NONO	2	0.349	0.106	0.243	1.00E-05	6.58E-04
SNHG1	NOP56	1	0.576	0.463	0.114	1.29E-03	1.16E-02
SNHG1	NPM1	2	0.479	0.363	0.116	8.50E-04	3.19E-03
SNHG1	NRAS	2	0.270	0.115	0.155	2.70E-04	3.29E-03
SNHG1	NUP188	2	0.288	0.074	0.214	2.00E-05	8.44E-04
SNHG1	NUP205	2	0.331	0.169	0.162	1.80E-04	2.62E-03
SNHG1	NUP58	1	0.441	0.158	0.283	1.00E-05	1.11E-03
SNHG1	OTUD3	1	0.415	0.289	0.126	2.35E-03	3.45E-02
SNHG1	PLAGL2	3	0.182	0.062	0.120	2.50E-03	1.53E-02

SNHG1	PLK1	2	0.390	0.179	0.211	1.00E-05	1.56E-04
SNHG1	PMPCA	1	0.338	0.118	0.220	6.00E-05	2.32E-02
SNHG1	POLE	2	0.411	0.281	0.129	5.90E-04	3.21E-03
SNHG1	POLQ	2	0.523	0.457	0.066	1.90E-02	3.63E-02
SNHG1	POP1	1	0.398	0.276	0.122	2.85E-03	3.81E-02
SNHG1	PPAT	2	0.500	0.323	0.177	1.00E-05	6.89E-05
SNHG1	PPM1G	2	0.356	0.088	0.268	1.00E-05	1.56E-04
SNHG1	PPP1CC	1	0.441	0.263	0.178	1.40E-04	7.59E-03
SNHG1	PPP2CA	2	0.256	0.051	0.205	2.00E-05	8.44E-04
SNHG1	PRDX4	3	0.205	-0.024	0.229	1.00E-05	3.52E-04
SNHG1	PRPF4	1	0.378	0.256	0.122	2.82E-03	3.79E-02
SNHG1	PSMA7	2	0.300	0.139	0.161	1.90E-04	2.67E-03
SNHG1	PSMB6	2	0.260	0.138	0.122	1.55E-03	9.72E-03
SNHG1	PSMC2	2	0.236	0.153	0.083	1.03E-02	4.70E-02
SNHG1	PSMD11	1	0.305	0.079	0.226	4.00E-05	1.91E-02
SNHG1	PSMD14	2	0.549	0.415	0.134	1.90E-04	9.51E-04
SNHG1	PTBP3	1	0.321	0.066	0.255	1.00E-05	6.80E-03
SNHG1	PTGES3	2	0.533	0.266	0.267	1.00E-05	6.89E-05
SNHG1	PTMA	2	0.434	0.258	0.175	2.00E-05	2.47E-04
SNHG1	PTPN2	1	0.365	0.254	0.112	4.47E-03	4.71E-02
SNHG1	PTPN3	2	0.154	0.046	0.108	2.61E-03	2.06E-02
SNHG1	PUF60	1	0.260	0.055	0.205	1.50E-04	3.07E-02
SNHG1	PYCR1	1	0.277	0.032	0.245	1.00E-05	6.80E-03
SNHG1	RAB10	1	0.293	0.089	0.204	1.50E-04	3.07E-02
SNHG1	RAB11A	2	0.329	0.180	0.150	3.60E-04	3.95E-03
SNHG1	RAD23B	2	0.272	0.043	0.229	1.00E-05	6.58E-04
SNHG1	RANBP1	1	0.493	0.382	0.111	2.96E-03	2.61E-02
SNHG1	RCN1	2	0.150	0.061	0.089	7.55E-03	3.91E-02
SNHG1	RRP1	2	0.335	0.131	0.204	2.00E-05	8.44E-04
SNHG1	RRP9	1	0.373	0.219	0.154	5.40E-04	1.63E-02
SNHG1	RTN3	1	0.385	0.174	0.210	1.00E-05	1.11E-03
SNHG1	SCAMP3	3	0.155	-0.006	0.161	1.80E-04	2.80E-03
SNHG1	SCML1	3	0.438	0.326	0.112	2.09E-03	5.67E-03
SNHG1	SFPQ	1	0.443	0.322	0.120	2.99E-03	3.87E-02
SNHG1	SGTA	2	0.183	0.060	0.123	1.01E-03	1.16E-02
SNHG1	SIGMAR1	2	0.290	0.172	0.119	1.86E-03	1.11E-02
SNHG1	SLC1A5	3	0.215	-0.062	0.277	1.00E-05	3.52E-04
SNHG1	SLC25A1	2	0.129	-0.030	0.160	7.00E-05	2.00E-03
SNHG1	SLC25A17	2	0.421	0.268	0.153	1.00E-04	8.26E-04
SNHG1	SLC29A2	2	0.462	0.310	0.152	1.00E-05	6.89E-05
SNHG1	SLC7A5	3	0.213	-0.077	0.290	1.00E-05	3.52E-04
SNHG1	SMC1A	1	0.257	0.010	0.247	1.00E-05	6.80E-03
SNHG1	SNRPA	1	0.492	0.369	0.123	1.60E-03	1.84E-02
SNHG1	SNRPB	2	0.504	0.347	0.157	1.00E-05	6.89E-05
SNHG1	SOCS6	3	0.114	-0.077	0.191	2.00E-05	6.62E-04

SNHG1	SPATA2	3	0.217	0.115	0.102	6.70E-03	2.96E-02
SNHG1	SQLE	3	0.327	0.072	0.255	1.00E-05	1.58E-04
SNHG1	SRI	2	0.213	0.113	0.100	4.11E-03	2.72E-02
SNHG1	SRSF10	2	0.703	0.556	0.147	1.00E-05	2.90E-05
SNHG1	SSRP1	3	0.455	0.195	0.261	1.00E-05	4.38E-05
SNHG1	STAG2	2	0.309	0.223	0.086	9.98E-03	3.28E-02
SNHG1	STMN1	2	0.490	0.386	0.105	1.76E-03	5.68E-03
SNHG1	STXBP3	3	0.353	0.177	0.176	3.00E-05	2.04E-04
SNHG1	SUPV3L1	1	0.521	0.426	0.095	6.38E-03	4.07E-02
SNHG1	SUZ12	2	0.383	0.113	0.270	1.00E-05	1.56E-04
SNHG1	SYPL1	4	0.166	0.033	0.133	2.21E-03	1.35E-02
SNHG1	TACC3	1	0.376	0.240	0.136	1.50E-03	2.86E-02
SNHG1	TARBP1	1	0.398	0.268	0.130	1.96E-03	3.24E-02
SNHG1	TFAP4	1	0.367	0.252	0.114	3.93E-03	4.42E-02
SNHG1	TFDP1	1	0.452	0.354	0.098	5.33E-03	3.65E-02
SNHG1	TFG	3	0.208	-0.062	0.270	1.00E-05	3.52E-04
SNHG1	TIMM8A	1	0.459	0.356	0.104	4.20E-03	3.20E-02
SNHG1	TMF1	2	0.131	0.046	0.084	9.88E-03	4.56E-02
SNHG1	TMPO	1	0.369	0.260	0.109	5.00E-03	4.96E-02
SNHG1	TOMM20	3	0.336	0.223	0.113	5.03E-03	1.80E-02
SNHG1	TONSL	1	0.467	0.346	0.121	1.70E-03	1.88E-02
SNHG1	TOP2A	2	0.487	0.325	0.162	1.00E-05	6.89E-05
SNHG1	TRAP1	2	0.291	0.074	0.217	2.00E-05	8.44E-04
SNHG1	TRIP13	1	0.484	0.361	0.124	1.53E-03	1.78E-02
SNHG1	TTI1	3	0.285	0.102	0.184	7.00E-05	8.79E-04
SNHG1	TTK	2	0.535	0.430	0.105	1.70E-03	5.54E-03
SNHG1	TUBA1B	2	0.205	0.091	0.115	1.61E-03	1.49E-02
SNHG1	UNG	3	0.359	0.072	0.287	1.00E-05	8.47E-05
SNHG1	URB2	2	0.182	-0.016	0.198	1.00E-05	6.53E-04
SNHG1	USP1	1	0.439	0.205	0.233	1.00E-05	1.11E-03
SNHG1	USP39	1	0.387	0.236	0.151	6.70E-04	1.82E-02
SNHG1	VEGFA	3	0.276	0.028	0.248	1.00E-05	1.58E-04
SNHG1	VPS13A	2	0.222	0.116	0.106	2.81E-03	2.14E-02
SNHG1	WDR43	3	0.602	0.395	0.207	1.00E-05	3.73E-05
SNHG1	WDR5	2	0.391	0.237	0.154	9.00E-05	7.80E-04
SNHG1	YWHAQ	2	0.327	0.147	0.180	1.00E-04	2.20E-03
SNHG1	ZBTB33	2	0.294	0.136	0.157	2.30E-04	2.94E-03
SNHG1	ZBTB39	5	0.227	0.112	0.116	7.32E-03	2.49E-02
SNHG1	SNX14	1	0.290	0.116	0.174	5.40E-04	4.35E-02
SNHG1	SNX5	1	0.469	0.361	0.108	3.44E-03	2.86E-02
SNHG1	SRRT	1	0.387	0.251	0.136	1.50E-03	2.86E-02
SNHG1	STK35	3	0.262	0.171	0.090	1.54E-02	3.90E-02
SNHG1	STMP1	2	0.358	0.265	0.093	4.87E-03	1.45E-02
SNHG1	TBC1D31	1	0.498	0.275	0.223	1.00E-05	6.97E-04
SNHG1	TC2N	2	0.159	0.073	0.087	8.65E-03	4.21E-02

SNHG1	TDP1	1	0.426	0.288	0.138	1.32E-03	2.65E-02
SNHG1	TDP2	2	0.307	0.187	0.120	1.71E-03	1.05E-02
SNHG1	TIMM13	1	0.382	0.272	0.110	4.81E-03	4.86E-02
SNHG1	TMEM167A	2	0.218	0.085	0.133	5.30E-04	7.59E-03
SNHG1	TMEM181	2	0.173	0.080	0.093	6.05E-03	3.40E-02
SNHG1	TMEM199	1	0.278	0.082	0.195	2.10E-04	3.26E-02
SNHG1	TMEM41A	3	0.366	0.211	0.155	1.10E-04	5.43E-04
SNHG1	TMEM87A	2	0.268	0.127	0.141	4.80E-04	4.46E-03
SNHG1	TMEM87B	2	0.205	0.123	0.082	1.14E-02	4.96E-02
SNHG1	TMUB1	2	0.126	-0.033	0.159	9.00E-05	2.44E-03
SNHG1	TOR2A	2	0.122	-0.107	0.229	1.00E-05	6.53E-04
SNHG1	TRIAP1	2	0.393	0.293	0.100	3.23E-03	1.08E-02
SNHG1	TRIM59	2	0.351	0.280	0.071	1.80E-02	3.88E-02
SNHG1	TRMT10C	2	0.441	0.360	0.081	9.91E-03	2.47E-02
SNHG1	TRMT6	1	0.443	0.330	0.112	4.37E-03	4.68E-02
SNHG1	TRMU	1	0.451	0.335	0.117	2.19E-03	2.19E-02
SNHG1	UBN2	3	0.270	0.164	0.106	7.21E-03	2.31E-02
SNHG1	UBXN11	2	0.347	0.256	0.091	7.80E-03	2.77E-02
SNHG1	UCKL1	1	0.452	0.325	0.127	1.26E-03	1.58E-02
SNHG1	UTP15	2	0.260	0.011	0.249	1.00E-05	6.58E-04
SNHG1	VMA21	3	0.370	0.142	0.228	1.00E-05	8.47E-05
SNHG1	WDR77	1	0.360	0.216	0.144	9.80E-04	2.28E-02
SNHG1	YEATS2	2	0.140	-0.058	0.197	1.00E-05	6.53E-04
SNHG1	YRDC	4	0.315	0.003	0.312	1.00E-05	1.36E-04
SNHG1	ZCCHC3	2	0.287	0.145	0.142	4.60E-04	4.33E-03
SNHG1	ZCCHC8	1	0.537	0.388	0.149	4.60E-04	9.48E-03
SNHG1	ZIC5	2	0.153	0.052	0.100	4.06E-03	2.70E-02
SNHG15	KMT5A	1	0.366	0.255	0.111	4.59E-03	4.75E-02
SNHG15	MZT1	1	0.503	0.406	0.097	5.60E-03	3.75E-02
SNHG15	ACP1	1	0.520	0.402	0.118	2.01E-03	2.07E-02
SNHG15	AEN	2	0.267	0.165	0.103	4.34E-03	1.92E-02
SNHG15	AHCY	1	0.456	0.330	0.126	1.32E-03	1.63E-02
SNHG15	ALYREF	1	0.407	0.274	0.133	1.73E-03	3.04E-02
SNHG15	ANLN	1	0.465	0.355	0.110	3.08E-03	2.67E-02
SNHG15	ANP32A	1	0.454	0.334	0.119	1.90E-03	2.02E-02
SNHG15	APEX1	1	0.469	0.344	0.125	1.44E-03	1.71E-02
SNHG15	ARL6IP6	1	0.502	0.402	0.100	5.07E-03	3.56E-02
SNHG15	ASF1B	1	0.479	0.345	0.135	9.70E-04	1.42E-02
SNHG15	ATIC	1	0.473	0.370	0.102	4.46E-03	3.31E-02
SNHG15	BCS1L	1	0.506	0.397	0.109	3.29E-03	2.79E-02
SNHG15	BIRC5	1	0.416	0.269	0.148	7.60E-04	1.94E-02
SNHG15	BUB1	1	0.406	0.291	0.115	3.85E-03	4.38E-02
SNHG15	BUB1B	1	0.438	0.324	0.114	3.97E-03	4.42E-02
SNHG15	BUB3	1	0.491	0.397	0.094	6.58E-03	4.15E-02
SNHG15	C19orf48	1	0.537	0.428	0.109	3.23E-03	2.75E-02

SNHG15	CCT3	2	0.451	0.275	0.176	1.00E-05	6.89E-05
SNHG15	CCT7	1	0.526	0.421	0.105	3.97E-03	3.11E-02
SNHG15	CDC25A	2	0.460	0.254	0.206	1.00E-05	6.89E-05
SNHG15	CDC6	2	0.435	0.262	0.173	2.00E-05	2.47E-04
SNHG15	CDCA5	1	0.458	0.309	0.149	4.50E-04	9.39E-03
SNHG15	CDCA8	2	0.441	0.242	0.199	1.00E-05	1.56E-04
SNHG15	CDK1	1	0.490	0.373	0.117	2.11E-03	2.14E-02
SNHG15	CENPF	1	0.336	0.168	0.168	7.50E-04	4.99E-02
SNHG15	CENPM	1	0.428	0.300	0.128	2.13E-03	3.32E-02
SNHG15	CENPN	1	0.377	0.247	0.130	1.96E-03	3.24E-02
SNHG15	CHAF1A	1	0.428	0.302	0.126	2.32E-03	3.43E-02
SNHG15	CHD7	1	0.350	0.221	0.130	2.01E-03	3.25E-02
SNHG15	CKAP2	2	0.434	0.317	0.117	1.21E-03	5.35E-03
SNHG15	CLN6	2	0.454	0.303	0.151	2.00E-05	1.32E-04
SNHG15	CNPY2	1	0.479	0.382	0.097	5.80E-03	3.83E-02
SNHG15	CPSF1	1	0.361	0.239	0.122	2.81E-03	3.79E-02
SNHG15	CSE1L	1	0.416	0.297	0.119	3.16E-03	3.96E-02
SNHG15	CYC1	1	0.431	0.313	0.118	3.32E-03	4.04E-02
SNHG15	CYHR1	1	0.409	0.298	0.111	4.57E-03	4.74E-02
SNHG15	DAZAP1	1	0.479	0.369	0.110	3.07E-03	2.67E-02
SNHG15	DCTPP1	2	0.280	0.149	0.131	8.70E-04	6.68E-03
SNHG15	DDX39A	1	0.490	0.371	0.119	1.91E-03	2.02E-02
SNHG15	DDX52	2	0.214	0.074	0.140	3.50E-04	5.78E-03
SNHG15	DHRS13	1	0.308	0.141	0.167	7.60E-04	4.99E-02
SNHG15	DPM2	2	0.513	0.411	0.102	2.16E-03	6.70E-03
SNHG15	EIF2B4	1	0.424	0.314	0.110	4.81E-03	4.86E-02
SNHG15	EIF6	1	0.492	0.397	0.095	6.38E-03	4.07E-02
SNHG15	FAM136A	1	0.612	0.507	0.105	2.16E-03	1.66E-02
SNHG15	FAM49B	2	0.379	0.203	0.176	2.00E-05	2.47E-04
SNHG15	FANCI	1	0.420	0.304	0.117	3.52E-03	4.18E-02
SNHG15	FKBPL	1	0.381	0.261	0.119	3.11E-03	3.92E-02
SNHG15	GIT1	2	0.338	0.207	0.131	9.20E-04	6.92E-03
SNHG15	GMNN	1	0.448	0.305	0.144	1.02E-03	2.35E-02
SNHG15	GNL3	1	0.446	0.337	0.109	4.92E-03	4.91E-02
SNHG15	GPN1	1	0.462	0.367	0.095	6.34E-03	4.05E-02
SNHG15	GTF3C2	1	0.366	0.247	0.119	3.23E-03	3.99E-02
SNHG15	HMBS	1	0.526	0.434	0.093	7.29E-03	4.44E-02
SNHG15	HMGB2	1	0.452	0.349	0.104	4.14E-03	3.18E-02
SNHG15	HNRNPF	1	0.456	0.359	0.097	5.70E-03	3.78E-02
SNHG15	ILF2	1	0.440	0.301	0.139	1.27E-03	2.59E-02
SNHG15	INO80E	2	0.309	0.232	0.077	1.59E-02	4.42E-02
SNHG15	KIF11	1	0.433	0.317	0.116	3.63E-03	4.24E-02
SNHG15	KIFC1	1	0.428	0.280	0.149	7.00E-04	1.85E-02
SNHG15	KPNA2	1	0.422	0.289	0.132	1.77E-03	3.08E-02
SNHG15	LIG1	2	0.315	0.126	0.189	7.00E-05	1.89E-03

SNHG15	LMNB1	2	0.317	0.126	0.190	5.00E-05	1.46E-03
SNHG15	LMNB2	1	0.399	0.273	0.126	2.32E-03	3.43E-02
SNHG15	MAD2L1	1	0.492	0.377	0.115	2.34E-03	2.28E-02
SNHG15	MAIP1	1	0.377	0.267	0.111	4.65E-03	4.78E-02
SNHG15	MCM4	1	0.358	0.222	0.136	1.51E-03	2.86E-02
SNHG15	MCM7	2	0.415	0.288	0.126	6.90E-04	3.54E-03
SNHG15	MIF	1	0.494	0.402	0.092	7.58E-03	4.55E-02
SNHG15	MRPS26	1	0.529	0.418	0.111	2.96E-03	2.61E-02
SNHG15	MTHFD1	1	0.365	0.241	0.124	2.58E-03	3.63E-02
SNHG15	MTHFD2	1	0.472	0.365	0.107	3.51E-03	2.87E-02
SNHG15	MYC	3	0.346	0.238	0.108	6.48E-03	2.15E-02
SNHG15	NCAPD2	2	0.264	0.084	0.180	1.00E-04	2.20E-03
SNHG15	NCAPG2	1	0.387	0.242	0.145	9.00E-04	2.16E-02
SNHG15	NCL	1	0.421	0.295	0.126	2.31E-03	3.43E-02
SNHG15	NDUFB9	2	0.456	0.356	0.100	2.42E-03	7.31E-03
SNHG15	NELFCD	1	0.441	0.309	0.132	1.82E-03	3.11E-02
SNHG15	NOLC1	1	0.368	0.254	0.113	4.13E-03	4.53E-02
SNHG15	NONO	1	0.391	0.276	0.114	3.96E-03	4.42E-02
SNHG15	NOP56	1	0.637	0.537	0.100	2.91E-03	2.05E-02
SNHG15	NUDCD1	1	0.452	0.347	0.105	3.94E-03	3.10E-02
SNHG15	NUP205	2	0.219	0.047	0.172	3.00E-05	1.11E-03
SNHG15	NUP37	1	0.507	0.411	0.096	5.91E-03	3.88E-02
SNHG15	NUSAP1	1	0.469	0.344	0.125	1.38E-03	1.67E-02
SNHG15	PATL1	1	0.361	0.248	0.113	4.14E-03	4.53E-02
SNHG15	PDRG1	1	0.490	0.380	0.110	3.07E-03	2.67E-02
SNHG15	PGAP2	1	0.497	0.369	0.128	1.22E-03	1.54E-02
SNHG15	PLAGL2	3	0.135	0.005	0.130	1.20E-03	9.16E-03
SNHG15	PLK1	2	0.426	0.238	0.188	1.00E-05	1.56E-04
SNHG15	POLD2	1	0.623	0.542	0.082	8.37E-03	4.20E-02
SNHG15	POLR1B	1	0.480	0.374	0.106	3.69E-03	2.97E-02
SNHG15	POLR3K	1	0.428	0.318	0.110	4.72E-03	4.82E-02
SNHG15	POP7	1	0.488	0.391	0.097	5.81E-03	3.84E-02
SNHG15	POU2F1	2	0.149	0.040	0.108	2.52E-03	2.01E-02
SNHG15	PPAT	1	0.459	0.342	0.117	2.10E-03	2.13E-02
SNHG15	PPIL1	1	0.413	0.297	0.116	3.64E-03	4.24E-02
SNHG15	PPM1G	1	0.479	0.365	0.114	2.54E-03	2.41E-02
SNHG15	PROSER1	1	0.358	0.239	0.119	3.11E-03	3.92E-02
SNHG15	PRPF19	1	0.426	0.289	0.137	1.40E-03	2.75E-02
SNHG15	PRPF4	1	0.443	0.331	0.112	4.38E-03	4.68E-02
SNHG15	PTDSS1	1	0.395	0.263	0.132	1.80E-03	3.11E-02
SNHG15	PTGES3	1	0.460	0.356	0.104	4.11E-03	3.16E-02
SNHG15	PUS1	1	0.566	0.473	0.093	4.39E-03	2.71E-02
SNHG15	RACGAP1	1	0.429	0.291	0.138	1.31E-03	2.64E-02
SNHG15	RAD21	1	0.382	0.268	0.114	3.94E-03	4.42E-02
SNHG15	RANBP1	1	0.464	0.364	0.100	5.11E-03	3.58E-02

SNHG15	RCC1	1	0.407	0.277	0.130	1.97E-03	3.25E-02
SNHG15	REPIN1	3	0.278	0.102	0.176	1.10E-04	1.15E-03
SNHG15	RRP1	2	0.453	0.289	0.164	1.00E-05	6.89E-05
SNHG15	RRP9	1	0.534	0.417	0.117	2.06E-03	2.10E-02
SNHG15	RRS1	1	0.485	0.382	0.102	4.46E-03	3.31E-02
SNHG15	SAMD1	1	0.405	0.282	0.122	2.79E-03	3.78E-02
SNHG15	SAPCD2	1	0.512	0.395	0.117	2.17E-03	2.18E-02
SNHG15	SELENOH	1	0.403	0.284	0.119	3.11E-03	3.92E-02
SNHG15	SF3B4	1	0.367	0.256	0.110	4.70E-03	4.80E-02
SNHG15	SFPQ	1	0.372	0.232	0.140	1.22E-03	2.53E-02
SNHG15	SGTA	1	0.382	0.272	0.109	4.89E-03	4.91E-02
SNHG15	SKA1	1	0.397	0.268	0.128	2.11E-03	3.32E-02
SNHG15	**SNHG1**	2	0.624	0.516	0.108	4.80E-04	1.51E-03
SNHG15	SNRPA	1	0.557	0.447	0.111	1.53E-03	1.31E-02
SNHG15	SORD	1	0.353	0.216	0.138	1.35E-03	2.68E-02
SNHG15	SRRT	1	0.454	0.329	0.125	1.43E-03	1.71E-02
SNHG15	SRSF7	1	0.577	0.485	0.092	4.50E-03	2.75E-02
SNHG15	SSRP1	1	0.417	0.267	0.150	6.80E-04	1.82E-02
SNHG15	STMN1	1	0.494	0.364	0.130	1.10E-03	1.48E-02
SNHG15	TACC3	1	0.391	0.254	0.137	1.44E-03	2.81E-02
SNHG15	TEDC1	1	0.418	0.308	0.110	4.80E-03	4.86E-02
SNHG15	TFDP1	2	0.442	0.334	0.108	2.04E-03	7.69E-03
SNHG15	TIMM13	2	0.520	0.445	0.075	1.16E-02	2.46E-02
SNHG15	TIMM8A	1	0.501	0.403	0.098	5.43E-03	3.69E-02
SNHG15	TMUB1	1	0.407	0.278	0.128	2.11E-03	3.32E-02
SNHG15	TONSL	1	0.460	0.333	0.127	1.26E-03	1.58E-02
SNHG15	TOP2A	2	0.425	0.256	0.169	3.00E-05	3.62E-04
SNHG15	TOR2A	2	0.373	0.222	0.151	1.00E-04	8.26E-04
SNHG15	TPX2	1	0.489	0.367	0.121	1.69E-03	1.88E-02
SNHG15	TRIP13	1	0.475	0.345	0.130	1.10E-03	1.48E-02
SNHG15	TRMT6	1	0.488	0.382	0.106	3.72E-03	2.98E-02
SNHG15	TRMU	1	0.404	0.273	0.130	1.94E-03	3.22E-02
SNHG15	TUBB4B	1	0.514	0.406	0.108	3.46E-03	2.86E-02
SNHG15	U2AF2	2	0.341	0.226	0.115	2.26E-03	1.26E-02
SNHG15	UNG	1	0.358	0.179	0.180	1.30E-04	7.59E-03
SNHG15	USP39	1	0.502	0.376	0.126	1.33E-03	1.64E-02
SNHG15	UTP4	1	0.473	0.381	0.092	7.65E-03	4.57E-02
SNHG15	WDR77	1	0.382	0.239	0.143	1.04E-03	2.37E-02
SNHG15	WRNIP1	2	0.377	0.255	0.122	9.40E-04	4.44E-03
SNHG15	YRDC	1	0.456	0.359	0.097	5.76E-03	3.81E-02
SNHG15	ZCCHC3	1	0.367	0.232	0.135	1.59E-03	2.91E-02
SNHG15	ZNF768	2	0.104	-0.012	0.116	1.50E-03	1.43E-02
SNHG17	AGO2	2	0.104	-0.047	0.151	1.60E-04	3.69E-03
SNHG17	ANLN	3	0.362	0.125	0.237	1.00E-05	8.47E-05
SNHG17	ARL5B	2	0.118	-0.054	0.172	3.00E-05	1.11E-03

SNHG17	ATF1	2	0.181	0.064	0.117	1.40E-03	1.38E-02
SNHG17	BIRC5	2	0.379	0.211	0.168	4.00E-05	4.49E-04
SNHG17	BUB3	1	0.390	0.267	0.123	2.72E-03	3.75E-02
SNHG17	C6orf62	2	0.150	0.011	0.139	3.50E-04	5.78E-03
SNHG17	CCT4	2	0.386	0.258	0.128	6.60E-04	3.51E-03
SNHG17	CDC6	2	0.420	0.265	0.154	9.00E-05	7.80E-04
SNHG17	CDK2AP1	2	0.166	0.083	0.084	1.01E-02	4.62E-02
SNHG17	CENPF	2	0.380	0.185	0.196	1.00E-05	1.56E-04
SNHG17	CENPN	1	0.370	0.228	0.142	1.09E-03	2.41E-02
SNHG17	CLPTM1L	2	0.173	0.051	0.122	1.10E-03	1.20E-02
SNHG17	CSE1L	2	0.510	0.381	0.128	3.40E-04	1.56E-03
SNHG17	DDX21	2	0.258	0.089	0.169	1.60E-04	2.62E-03
SNHG17	EIF2AK1	1	0.492	0.386	0.106	3.82E-03	3.04E-02
SNHG17	FAM91A1	2	0.292	0.124	0.168	1.60E-04	2.62E-03
SNHG17	FARSB	2	0.351	0.236	0.115	1.46E-03	6.18E-03
SNHG17	FZD6	2	0.131	0.009	0.122	1.06E-03	1.18E-02
SNHG17	G3BP1	2	0.149	-0.046	0.195	1.00E-05	6.53E-04
SNHG17	GMNN	2	0.428	0.287	0.141	2.00E-04	1.34E-03
SNHG17	HM13	1	0.441	0.328	0.112	4.36E-03	4.68E-02
SNHG17	HSP90AA1	1	0.355	0.244	0.111	4.57E-03	4.74E-02
SNHG17	HSPH1	2	0.292	0.149	0.143	4.50E-04	4.29E-03
SNHG17	IGF2BP1	2	0.270	0.196	0.074	1.81E-02	4.81E-02
SNHG17	KIF23	2	0.405	0.224	0.181	1.00E-05	1.56E-04
SNHG17	MAD2L1	2	0.431	0.253	0.178	2.00E-05	2.47E-04
SNHG17	MAL2	2	0.277	0.158	0.119	1.82E-03	1.09E-02
SNHG17	MYBL2	2	0.517	0.403	0.114	9.50E-04	3.50E-03
SNHG17	MYO1B	2	0.125	-0.011	0.136	3.80E-04	6.02E-03
SNHG17	NCAPG2	2	0.314	0.105	0.209	2.00E-05	8.44E-04
SNHG17	NUSAP1	1	0.421	0.267	0.154	5.30E-04	1.61E-02
SNHG17	PMAIP1	2	0.235	0.118	0.117	1.42E-03	1.39E-02
SNHG17	PROSER1	3	0.420	0.258	0.162	7.00E-05	3.66E-04
SNHG17	RRM2	2	0.337	0.168	0.169	1.60E-04	2.62E-03
SNHG17	SCD	2	0.186	-0.012	0.198	1.00E-05	6.53E-04
SNHG17	SLC20A1	2	0.284	0.144	0.141	4.90E-04	4.50E-03
SNHG17	SLC37A4	2	0.404	0.291	0.113	1.55E-03	6.39E-03
SNHG17	SLC7A5	2	0.214	0.064	0.149	1.90E-04	4.20E-03
SNHG17	SLC7A6	2	0.158	0.046	0.112	2.06E-03	1.79E-02
SNHG17	TBRG4	1	0.451	0.350	0.101	4.89E-03	3.49E-02
SNHG17	TENT4A	2	0.179	0.035	0.144	2.80E-04	5.36E-03
SNHG17	TPX2	1	0.571	0.466	0.105	2.13E-03	1.64E-02
SNHG17	TRMT10C	2	0.325	0.209	0.116	2.11E-03	1.20E-02
SNHG17	TWNK	2	0.348	0.240	0.108	3.32E-03	1.61E-02
SNHG17	TYMS	2	0.264	0.115	0.149	3.60E-04	3.95E-03
SNHG17	UTP23	2	0.283	0.190	0.093	6.83E-03	2.55E-02
SNHG17	VEGFA	2	0.347	0.230	0.117	2.00E-03	1.16E-02

SNHG17	YWHAG	2	0.129	-0.032	0.161	7.00E-05	2.00E-03
SNHG17	YWHAZ	2	0.390	0.240	0.149	1.20E-04	9.37E-04
SNHG3	ANKRD46	2	0.314	0.201	0.113	2.49E-03	1.34E-02
SNHG3	CDCA8	2	0.354	0.263	0.091	5.51E-03	1.58E-02
SNHG3	CLN6	2	0.198	0.104	0.094	5.88E-03	3.36E-02
SNHG3	GMNN	2	0.326	0.228	0.098	5.36E-03	2.17E-02
SNHG3	MRPS2	2	0.339	0.263	0.076	1.65E-02	4.52E-02
SNHG3	NCAPD2	2	0.181	0.094	0.087	8.38E-03	4.14E-02
SNHG3	NOLC1	2	0.302	0.222	0.081	1.31E-02	3.91E-02
SNHG3	NUP107	2	0.358	0.254	0.104	2.57E-03	9.06E-03
SNHG3	PILRB	2	0.390	0.318	0.071	1.74E-02	3.79E-02
SNHG3	PKMYT1	3	0.270	0.175	0.095	1.24E-02	3.38E-02
SNHG3	PRMT5	2	0.280	0.202	0.078	1.47E-02	4.21E-02
SNHG3	PTDSS1	2	0.179	0.074	0.105	3.03E-03	2.25E-02
SNHG3	PUS1	2	0.407	0.335	0.072	1.67E-02	3.67E-02
SNHG3	RCC2	2	0.240	0.144	0.096	5.17E-03	3.13E-02
SNHG3	SCAMP3	2	0.131	0.037	0.095	5.54E-03	3.22E-02
SNHG3	SF3B4	2	0.233	0.140	0.093	6.09E-03	3.42E-02
SNHG3	**SNHG12**	4	0.774	0.724	0.050	4.06E-03	4.77E-03
SNHG3	CCNF	2	0.238	0.140	0.098	4.66E-03	2.92E-02
SNHG3	CYC1	2	0.291	0.209	0.082	1.24E-02	3.78E-02
SNHG3	ENO1	2	0.245	0.157	0.088	8.20E-03	4.10E-02
SNHG3	KPNA2	2	0.364	0.275	0.089	6.14E-03	1.72E-02
SNHG3	MCM7	2	0.186	0.080	0.107	2.73E-03	2.11E-02
SNHG3	MSH6	2	0.115	0.021	0.094	5.77E-03	3.32E-02
SNHG3	POLE	3	0.268	0.154	0.113	4.92E-03	1.77E-02
SNHG3	RCC1	2	0.337	0.252	0.086	1.04E-02	3.37E-02
SNHG3	TOP2A	2	0.338	0.253	0.085	1.08E-02	3.46E-02
SNHG3	UMPS	2	0.268	0.188	0.080	1.39E-02	4.05E-02
SNHG3	XPO1	2	0.416	0.342	0.074	1.50E-02	3.39E-02
SNHG3	WDR77	2	0.338	0.260	0.078	1.49E-02	4.26E-02
SNHG3	ZCCHC3	2	0.234	0.142	0.092	6.40E-03	3.53E-02
SNHG3	ZNF37BP	2	0.243	0.145	0.098	4.62E-03	2.90E-02
SNHG3	ZNF587	2	0.127	0.041	0.086	8.74E-03	4.24E-02
SNHG7	ARL6IP6	2	0.271	0.171	0.100	4.86E-03	2.04E-02
SNHG7	CDCA5	2	0.261	0.130	0.131	8.90E-04	6.78E-03
SNHG7	DTD1	2	0.239	0.156	0.083	1.07E-02	4.79E-02
SNHG7	SAPCD2	2	0.435	0.358	0.078	1.25E-02	2.95E-02
SNHG7	**SNHG6**	2	0.570	0.514	0.056	2.04E-02	3.51E-02
SNHG7	CCNF	3	0.169	0.044	0.125	1.75E-03	1.20E-02
SNHG7	CCT3	2	0.375	0.246	0.128	6.50E-04	3.48E-03
SNHG7	CDC25A	2	0.243	0.103	0.140	3.40E-04	5.78E-03
SNHG7	CDK1	2	0.292	0.185	0.107	3.51E-03	1.68E-02
SNHG7	CDK5R1	2	0.102	0.019	0.083	1.09E-02	4.85E-02
SNHG7	CENPM	2	0.275	0.169	0.106	3.71E-03	1.74E-02

SNHG7	CHD7	2	0.298	0.182	0.116	2.13E-03	1.20E-02
SNHG7	CKAP2	3	0.348	0.243	0.106	7.22E-03	2.32E-02
SNHG7	CLN6	2	0.274	0.138	0.136	7.60E-04	6.31E-03
SNHG7	CRLS1	2	0.296	0.192	0.104	4.12E-03	1.86E-02
SNHG7	FANCI	2	0.152	0.037	0.115	1.58E-03	1.47E-02
SNHG7	IDH2	2	0.108	0.025	0.083	1.06E-02	4.79E-02
SNHG7	IGF2BP1	2	0.103	-0.010	0.113	1.86E-03	1.67E-02
SNHG7	KIFC1	2	0.275	0.146	0.129	9.90E-04	7.22E-03
SNHG7	LMNB1	3	0.171	0.068	0.103	6.39E-03	2.86E-02
SNHG7	MOCS3	3	0.139	0.022	0.117	2.83E-03	1.66E-02
SNHG7	NCAPD2	2	0.181	0.068	0.112	2.00E-03	1.75E-02
SNHG7	NOLC1	2	0.282	0.207	0.075	1.72E-02	4.64E-02
SNHG7	NUDCD1	2	0.281	0.169	0.112	2.65E-03	1.39E-02
SNHG7	PFDN2	2	0.384	0.294	0.090	5.73E-03	1.63E-02
SNHG7	POLD2	2	0.359	0.248	0.111	1.73E-03	6.85E-03
SNHG7	RACGAP1	2	0.256	0.124	0.132	8.50E-04	6.55E-03
SNHG7	**SNHG1**	3	0.464	0.391	0.073	1.83E-02	2.93E-02
SNHG7	SQLE	2	0.151	0.002	0.149	2.00E-04	4.30E-03
SNHG7	STMN1	2	0.372	0.286	0.086	7.30E-03	1.97E-02
SNHG7	TOP2A	2	0.227	0.110	0.117	1.39E-03	1.38E-02
SNHG7	TRIP13	2	0.292	0.169	0.123	1.41E-03	9.16E-03
SNHG7	WDR77	2	0.236	0.110	0.126	8.50E-04	1.03E-02

miRNA	Coefficient	miRNA target
hsa-let-7g	-0.446	MSL3P1
hsa-let-7g	-0.192	PKMYT1
hsa-let-7g	-0.169	CYC1
hsa-let-7g	-0.168	PRMT5
hsa-let-7g	-0.153	CDCA8
hsa-let-7g	-0.146	RCC1
hsa-let-7g	-0.145	MRPS2
hsa-let-7g	-0.144	AURKA
hsa-let-7g	-0.143	ENO1
hsa-let-7g	-0.141	GRPEL2
hsa-let-7g	-0.137	TOP2A
hsa-let-7g	-0.135	TRIB3
hsa-let-7g	-0.131	SNHG3
hsa-let-7g	-0.130	UMPS
hsa-let-7g	-0.120	DPM2
hsa-let-7g	-0.120	MEN1
hsa-let-7g	-0.112	CTPS1
hsa-let-7g	-0.103	IGF2BP1
hsa-let-7g	-0.102	NOLC1
hsa-let-7g	-0.091	CCNF
hsa-let-7g	-0.090	BLM
hsa-let-7g	-0.089	MSH6
hsa-let-7g	-0.087	POLQ
hsa-let-7g	-0.084	RAD54B
hsa-let-7g	-0.081	CSNK1E
hsa-let-7g	-0.079	HSPH1
hsa-let-7g	-0.072	SCAMP3
hsa-let-7g	-0.069	PUS1
hsa-let-7g	-0.068	LRRC8B
hsa-let-7g	-0.068	TOMM20
hsa-let-7g	-0.068	GLO1
hsa-let-7g	-0.062	RCC2
hsa-let-7g	-0.061	KPNA2
hsa-let-7g	-0.058	SF3B4
hsa-let-7g	-0.056	LIN7C
hsa-let-7g	-0.056	GMNN
hsa-let-7g	-0.055	SMC1A
hsa-let-7g	-0.055	NCAPD2
hsa-let-7g	-0.054	XPO1
hsa-let-7g	-0.051	MAD2L1
hsa-let-7i	-0.904	WNK2
hsa-let-7i	-0.586	CMTM8
hsa-let-7i	-0.383	C17orf100
hsa-let-7i	-0.362	C6orf136

hsa-let-7i	-0.327	PLAGL2
hsa-let-7i	-0.232	TRIB3
hsa-let-7i	-0.190	EIF2AK1
hsa-let-7i	-0.173	NELFCD
hsa-let-7i	-0.167	SPRYD4
hsa-let-7i	-0.165	SIGMAR1
hsa-let-7i	-0.151	MOCS3
hsa-let-7i	-0.150	PLEKHA1
hsa-let-7i	-0.141	ZNF587
hsa-let-7i	-0.128	NAA20
hsa-let-7i	-0.126	NR6A1
hsa-let-7i	-0.119	BLM
hsa-let-7i	-0.117	SLC25A39
hsa-let-7i	-0.113	CNOT11
hsa-let-7i	-0.109	TOMM20
hsa-let-7i	-0.107	RAD54B
hsa-let-7i	-0.105	CUL2
hsa-let-7i	-0.101	PVR
hsa-let-7i	-0.096	SRSF10
hsa-let-7i	-0.095	TTI1
hsa-let-7i	-0.093	GPSM2
hsa-let-7i	-0.089	AURKA
hsa-let-7i	-0.087	CDCA8
hsa-let-7i	-0.082	SF3B4
hsa-let-7i	-0.081	SLC37A4
hsa-let-7i	-0.079	CENPA
hsa-let-7i	-0.076	SBNO1
hsa-let-7i	-0.076	DSP
hsa-let-7i	-0.075	DNAAF5
hsa-let-7i	-0.074	ENO1
hsa-let-7i	-0.073	ANKRD46
hsa-let-7i	-0.070	MEN1
hsa-let-7i	-0.070	SPATA2
hsa-let-7i	-0.067	FBXO45
hsa-let-7i	-0.067	TOP2A
hsa-let-7i	-0.065	HSPA14
hsa-let-7i	-0.063	GMNN
hsa-let-7i	-0.062	ZCCHC3
hsa-let-7i	-0.056	RAB11A
hsa-let-7i	-0.054	CHD7
hsa-let-7i	-0.054	GLO1
hsa-let-7i	-0.054	MAPKAPK5-AS1
hsa-let-7i	-0.054	PUS1
hsa-let-7i	-0.051	SCAMP3
hsa-let-7i	-0.050	E2F3

hsa-miR-1226	-0.091	SNHG7
hsa-miR-125a	-0.393	GINS3
hsa-miR-125a	-0.289	POP1
hsa-miR-125a	-0.279	BUB1B
hsa-miR-125a	-0.255	VPS13A
hsa-miR-125a	-0.233	NPM1
hsa-miR-125a	-0.202	SUPV3L1
hsa-miR-125a	-0.199	BUB1
hsa-miR-125a	-0.195	MTHFD1
hsa-miR-125a	-0.157	PTPN2
hsa-miR-125a	-0.151	TOR2A
hsa-miR-125a	-0.149	TOP2A
hsa-miR-125a	-0.147	CDC6
hsa-miR-125a	-0.139	MTHFD1L
hsa-miR-125a	-0.137	PLK1
hsa-miR-125a	-0.131	SGO2
hsa-miR-125a	-0.130	ZBTB33
hsa-miR-125a	-0.129	CTPS1
hsa-miR-125a	-0.127	CDCA8
hsa-miR-125a	-0.122	RRP1
hsa-miR-125a	-0.118	GPSM2
hsa-miR-125a	-0.118	TIMM13
hsa-miR-125a	-0.117	RANBP1
hsa-miR-125a	-0.117	NUP37
hsa-miR-125a	-0.117	FAM120A
hsa-miR-125a	-0.115	MKI67
hsa-miR-125a	-0.113	SINHCAF
hsa-miR-125a	-0.110	TUBA1B
hsa-miR-125a	-0.102	NCAPD2
hsa-miR-125a	-0.101	CAPZA1
hsa-miR-125a	-0.101	GTF3C5
hsa-miR-125a	-0.100	AEN
hsa-miR-125a	-0.099	PLAGL2
hsa-miR-125a	-0.097	ADIPOR2
hsa-miR-125a	-0.096	SNHG15
hsa-miR-125a	-0.096	YWHAQ
hsa-miR-125a	-0.092	MTHFD2
hsa-miR-125a	-0.086	MYC
hsa-miR-125a	-0.084	DDX52
hsa-miR-125a	-0.084	NAA15
hsa-miR-125a	-0.082	HMGB3
hsa-miR-125a	-0.080	PRRG4
hsa-miR-125a	-0.080	CEP128
hsa-miR-125a	-0.079	LIG1
hsa-miR-125a	-0.079	CDC25A

hsa-miR-125a	-0.077	SNHG1
hsa-miR-125a	-0.077	YRDC
hsa-miR-125a	-0.076	LYPLA1
hsa-miR-125a	-0.075	UBN2
hsa-miR-125a	-0.075	DPM2
hsa-miR-125a	-0.075	RAB11A
hsa-miR-125a	-0.074	HSPA4
hsa-miR-125a	-0.073	TRIAP1
hsa-miR-125a	-0.073	NUP205
hsa-miR-125a	-0.071	LIN7C
hsa-miR-125a	-0.071	HNRNPD
hsa-miR-125a	-0.071	SNX5
hsa-miR-125a	-0.068	NME1
hsa-miR-125a	-0.068	REPIN1
hsa-miR-125a	-0.067	LCLAT1
hsa-miR-125a	-0.067	LMNB1
hsa-miR-125a	-0.067	AGPS
hsa-miR-125a	-0.065	SBNO1
hsa-miR-125a	-0.063	BTBD1
hsa-miR-125a	-0.061	CLN6
hsa-miR-125a	-0.061	CHD1
hsa-miR-125a	-0.059	NRAS
hsa-miR-125a	-0.059	WDR5
hsa-miR-125a	-0.058	STXBP3
hsa-miR-125a	-0.058	CUL1
hsa-miR-125a	-0.056	PTGES3
hsa-miR-125a	-0.055	DHX9
hsa-miR-125a	-0.055	DYNLT1
hsa-miR-125a	-0.053	FBXO45
hsa-miR-125a	-0.052	GRSF1
hsa-miR-125a	-0.051	LARP4
hsa-miR-125a	-0.051	PPP2CA
hsa-miR-125a	-0.050	PSMD14
hsa-miR-125a	-0.050	AMD1
hsa-miR-1306	-0.097	SNHG3
hsa-miR-1306	-0.090	RMND5A
hsa-miR-1306	-0.081	ZCCHC8
hsa-miR-1306	-0.061	TIMM13
hsa-miR-1306	-0.059	ZIC5
hsa-miR-1306	-0.054	TDP2
hsa-miR-1306	-0.051	PPP1CC
hsa-miR-140	-0.468	IGF2BP1
hsa-miR-140	-0.372	CDC6
hsa-miR-140	-0.262	HMGA1
hsa-miR-140	-0.217	TWNK

hsa-miR-140	-0.207	RTN3
hsa-miR-140	-0.186	MYBL2
hsa-miR-140	-0.186	ANLN
hsa-miR-140	-0.178	VEGFA
hsa-miR-140	-0.173	SELENOH
hsa-miR-140	-0.160	PMAIP1
hsa-miR-140	-0.160	YWHAG
hsa-miR-140	-0.145	CKAP2
hsa-miR-140	-0.143	UTP23
hsa-miR-140	-0.137	FZD6
hsa-miR-140	-0.136	HSPH1
hsa-miR-140	-0.132	RACGAP1
hsa-miR-140	-0.117	KIF23
hsa-miR-140	-0.117	FARSB
hsa-miR-140	-0.111	NAA40
hsa-miR-140	-0.110	SNHG17
hsa-miR-140	-0.109	CDCA4
hsa-miR-140	-0.107	SCD
hsa-miR-140	-0.102	DDX52
hsa-miR-140	-0.096	CDK16
hsa-miR-140	-0.096	CNOT11
hsa-miR-140	-0.094	CDK2AP1
hsa-miR-140	-0.092	SLC7A5
hsa-miR-140	-0.088	YRDC
hsa-miR-140	-0.086	MAL2
hsa-miR-140	-0.085	BIRC5
hsa-miR-140	-0.085	AGO2
hsa-miR-140	-0.085	GMNN
hsa-miR-140	-0.082	CLN6
hsa-miR-140	-0.077	NUDCD1
hsa-miR-140	-0.072	MRPL20
hsa-miR-140	-0.070	SLC37A4
hsa-miR-140	-0.066	ATF1
hsa-miR-140	-0.064	BTBD1
hsa-miR-140	-0.061	TYMS
hsa-miR-140	-0.060	FAM91A1
hsa-miR-140	-0.057	CCT4
hsa-miR-140	-0.057	SLC20A1
hsa-miR-140	-0.056	RRM2
hsa-miR-140	-0.056	NCAPG2
hsa-miR-140	-0.055	FANCA
hsa-miR-140	-0.054	YEATS2
hsa-miR-140	-0.054	TRMT10C
hsa-miR-140	-0.053	PROSER1
hsa-miR-140	-0.051	YWHAZ

hsa-miR-142	-0.156	CCNE1
hsa-miR-142	-0.146	SNHG6
hsa-miR-142	-0.145	INSIG2
hsa-miR-142	-0.143	SQLE
hsa-miR-142	-0.093	TMEM181
hsa-miR-142	-0.084	CRLS1
hsa-miR-142	-0.078	PERP
hsa-miR-142	-0.078	PFDN2
hsa-miR-142	-0.073	DTD1
hsa-miR-142	-0.068	STMN1
hsa-miR-142	-0.059	CKAP2
hsa-miR-142	-0.051	SNHG7
hsa-miR-148a	-0.154	FZD6
hsa-miR-148a	-0.077	BTBD1
hsa-miR-148a	-0.074	MYC
hsa-miR-148a	-0.062	TRIM59
hsa-miR-148a	-0.058	ELOC
hsa-miR-148a	-0.056	SRSF10
hsa-miR-148a	-0.055	SNHG7
hsa-miR-148b	-0.198	GPSM2
hsa-miR-148b	-0.146	FARSB
hsa-miR-148b	-0.145	MYC
hsa-miR-148b	-0.143	ARL6IP6
hsa-miR-148b	-0.132	PAN3
hsa-miR-148b	-0.123	SRI
hsa-miR-148b	-0.118	BAZ1A
hsa-miR-148b	-0.115	UBXN11
hsa-miR-148b	-0.112	PSMB6
hsa-miR-148b	-0.108	PRRG4
hsa-miR-148b	-0.104	DSCC1
hsa-miR-148b	-0.086	TRAP1
hsa-miR-148b	-0.083	DEK
hsa-miR-148b	-0.077	CBX3
hsa-miR-148b	-0.071	SNHG1
hsa-miR-148b	-0.070	NUP188
hsa-miR-148b	-0.066	ENO1
hsa-miR-148b	-0.065	CUL1
hsa-miR-148b	-0.064	CCT4
hsa-miR-148b	-0.064	SOCS6
hsa-miR-148b	-0.062	CNIH1
hsa-miR-148b	-0.061	SIGMAR1
hsa-miR-148b	-0.059	SCML1
hsa-miR-148b	-0.059	TRIM59
hsa-miR-148b	-0.058	NDUFV1
hsa-miR-148b	-0.053	FAM120A

hsa-miR-151a	-0.162	PKMYT1
hsa-miR-151a	-0.137	MIRLET7BHG
hsa-miR-151a	-0.130	PARD6B
hsa-miR-151a	-0.093	SMC1A
hsa-miR-151a	-0.090	HIVEP2
hsa-miR-151a	-0.066	PPP2CA
hsa-miR-15a	-0.597	CCNE1
hsa-miR-15a	-0.368	KRT18
hsa-miR-15a	-0.286	SLC25A1
hsa-miR-15a	-0.207	TMEM41A
hsa-miR-15a	-0.198	PARD6B
hsa-miR-15a	-0.196	HMGA1
hsa-miR-15a	-0.183	SLC25A39
hsa-miR-15a	-0.167	OTUB1
hsa-miR-15a	-0.162	UNG
hsa-miR-15a	-0.160	CDCA5
hsa-miR-15a	-0.159	CENPN
hsa-miR-15a	-0.152	SLC37A4
hsa-miR-15a	-0.143	MEX3A
hsa-miR-15a	-0.135	GALNT3
hsa-miR-15a	-0.134	DHRS13
hsa-miR-15a	-0.129	BIRC5
hsa-miR-15a	-0.129	ADORA2B
hsa-miR-15a	-0.124	SQLE
hsa-miR-15a	-0.124	PPIL1
hsa-miR-15a	-0.110	CBX4
hsa-miR-15a	-0.105	HSPA1B
hsa-miR-15a	-0.102	C19orf48
hsa-miR-15a	-0.102	GEMIN4
hsa-miR-15a	-0.101	SNRPB
hsa-miR-15a	-0.100	DNAAF5
hsa-miR-15a	-0.097	SNHG1
hsa-miR-15a	-0.094	SLC25A22
hsa-miR-15a	-0.091	TTK
hsa-miR-15a	-0.091	SLC29A2
hsa-miR-15a	-0.088	DESI1
hsa-miR-15a	-0.079	SPATA2
hsa-miR-15a	-0.079	ZBTB39
hsa-miR-15a	-0.079	MRPS2
hsa-miR-15a	-0.076	TBRG4
hsa-miR-15a	-0.071	SINHCAF
hsa-miR-15a	-0.070	YRDC
hsa-miR-15a	-0.068	CHORDC1
hsa-miR-15a	-0.066	TOMM20
hsa-miR-15a	-0.066	TMUB1

hsa-miR-15a	-0.066	BAMBI
hsa-miR-15a	-0.065	LRFN4
hsa-miR-15a	-0.064	PGAM5
hsa-miR-15a	-0.064	TFG
hsa-miR-15a	-0.064	CDCA4
hsa-miR-15a	-0.061	SFXN1
hsa-miR-15a	-0.059	SYPL1
hsa-miR-15a	-0.058	NPM1
hsa-miR-15a	-0.057	PSMC2
hsa-miR-15a	-0.055	CHKB-DT
hsa-miR-15a	-0.054	MAIP1
hsa-miR-15a	-0.051	MED17
hsa-miR-15a	-0.051	KCMF1
hsa-miR-15b	-0.232	STXBP3
hsa-miR-15b	-0.150	KTN1
hsa-miR-15b	-0.143	PLEKHA1
hsa-miR-15b	-0.113	HIVEP2
hsa-miR-15b	-0.113	VPS13A
hsa-miR-15b	-0.112	SLC7A6
hsa-miR-15b	-0.100	SOCS6
hsa-miR-15b	-0.099	NAA20
hsa-miR-15b	-0.098	PARD6B
hsa-miR-15b	-0.096	ZCCHC3
hsa-miR-15b	-0.095	STK35
hsa-miR-15b	-0.093	SPATA2
hsa-miR-15b	-0.091	INSIG2
hsa-miR-15b	-0.087	ZNF37BP
hsa-miR-15b	-0.085	PLAGL2
hsa-miR-15b	-0.085	VEGFA
hsa-miR-15b	-0.072	TDP2
hsa-miR-15b	-0.069	PDIK1L
hsa-miR-15b	-0.062	SYPL1
hsa-miR-15b	-0.062	TMEM181
hsa-miR-15b	-0.060	TMEM87B
hsa-miR-15b	-0.060	IGF2BP1
hsa-miR-15b	-0.052	SNHG1
hsa-miR-15b	-0.051	CHD7
hsa-miR-185	-0.217	MCM7
hsa-miR-185	-0.207	CDK4
hsa-miR-185	-0.193	NR6A1
hsa-miR-185	-0.189	DCTPP1
hsa-miR-185	-0.142	WRNIP1
hsa-miR-185	-0.138	CKAP2
hsa-miR-185	-0.129	U2AF2
hsa-miR-185	-0.094	TFDP1

hsa-miR-185	-0.085	DSP
hsa-miR-185	-0.085	NDUFB9
hsa-miR-185	-0.079	HDGF
hsa-miR-185	-0.073	ZNF768
hsa-miR-185	-0.072	CDCA4
hsa-miR-185	-0.071	INO80E
hsa-miR-185	-0.069	ZNF37BP
hsa-miR-185	-0.068	REPIN1
hsa-miR-185	-0.067	WDR43
hsa-miR-185	-0.063	PLAGL2
hsa-miR-185	-0.060	SNHG15
hsa-miR-185	-0.060	MYC
hsa-miR-185	-0.057	AHSA1
hsa-miR-1976	-0.145	NOP56
hsa-miR-1976	-0.107	SNHG17
hsa-miR-1976	-0.089	YWHAQ
hsa-miR-1976	-0.073	C19orf48
hsa-miR-1976	-0.060	AEN
hsa-miR-1976	-0.054	ZNF768
hsa-miR-20b	-0.111	PKMYT1
hsa-miR-20b	-0.094	SNHG3
hsa-miR-20b	-0.089	HMGB3
hsa-miR-20b	-0.070	SNHG12
hsa-miR-20b	-0.062	OSBPL3
hsa-miR-20b	-0.054	POLE
hsa-miR-20b	-0.051	YWHAZ
hsa-miR-216b	-0.178	PRRG4
hsa-miR-216b	-0.163	SNHG1
hsa-miR-216b	-0.087	MYO6
hsa-miR-216b	-0.084	WDR43
hsa-miR-216b	-0.069	ESCO2
hsa-miR-216b	-0.064	SNHG7
hsa-miR-216b	-0.056	TRMT10C
hsa-miR-216b	-0.054	TMF1
hsa-miR-216b	-0.054	NAA15
hsa-miR-22	-0.801	SAPCD2
hsa-miR-22	-0.496	SORD
hsa-miR-22	-0.468	MEX3A
hsa-miR-22	-0.404	TEDC1
hsa-miR-22	-0.404	CYC1
hsa-miR-22	-0.375	IGF2BP1
hsa-miR-22	-0.366	MSL3P1
hsa-miR-22	-0.365	KIFC1
hsa-miR-22	-0.358	TRMT6
hsa-miR-22	-0.344	BCS1L

hsa-miR-22	-0.343	RRP1
hsa-miR-22	-0.338	CDK5R1
hsa-miR-22	-0.329	RCC1
hsa-miR-22	-0.325	FKBPL
hsa-miR-22	-0.323	WDR77
hsa-miR-22	-0.321	PGAP2
hsa-miR-22	-0.317	AHCY
hsa-miR-22	-0.316	BAMBI
hsa-miR-22	-0.316	SAMD1
hsa-miR-22	-0.309	CDCA5
hsa-miR-22	-0.308	MIF
hsa-miR-22	-0.306	CENPW
hsa-miR-22	-0.305	HMBS
hsa-miR-22	-0.305	NOP56
hsa-miR-22	-0.303	MRPS26
hsa-miR-22	-0.299	NELFCD
hsa-miR-22	-0.297	CNPY2
hsa-miR-22	-0.295	DHRS13
hsa-miR-22	-0.292	RRP9
hsa-miR-22	-0.291	PPAT
hsa-miR-22	-0.290	STMN1
hsa-miR-22	-0.288	CDCA8
hsa-miR-22	-0.288	SQLE
hsa-miR-22	-0.284	TRMU
hsa-miR-22	-0.279	DTD1
hsa-miR-22	-0.279	CYHR1
hsa-miR-22	-0.279	RRS1
hsa-miR-22	-0.277	NDUFB9
hsa-miR-22	-0.268	UNG
hsa-miR-22	-0.264	USP39
hsa-miR-22	-0.262	CENPM
hsa-miR-22	-0.261	MRPL52
hsa-miR-22	-0.260	PTDSS1
hsa-miR-22	-0.254	TONSL
hsa-miR-22	-0.247	ARL6IP6
hsa-miR-22	-0.246	TDP1
hsa-miR-22	-0.244	RCC2
hsa-miR-22	-0.239	TMUB1
hsa-miR-22	-0.239	POLD2
hsa-miR-22	-0.237	CDC6
hsa-miR-22	-0.236	SNHG7
hsa-miR-22	-0.232	FAM136A
hsa-miR-22	-0.230	POLR3K
hsa-miR-22	-0.229	UBXN11
hsa-miR-22	-0.226	GMNN

hsa-miR-22	-0.224	ASF1B
hsa-miR-22	-0.222	ALYREF
hsa-miR-22	-0.219	APEX1
hsa-miR-22	-0.216	FANCI
hsa-miR-22	-0.211	DCTPP1
hsa-miR-22	-0.205	UTP4
hsa-miR-22	-0.205	DPM2
hsa-miR-22	-0.205	CCNF
hsa-miR-22	-0.204	EPCAM
hsa-miR-22	-0.203	LIG1
hsa-miR-22	-0.202	EIF2B4
hsa-miR-22	-0.201	TRIP13
hsa-miR-22	-0.198	SIGMAR1
hsa-miR-22	-0.198	PRPF19
hsa-miR-22	-0.196	TOR2A
hsa-miR-22	-0.193	DDX39A
hsa-miR-22	-0.188	C5orf34
hsa-miR-22	-0.188	ERG28
hsa-miR-22	-0.188	TIMM8A
hsa-miR-22	-0.186	ZBTB39
hsa-miR-22	-0.186	CDC25A
hsa-miR-22	-0.184	CKAP2
hsa-miR-22	-0.183	NAA20
hsa-miR-22	-0.183	GNL3
hsa-miR-22	-0.183	PTMA
hsa-miR-22	-0.182	SNRPA
hsa-miR-22	-0.181	KPNA2
hsa-miR-22	-0.181	SNHG1
hsa-miR-22	-0.178	REPIN1
hsa-miR-22	-0.177	CRLS1
hsa-miR-22	-0.177	GIT1
hsa-miR-22	-0.176	OSBPL3
hsa-miR-22	-0.172	POP7
hsa-miR-22	-0.171	PFDN2
hsa-miR-22	-0.170	KMT5A
hsa-miR-22	-0.168	PLK1
hsa-miR-22	-0.168	TACC3
hsa-miR-22	-0.159	ZNF768
hsa-miR-22	-0.159	SELENOH
hsa-miR-22	-0.157	DAZAP1
hsa-miR-22	-0.157	PDRG1
hsa-miR-22	-0.156	PLAGL2
hsa-miR-22	-0.155	GPN1
hsa-miR-22	-0.155	MCM7
hsa-miR-22	-0.155	PUS1

hsa-miR-22	-0.152	UMPS
hsa-miR-22	-0.150	CDK1
hsa-miR-22	-0.150	KIF11
hsa-miR-22	-0.147	SGTA
hsa-miR-22	-0.147	NONO
hsa-miR-22	-0.146	CCT3
hsa-miR-22	-0.144	PDIK1L
hsa-miR-22	-0.143	RCN1
hsa-miR-22	-0.139	PRPF4
hsa-miR-22	-0.139	MSH6
hsa-miR-22	-0.139	CHAF1A
hsa-miR-22	-0.138	ACP1
hsa-miR-22	-0.136	TTI1
hsa-miR-22	-0.135	ALG14
hsa-miR-22	-0.134	TMEM41A
hsa-miR-22	-0.132	CCDC59
hsa-miR-22	-0.131	SNHG15
hsa-miR-22	-0.130	WRNIP1
hsa-miR-22	-0.130	NUDCD1
hsa-miR-22	-0.128	ATIC
hsa-miR-22	-0.127	CCT7
hsa-miR-22	-0.126	POLR1B
hsa-miR-22	-0.123	HMGB2
hsa-miR-22	-0.123	SNHG3
hsa-miR-22	-0.123	PATL1
hsa-miR-22	-0.122	PRMT5
hsa-miR-22	-0.120	IDH2
hsa-miR-22	-0.120	ANP32A
hsa-miR-22	-0.120	SNHG12
hsa-miR-22	-0.120	SSRP1
hsa-miR-22	-0.119	CHD7
hsa-miR-22	-0.119	RACGAP1
hsa-miR-22	-0.115	NUP107
hsa-miR-22	-0.114	SRRT
hsa-miR-22	-0.114	PPIL1
hsa-miR-22	-0.113	POLE
hsa-miR-22	-0.112	SLC7A5
hsa-miR-22	-0.112	NOLC1
hsa-miR-22	-0.111	CLN6
hsa-miR-22	-0.109	ZCCHC3
hsa-miR-22	-0.109	CPSF1
hsa-miR-22	-0.108	EIF6
hsa-miR-22	-0.107	POU2F1
hsa-miR-22	-0.106	C19orf48
hsa-miR-22	-0.104	MCM6

hsa-miR-22	-0.103	CSNK1E
hsa-miR-22	-0.102	FAM49B
hsa-miR-22	-0.101	MOCS3
hsa-miR-22	-0.099	CHTOP
hsa-miR-22	-0.099	INO80E
hsa-miR-22	-0.099	SCML1
hsa-miR-22	-0.098	RAD21
hsa-miR-22	-0.095	DDX52
hsa-miR-22	-0.094	SUZ12
hsa-miR-22	-0.092	MCM4
hsa-miR-22	-0.089	LMNB2
hsa-miR-22	-0.089	ANKRD46
hsa-miR-22	-0.088	TOP2A
hsa-miR-22	-0.084	ABCF2
hsa-miR-22	-0.084	ILF2
hsa-miR-22	-0.083	U2AF2
hsa-miR-22	-0.082	TFDP1
hsa-miR-22	-0.082	SF3B4
hsa-miR-22	-0.081	TOMM20
hsa-miR-22	-0.081	ATXN2L
hsa-miR-22	-0.081	ENO1
hsa-miR-22	-0.078	BRAT1
hsa-miR-22	-0.078	URB2
hsa-miR-22	-0.077	TUBB4B
hsa-miR-22	-0.077	NCL
hsa-miR-22	-0.075	GTF3C2
hsa-miR-22	-0.074	PPM1G
hsa-miR-22	-0.074	STMP1
hsa-miR-22	-0.074	NCAPD2
hsa-miR-22	-0.073	BIRC5
hsa-miR-22	-0.072	DLG3
hsa-miR-22	-0.072	SRSF7
hsa-miR-22	-0.071	SCAMP3
hsa-miR-22	-0.070	MRPS2
hsa-miR-22	-0.068	SNHG6
hsa-miR-22	-0.068	HNRNPF
hsa-miR-22	-0.068	MYC
hsa-miR-22	-0.067	MAIP1
hsa-miR-22	-0.064	AEN
hsa-miR-22	-0.063	LMNB1
hsa-miR-22	-0.062	NAA25
hsa-miR-22	-0.062	ANAPC5
hsa-miR-22	-0.060	SFPQ
hsa-miR-22	-0.060	RAD23B
hsa-miR-22	-0.060	MAP3K21

hsa-miR-22	-0.059	DCAF12
hsa-miR-22	-0.058	TMPO
hsa-miR-22	-0.058	SLC25A17
hsa-miR-22	-0.057	ILF3
hsa-miR-22	-0.055	PTPN3
hsa-miR-22	-0.055	NUP205
hsa-miR-22	-0.055	NDUFV1
hsa-miR-22	-0.054	MZT1
hsa-miR-22	-0.054	PSMA7
hsa-miR-22	-0.052	SLC39A10
hsa-miR-22	-0.051	FZD6
hsa-miR-223	-0.087	SNHG7
hsa-miR-223	-0.068	VEGFA
hsa-miR-2355	-0.254	FDXR
hsa-miR-2355	-0.137	FANCA
hsa-miR-2355	-0.089	SNHG1
hsa-miR-2355	-0.089	SLC1A5
hsa-miR-2355	-0.078	MCM7
hsa-miR-2355	-0.075	HACD3
hsa-miR-2355	-0.073	POLE
hsa-miR-2355	-0.071	STAG2
hsa-miR-2355	-0.070	PKMYT1
hsa-miR-2355	-0.070	TMEM167A
hsa-miR-2355	-0.069	SLC25A39
hsa-miR-2355	-0.069	MAP3K4
hsa-miR-2355	-0.069	HMGCR
hsa-miR-2355	-0.058	SNHG3
hsa-miR-2355	-0.052	DNAAF5
hsa-miR-28	-0.295	SKA1
hsa-miR-28	-0.271	CENPF
hsa-miR-28	-0.267	HM13
hsa-miR-28	-0.263	TPX2
hsa-miR-28	-0.257	NUSAP1
hsa-miR-28	-0.249	NCAPG2
hsa-miR-28	-0.237	IGF2BP1
hsa-miR-28	-0.207	TENT4A
hsa-miR-28	-0.194	CENPN
hsa-miR-28	-0.163	MAL2
hsa-miR-28	-0.156	ANLN
hsa-miR-28	-0.148	SLC37A4
hsa-miR-28	-0.144	SLC7A6
hsa-miR-28	-0.136	NUP188
hsa-miR-28	-0.134	EIF2AK1
hsa-miR-28	-0.133	PTBP3
hsa-miR-28	-0.131	CLPTM1L

hsa-miR-28	-0.127	GRPEL2
hsa-miR-28	-0.122	ARL5B
hsa-miR-28	-0.122	MAD2L1
hsa-miR-28	-0.109	CSE1L
hsa-miR-28	-0.100	BUB3
hsa-miR-28	-0.098	SNHG17
hsa-miR-28	-0.096	SNHG15
hsa-miR-28	-0.095	FAM49B
hsa-miR-28	-0.093	E2F3
hsa-miR-28	-0.093	G3BP1
hsa-miR-28	-0.092	HSPA14
hsa-miR-28	-0.082	PROSER1
hsa-miR-28	-0.081	TBRG4
hsa-miR-28	-0.075	SCD
hsa-miR-28	-0.065	GIT1
hsa-miR-28	-0.065	ATF1
hsa-miR-28	-0.064	C6orf62
hsa-miR-28	-0.062	MYO1B
hsa-miR-28	-0.056	SBNO1
hsa-miR-28	-0.055	POU2F1
hsa-miR-28	-0.053	DDX21
hsa-miR-28	-0.050	CCT3
hsa-miR-30d	-0.345	MYBL2
hsa-miR-30d	-0.312	CCNF
hsa-miR-30d	-0.306	MSL3P1
hsa-miR-30d	-0.264	TRIB3
hsa-miR-30d	-0.219	LMNB1
hsa-miR-30d	-0.217	GMNN
hsa-miR-30d	-0.182	ZBTB39
hsa-miR-30d	-0.171	C6orf136
hsa-miR-30d	-0.160	KIF11
hsa-miR-30d	-0.151	SGO1
hsa-miR-30d	-0.150	ESCO2
hsa-miR-30d	-0.147	TYMS
hsa-miR-30d	-0.138	NCAPG
hsa-miR-30d	-0.127	E2F7
hsa-miR-30d	-0.124	KPNA2
hsa-miR-30d	-0.120	EPCAM
hsa-miR-30d	-0.115	KIF23
hsa-miR-30d	-0.112	FAM111B
hsa-miR-30d	-0.110	PRPF19
hsa-miR-30d	-0.108	SSRP1
hsa-miR-30d	-0.102	ANP32A
hsa-miR-30d	-0.101	SNHG1
hsa-miR-30d	-0.099	TTI1

hsa-miR-30d	-0.096	DNAJC9
hsa-miR-30d	-0.095	BRCA2
hsa-miR-30d	-0.095	MRPS2
hsa-miR-30d	-0.093	STMN1
hsa-miR-30d	-0.091	SGTA
hsa-miR-30d	-0.090	CDK1
hsa-miR-30d	-0.089	ANAPC5
hsa-miR-30d	-0.088	LMNB2
hsa-miR-30d	-0.087	TRIAP1
hsa-miR-30d	-0.086	CHORDC1
hsa-miR-30d	-0.081	PMAIP1
hsa-miR-30d	-0.078	SNHG6
hsa-miR-30d	-0.077	MZT1
hsa-miR-30d	-0.074	DSP
hsa-miR-30d	-0.071	CSE1L
hsa-miR-30d	-0.070	CDCA4
hsa-miR-30d	-0.069	CCDC43
hsa-miR-30d	-0.068	POLQ
hsa-miR-30d	-0.067	PRDX4
hsa-miR-30d	-0.064	RRM2
hsa-miR-30d	-0.059	BAZ1A
hsa-miR-30d	-0.058	CBFB
hsa-miR-30d	-0.057	SLC39A10
hsa-miR-30d	-0.056	CEP128
hsa-miR-30d	-0.055	TC2N
hsa-miR-30d	-0.054	C5orf22
hsa-miR-30d	-0.053	SCAMP3
hsa-miR-30e	-0.613	GALNT3
hsa-miR-30e	-0.524	TTK
hsa-miR-30e	-0.485	VEGFA
hsa-miR-30e	-0.481	MAD2L1
hsa-miR-30e	-0.440	ZIC5
hsa-miR-30e	-0.440	MYO1B
hsa-miR-30e	-0.411	PSAT1
hsa-miR-30e	-0.410	MYO6
hsa-miR-30e	-0.407	CDC6
hsa-miR-30e	-0.379	PPAT
hsa-miR-30e	-0.376	FAM91A1
hsa-miR-30e	-0.371	HSPE1
hsa-miR-30e	-0.363	HSP90AA1
hsa-miR-30e	-0.358	POLQ
hsa-miR-30e	-0.348	DSCC1
hsa-miR-30e	-0.345	TRIB3
hsa-miR-30e	-0.341	FZD6
hsa-miR-30e	-0.332	TC2N

hsa-miR-30e	-0.328	CENPA
hsa-miR-30e	-0.325	CDK1
hsa-miR-30e	-0.323	MSL3P1
hsa-miR-30e	-0.313	KIF23
hsa-miR-30e	-0.313	TMEM41A
hsa-miR-30e	-0.312	DSP
hsa-miR-30e	-0.297	HSPA5
hsa-miR-30e	-0.261	YWHAZ
hsa-miR-30e	-0.259	MAP3K21
hsa-miR-30e	-0.257	CBX3
hsa-miR-30e	-0.252	PTPN3
hsa-miR-30e	-0.251	BAZ1A
hsa-miR-30e	-0.249	FBXO45
hsa-miR-30e	-0.243	NCAPG
hsa-miR-30e	-0.241	SYPL1
hsa-miR-30e	-0.235	LYPLA1
hsa-miR-30e	-0.234	MTHFD2
hsa-miR-30e	-0.223	STAG2
hsa-miR-30e	-0.221	SLC20A1
hsa-miR-30e	-0.220	SGO1
hsa-miR-30e	-0.215	CSE1L
hsa-miR-30e	-0.212	CLDN12
hsa-miR-30e	-0.211	ANLN
hsa-miR-30e	-0.205	ADIPOR2
hsa-miR-30e	-0.205	DLG3
hsa-miR-30e	-0.205	TMEM181
hsa-miR-30e	-0.204	MYBL2
hsa-miR-30e	-0.203	GOLT1B
hsa-miR-30e	-0.202	C5orf34
hsa-miR-30e	-0.202	PSMD14
hsa-miR-30e	-0.201	KPNA2
hsa-miR-30e	-0.197	OSBPL3
hsa-miR-30e	-0.196	SLC39A10
hsa-miR-30e	-0.196	PMAIP1
hsa-miR-30e	-0.195	TRIM59
hsa-miR-30e	-0.195	FAM111B
hsa-miR-30e	-0.188	AMD1
hsa-miR-30e	-0.180	BRCA2
hsa-miR-30e	-0.177	TMEM167A
hsa-miR-30e	-0.172	DYNLT1
hsa-miR-30e	-0.172	WDR43
hsa-miR-30e	-0.170	PSMA7
hsa-miR-30e	-0.170	CHORDC1
hsa-miR-30e	-0.169	PDIK1L
hsa-miR-30e	-0.168	RRM2

hsa-miR-30e	-0.164	SLC7A6
hsa-miR-30e	-0.163	UBN2
hsa-miR-30e	-0.162	MKI67
hsa-miR-30e	-0.160	SLC26A6
hsa-miR-30e	-0.159	TMEM87B
hsa-miR-30e	-0.159	CCNB1
hsa-miR-30e	-0.158	FAM136A
hsa-miR-30e	-0.156	PSMC2
hsa-miR-30e	-0.155	RCN1
hsa-miR-30e	-0.155	SCML1
hsa-miR-30e	-0.153	TYMS
hsa-miR-30e	-0.152	TWNK
hsa-miR-30e	-0.151	STMP1
hsa-miR-30e	-0.147	CCT4
hsa-miR-30e	-0.145	STK35
hsa-miR-30e	-0.144	HSPH1
hsa-miR-30e	-0.144	TRMT10C
hsa-miR-30e	-0.142	PRDX4
hsa-miR-30e	-0.142	SLC25A17
hsa-miR-30e	-0.140	SPATA2
hsa-miR-30e	-0.140	ESCO2
hsa-miR-30e	-0.140	AGPS
hsa-miR-30e	-0.140	GMNN
hsa-miR-30e	-0.138	KIF11
hsa-miR-30e	-0.136	TMF1
hsa-miR-30e	-0.135	CENPF
hsa-miR-30e	-0.134	SLC1A5
hsa-miR-30e	-0.133	SLC7A5
hsa-miR-30e	-0.132	TENT4A
hsa-miR-30e	-0.130	FARSB
hsa-miR-30e	-0.128	UTP15
hsa-miR-30e	-0.127	ASNSD1
hsa-miR-30e	-0.126	PARD6B
hsa-miR-30e	-0.125	SRSF10
hsa-miR-30e	-0.125	TFG
hsa-miR-30e	-0.124	BTBD1
hsa-miR-30e	-0.123	CSNK1E
hsa-miR-30e	-0.122	CBFB
hsa-miR-30e	-0.119	CCDC43
hsa-miR-30e	-0.119	LCLAT1
hsa-miR-30e	-0.118	SFXN1
hsa-miR-30e	-0.118	ZBTB33
hsa-miR-30e	-0.116	FAM120A
hsa-miR-30e	-0.116	CDK2AP1
hsa-miR-30e	-0.114	GLO1

hsa-miR-30e	-0.112	TMEM87A
hsa-miR-30e	-0.110	CHD1
hsa-miR-30e	-0.108	E2F7
hsa-miR-30e	-0.107	VMA21
hsa-miR-30e	-0.106	TOMM20
hsa-miR-30e	-0.106	CHD7
hsa-miR-30e	-0.104	RAB11A
hsa-miR-30e	-0.102	LARP4
hsa-miR-30e	-0.100	URB2
hsa-miR-30e	-0.096	DDX21
hsa-miR-30e	-0.095	ACP1
hsa-miR-30e	-0.094	HSPA4
hsa-miR-30e	-0.091	MYC
hsa-miR-30e	-0.088	ARL5B
hsa-miR-30e	-0.087	C6orf62
hsa-miR-30e	-0.085	NAA25
hsa-miR-30e	-0.084	CDK4
hsa-miR-30e	-0.081	C6orf136
hsa-miR-30e	-0.080	LIN7C
hsa-miR-30e	-0.077	NCL
hsa-miR-30e	-0.074	PROSER1
hsa-miR-30e	-0.073	LMBR1
hsa-miR-30e	-0.072	C5orf22
hsa-miR-30e	-0.071	DCAF12
hsa-miR-30e	-0.071	SENP2
hsa-miR-30e	-0.070	AGO2
hsa-miR-30e	-0.068	SCAMP3
hsa-miR-30e	-0.067	NRAS
hsa-miR-30e	-0.066	DNAAF5
hsa-miR-30e	-0.066	HACD3
hsa-miR-30e	-0.064	TTI1
hsa-miR-30e	-0.064	WDR5
hsa-miR-30e	-0.064	BIRC5
hsa-miR-30e	-0.062	G3BP1
hsa-miR-30e	-0.060	YEATS2
hsa-miR-30e	-0.060	UTP23
hsa-miR-30e	-0.059	YWHAG
hsa-miR-30e	-0.057	SNHG17
hsa-miR-30e	-0.057	GRSF1
hsa-miR-30e	-0.056	CLPTM1L
hsa-miR-30e	-0.054	CAPZA1
hsa-miR-30e	-0.052	SNHG1
hsa-miR-30e	-0.051	LRRC8B
hsa-miR-30e	-0.050	SBNO1
hsa-miR-320e	-0.117	HSPH1

hsa-miR-320e	-0.099	LCLAT1
hsa-miR-320e	-0.091	SNHG3
hsa-miR-320e	-0.088	SFXN1
hsa-miR-320e	-0.081	FDXR
hsa-miR-320e	-0.073	WDR77
hsa-miR-320e	-0.069	CLN6
hsa-miR-320e	-0.058	PTDSS1
hsa-miR-320e	-0.051	ZNF37BP
hsa-miR-326	-0.138	SNHG12
hsa-miR-326	-0.105	BIRC5
hsa-miR-326	-0.101	XPO1
hsa-miR-326	-0.101	PILRB
hsa-miR-326	-0.098	ZNF37BP
hsa-miR-326	-0.082	NUP107
hsa-miR-326	-0.074	SNHG3
hsa-miR-326	-0.072	CSE1L
hsa-miR-326	-0.072	ZNF587
hsa-miR-326	-0.060	ANKRD46
hsa-miR-326	-0.057	BAZ1A
hsa-miR-331	-0.101	TMF1
hsa-miR-331	-0.077	MIRLET7BHG
hsa-miR-340	-0.353	SAPCD2
hsa-miR-340	-0.228	AGO2
hsa-miR-340	-0.181	OSBPL3
hsa-miR-340	-0.174	POP1
hsa-miR-340	-0.167	SQLE
hsa-miR-340	-0.165	SYPL1
hsa-miR-340	-0.163	MAL2
hsa-miR-340	-0.154	PTBP3
hsa-miR-340	-0.153	PMAIP1
hsa-miR-340	-0.119	NUP205
hsa-miR-340	-0.117	HSPH1
hsa-miR-340	-0.114	HACD3
hsa-miR-340	-0.098	ATXN2L
hsa-miR-340	-0.094	SOCS6
hsa-miR-340	-0.094	MIRLET7BHG
hsa-miR-340	-0.091	LCLAT1
hsa-miR-340	-0.085	KIF23
hsa-miR-340	-0.075	PSAT1
hsa-miR-340	-0.075	AGPS
hsa-miR-340	-0.071	SLC39A10
hsa-miR-340	-0.069	PFDN2
hsa-miR-340	-0.059	NUP37
hsa-miR-340	-0.058	ARL6IP6
hsa-miR-340	-0.057	ANLN

hsa-miR-340	-0.056	SMC1A
hsa-miR-340	-0.056	DDX21
hsa-miR-340	-0.055	FAM136A
hsa-miR-340	-0.052	ANKRD46
hsa-miR-340	-0.051	TMF1
hsa-miR-340	-0.051	INSIG2
hsa-miR-342	-0.147	POLD2
hsa-miR-342	-0.115	NME1
hsa-miR-342	-0.114	TBRG4
hsa-miR-342	-0.099	RRM2
hsa-miR-342	-0.098	LMNB1
hsa-miR-342	-0.091	WDR77
hsa-miR-342	-0.088	MOCS3
hsa-miR-342	-0.086	CCT3
hsa-miR-342	-0.081	CCNF
hsa-miR-342	-0.081	CDCA4
hsa-miR-342	-0.074	PARD6B
hsa-miR-342	-0.073	SRI
hsa-miR-342	-0.069	TUBA1B
hsa-miR-342	-0.062	GLO1
hsa-miR-342	-0.053	CLN6
hsa-miR-342	-0.052	SNHG7
hsa-miR-342	-0.051	FDXR
hsa-miR-34a	-0.715	IGF2BP1
hsa-miR-34a	-0.714	ZIC5
hsa-miR-34a	-0.601	WNK2
hsa-miR-34a	-0.225	BUB1B
hsa-miR-34a	-0.214	TTK
hsa-miR-34a	-0.194	TRIB3
hsa-miR-34a	-0.189	CDCA5
hsa-miR-34a	-0.185	CENPA
hsa-miR-34a	-0.182	BUB1
hsa-miR-34a	-0.157	RAD54B
hsa-miR-34a	-0.155	RACGAP1
hsa-miR-34a	-0.154	CKAP2
hsa-miR-34a	-0.150	CDK1
hsa-miR-34a	-0.149	BLM
hsa-miR-34a	-0.148	ANLN
hsa-miR-34a	-0.144	NCAPD2
hsa-miR-34a	-0.144	C17orf100
hsa-miR-34a	-0.144	TOP2A
hsa-miR-34a	-0.140	DSCC1
hsa-miR-34a	-0.138	ADIPOR2
hsa-miR-34a	-0.131	NUDCD1
hsa-miR-34a	-0.130	SEH1L

hsa-miR-34a	-0.126	MAD2L1
hsa-miR-34a	-0.124	GPSM2
hsa-miR-34a	-0.123	SLC39A10
hsa-miR-34a	-0.116	SNHG7
hsa-miR-34a	-0.114	IDH2
hsa-miR-34a	-0.113	ARL5B
hsa-miR-34a	-0.112	SGO2
hsa-miR-34a	-0.107	NUP37
hsa-miR-34a	-0.105	NCAPG
hsa-miR-34a	-0.103	SLC7A5
hsa-miR-34a	-0.100	CDC25A
hsa-miR-34a	-0.099	KIF22
hsa-miR-34a	-0.099	ARL6IP6
hsa-miR-34a	-0.095	TWNK
hsa-miR-34a	-0.095	AURKA
hsa-miR-34a	-0.092	PERP
hsa-miR-34a	-0.090	MYBL2
hsa-miR-34a	-0.089	PVR
hsa-miR-34a	-0.088	E2F3
hsa-miR-34a	-0.088	KIFC1
hsa-miR-34a	-0.081	TBC1D31
hsa-miR-34a	-0.078	SPRYD4
hsa-miR-34a	-0.074	TRIP13
hsa-miR-34a	-0.071	FAM49B
hsa-miR-34a	-0.071	TRIM59
hsa-miR-34a	-0.070	FOXN2
hsa-miR-34a	-0.070	MOCS3
hsa-miR-34a	-0.069	TARBP1
hsa-miR-34a	-0.068	CBX3
hsa-miR-34a	-0.066	SLC7A6
hsa-miR-34a	-0.065	TPX2
hsa-miR-34a	-0.064	NR6A1
hsa-miR-34a	-0.064	LMNB1
hsa-miR-34a	-0.063	TYMS
hsa-miR-34a	-0.063	MAPKAPK5-AS1
hsa-miR-34a	-0.060	CCNF
hsa-miR-34a	-0.060	SINHCAF
hsa-miR-34a	-0.060	SAPCD2
hsa-miR-34a	-0.058	EPCAM
hsa-miR-34a	-0.056	POP1
hsa-miR-34a	-0.055	SKA1
hsa-miR-34a	-0.055	SMIM13
hsa-miR-34a	-0.053	PROSER1
hsa-miR-34a	-0.053	FANCI
hsa-miR-34a	-0.052	PMPCA

hsa-miR-34a	-0.051	LARP4
hsa-miR-34a	-0.051	CDK5R1
hsa-miR-34a	-0.051	BRCA2
hsa-miR-34a	-0.051	ATF1
hsa-miR-34a	-0.050	MEN1
hsa-miR-34a	-0.050	CHD7
hsa-miR-3619	-0.113	SNHG3
hsa-miR-3619	-0.073	SNHG17
hsa-miR-3677	-0.164	PILRB
hsa-miR-3677	-0.065	SNHG7
hsa-miR-374a	-0.314	PRRG4
hsa-miR-374a	-0.196	TEDC1
hsa-miR-374a	-0.181	PARD6B
hsa-miR-374a	-0.151	PERP
hsa-miR-374a	-0.147	CYC1
hsa-miR-374a	-0.125	TC2N
hsa-miR-374a	-0.112	OSBPL3
hsa-miR-374a	-0.098	HSPH1
hsa-miR-374a	-0.098	ADORA2B
hsa-miR-374a	-0.095	TIMM8A
hsa-miR-374a	-0.094	DESI1
hsa-miR-374a	-0.090	SQLE
hsa-miR-374a	-0.088	FANCA
hsa-miR-374a	-0.087	NAA15
hsa-miR-374a	-0.086	TMEM181
hsa-miR-374a	-0.082	HSPA1B
hsa-miR-374a	-0.080	GEMIN4
hsa-miR-374a	-0.080	NCAPD2
hsa-miR-374a	-0.078	SFXN1
hsa-miR-374a	-0.077	LRFN4
hsa-miR-374a	-0.074	MAL2
hsa-miR-374a	-0.072	GNL3
hsa-miR-374a	-0.066	MIRLET7BHG
hsa-miR-374a	-0.065	TACC3
hsa-miR-374a	-0.055	POLR1B
hsa-miR-374a	-0.053	TRAP1
hsa-miR-374a	-0.052	SRI
hsa-miR-423	-0.210	ALG14
hsa-miR-423	-0.174	FAM49B
hsa-miR-423	-0.159	SMIM13
hsa-miR-423	-0.151	MYC
hsa-miR-423	-0.148	CCNF
hsa-miR-423	-0.101	STK35
hsa-miR-423	-0.099	TWNK
hsa-miR-423	-0.097	HMGCR

hsa-miR-423	-0.090	MRPL52
hsa-miR-423	-0.085	YRDC
hsa-miR-423	-0.082	ARL5B
hsa-miR-423	-0.081	HIVEP2
hsa-miR-423	-0.079	HSPA4
hsa-miR-423	-0.078	KMT5A
hsa-miR-423	-0.075	PDIK1L
hsa-miR-423	-0.067	SIKE1
hsa-miR-423	-0.064	ZBTB39
hsa-miR-423	-0.063	CNIH1
hsa-miR-423	-0.062	CCT4
hsa-miR-423	-0.060	MTHFD1L
hsa-miR-423	-0.059	SNHG1
hsa-miR-423	-0.057	TUBA1B
hsa-miR-423	-0.053	CCT7
hsa-miR-424	-0.149	VPS13A
hsa-miR-424	-0.127	ZNF37BP
hsa-miR-424	-0.110	CUL2
hsa-miR-424	-0.101	UBN2
hsa-miR-424	-0.100	TFAP4
hsa-miR-424	-0.090	SYPL1
hsa-miR-424	-0.081	RMND5A
hsa-miR-424	-0.075	QTRT2
hsa-miR-424	-0.074	MAPKAPK5-AS1
hsa-miR-424	-0.074	HSPA14
hsa-miR-424	-0.062	PTBP3
hsa-miR-424	-0.062	TENT4A
hsa-miR-424	-0.062	GRPEL2
hsa-miR-424	-0.061	SBNO1
hsa-miR-424	-0.059	OTUD3
hsa-miR-424	-0.052	SOCS6
hsa-miR-424	-0.052	E2F7
hsa-miR-424	-0.052	CLDN12
hsa-miR-424	-0.051	NAA40
hsa-miR-4726	-0.083	PILRB
hsa-miR-4726	-0.071	SNHG15
hsa-miR-4726	-0.062	TIMM13
hsa-miR-484	-0.153	SNHG7
hsa-miR-484	-0.125	CLDN12
hsa-miR-484	-0.124	TWNK
hsa-miR-484	-0.124	HIVEP2
hsa-miR-484	-0.113	FZD6
hsa-miR-484	-0.090	NOLC1
hsa-miR-484	-0.089	MIRLET7BHG
hsa-miR-484	-0.082	C19orf48

hsa-miR-484	-0.067	SNHG1
hsa-miR-484	-0.057	VMA21
hsa-miR-497	-0.318	SLC7A5
hsa-miR-497	-0.295	TBC1D31
hsa-miR-497	-0.230	EIF4E
hsa-miR-497	-0.222	LRFN4
hsa-miR-497	-0.216	OTUD3
hsa-miR-497	-0.207	PERP
hsa-miR-497	-0.188	ZIC5
hsa-miR-497	-0.180	ADORA2B
hsa-miR-497	-0.180	SYPL1
hsa-miR-497	-0.169	GTF3C5
hsa-miR-497	-0.166	SEH1L
hsa-miR-497	-0.165	STXBP3
hsa-miR-497	-0.160	PSAT1
hsa-miR-497	-0.160	SNHG1
hsa-miR-497	-0.159	FDXR
hsa-miR-497	-0.156	CHORDC1
hsa-miR-497	-0.156	MAPKAPK5
hsa-miR-497	-0.155	DCUN1D5
hsa-miR-497	-0.155	ENTR1
hsa-miR-497	-0.149	HMGCR
hsa-miR-497	-0.149	SMC1A
hsa-miR-497	-0.148	PYCR1
hsa-miR-497	-0.143	SNX14
hsa-miR-497	-0.141	PTGES2
hsa-miR-497	-0.135	IER3IP1
hsa-miR-497	-0.134	DEK
hsa-miR-497	-0.131	KIF22
hsa-miR-497	-0.130	GEMIN4
hsa-miR-497	-0.127	SRI
hsa-miR-497	-0.125	CLNS1A
hsa-miR-497	-0.125	PUF60
hsa-miR-497	-0.125	MED17
hsa-miR-497	-0.125	ERG28
hsa-miR-497	-0.124	SLC29A2
hsa-miR-497	-0.124	MRPL20
hsa-miR-497	-0.122	HAUS3
hsa-miR-497	-0.122	ZCCHC8
hsa-miR-497	-0.122	PTGES3
hsa-miR-497	-0.122	YWHAQ
hsa-miR-497	-0.122	SRSF10
hsa-miR-497	-0.121	AHSA1
hsa-miR-497	-0.121	YEATS2
hsa-miR-497	-0.121	BIRC5

hsa-miR-497	-0.119	GRPEL2
hsa-miR-497	-0.117	SOCS6
hsa-miR-497	-0.115	QTRT2
hsa-miR-497	-0.113	VEGFA
hsa-miR-497	-0.113	DNAJC9
hsa-miR-497	-0.112	NAA40
hsa-miR-497	-0.111	PGAM5
hsa-miR-497	-0.111	ATP6V0B
hsa-miR-497	-0.111	ASNSD1
hsa-miR-497	-0.110	SLC1A5
hsa-miR-497	-0.110	TFAP4
hsa-miR-497	-0.105	MTHFD2
hsa-miR-497	-0.105	CCNE1
hsa-miR-497	-0.105	PSMB6
hsa-miR-497	-0.104	TARBP1
hsa-miR-497	-0.104	UTP15
hsa-miR-497	-0.103	DENR
hsa-miR-497	-0.103	BRAT1
hsa-miR-497	-0.102	SMIM13
hsa-miR-497	-0.101	PMPCA
hsa-miR-497	-0.099	AP5M1
hsa-miR-497	-0.099	PTMA
hsa-miR-497	-0.096	CDCA4
hsa-miR-497	-0.096	UNG
hsa-miR-497	-0.095	FANCA
hsa-miR-497	-0.094	NUP58
hsa-miR-497	-0.094	KIF23
hsa-miR-497	-0.094	E2F7
hsa-miR-497	-0.094	CSE1L
hsa-miR-497	-0.094	PTPMT1
hsa-miR-497	-0.092	FEN1
hsa-miR-497	-0.092	SNRPB
hsa-miR-497	-0.089	FBXO45
hsa-miR-497	-0.089	KCMF1
hsa-miR-497	-0.089	CBX4
hsa-miR-497	-0.088	NAA20
hsa-miR-497	-0.087	HSPA9
hsa-miR-497	-0.087	NFYA
hsa-miR-497	-0.086	HSPA1B
hsa-miR-497	-0.085	INSIG2
hsa-miR-497	-0.085	DESI1
hsa-miR-497	-0.083	SLC25A22
hsa-miR-497	-0.082	UBN2
hsa-miR-497	-0.082	CDK4
hsa-miR-497	-0.080	SENP2

hsa-miR-497	-0.080	CCDC59
hsa-miR-497	-0.079	NONO
hsa-miR-497	-0.079	LMBR1
hsa-miR-497	-0.078	RTN3
hsa-miR-497	-0.078	PLEKHA1
hsa-miR-497	-0.077	ATXN2L
hsa-miR-497	-0.076	ZBTB39
hsa-miR-497	-0.076	GLO1
hsa-miR-497	-0.075	DHRS13
hsa-miR-497	-0.075	UCKL1
hsa-miR-497	-0.075	CDK16
hsa-miR-497	-0.073	CNIH1
hsa-miR-497	-0.073	C6orf136
hsa-miR-497	-0.073	USP1
hsa-miR-497	-0.072	MAP3K4
hsa-miR-497	-0.072	SIKE1
hsa-miR-497	-0.071	WDR43
hsa-miR-497	-0.071	YRDC
hsa-miR-497	-0.071	NUP188
hsa-miR-497	-0.070	CHKB-DT
hsa-miR-497	-0.069	BZW1
hsa-miR-497	-0.068	ELOC
hsa-miR-497	-0.068	PTBP3
hsa-miR-497	-0.067	PPP2CA
hsa-miR-497	-0.066	PRDX4
hsa-miR-497	-0.065	OTUB1
hsa-miR-497	-0.065	HMGA1
hsa-miR-497	-0.064	LRRC8B
hsa-miR-497	-0.064	CCNB1
hsa-miR-497	-0.063	CPSF6
hsa-miR-497	-0.063	CBFB
hsa-miR-497	-0.062	FOXN2
hsa-miR-497	-0.062	TRAP1
hsa-miR-497	-0.061	PPM1G
hsa-miR-497	-0.060	G3BP1
hsa-miR-497	-0.060	TDP2
hsa-miR-497	-0.060	KRT18
hsa-miR-497	-0.060	PSMD11
hsa-miR-497	-0.059	SQLE
hsa-miR-497	-0.059	PI4K2B
hsa-miR-497	-0.058	PAN3
hsa-miR-497	-0.058	CCDC14
hsa-miR-497	-0.058	TMEM199
hsa-miR-497	-0.057	RMND5A
hsa-miR-497	-0.057	SLC26A6

hsa-miR-497	-0.057	NARF
hsa-miR-497	-0.057	TMEM87A
hsa-miR-497	-0.056	SLC25A1
hsa-miR-497	-0.056	SSRP1
hsa-miR-497	-0.055	TFG
hsa-miR-497	-0.054	ABCF2
hsa-miR-497	-0.054	SUZ12
hsa-miR-497	-0.054	HSPE1
hsa-miR-497	-0.053	GOLT1B
hsa-miR-497	-0.053	HDGF
hsa-miR-497	-0.053	RAD23B
hsa-miR-497	-0.053	PPP1CC
hsa-miR-497	-0.052	KTN1
hsa-miR-497	-0.051	HSPA5
hsa-miR-497	-0.051	VMA21
hsa-miR-497	-0.050	RAB10
hsa-miR-497	-0.050	SLC25A39
hsa-miR-4999	-0.091	SNHG3
hsa-miR-5008	-0.247	ZNF587
hsa-miR-5008	-0.238	SNHG3
hsa-miR-5008	-0.153	PILRB
hsa-miR-5008	-0.088	ZCCHC3
hsa-miR-503	-0.139	PERP
hsa-miR-503	-0.133	TRAP1
hsa-miR-503	-0.108	FAM120A
hsa-miR-503	-0.100	MRPL20
hsa-miR-503	-0.080	CHORDC1
hsa-miR-503	-0.072	UTP15
hsa-miR-503	-0.064	TMEM181
hsa-miR-503	-0.063	SNHG12
hsa-miR-503	-0.059	GOLT1B
hsa-miR-503	-0.053	SNHG3
hsa-miR-505	-0.148	MIRLET7BHG
hsa-miR-505	-0.120	SFXN1
hsa-miR-505	-0.094	TOP2A
hsa-miR-505	-0.082	STK35
hsa-miR-505	-0.062	PARD6B
hsa-miR-505	-0.059	UBN2
hsa-miR-522	-0.153	MAL2
hsa-miR-522	-0.124	PRRG4
hsa-miR-522	-0.121	WNK2
hsa-miR-522	-0.112	DLG3
hsa-miR-522	-0.072	TRIB3
hsa-miR-522	-0.069	MIRLET7BHG
hsa-miR-522	-0.068	SRI

hsa-miR-522	-0.067	DYNLT1
hsa-miR-522	-0.062	ASF1B
hsa-miR-522	-0.061	GALNT3
hsa-miR-522	-0.054	TIMM8A
hsa-miR-522	-0.051	MYO6
hsa-miR-660	-0.097	CDK4
hsa-miR-660	-0.087	SNHG7
hsa-miR-660	-0.086	C6orf136
hsa-miR-660	-0.063	CENPM
hsa-miR-660	-0.059	BTBD1
hsa-miR-660	-0.051	INO80E
hsa-miR-873	-0.132	PILRB
hsa-miR-873	-0.097	MIRLET7BHG
hsa-miR-873	-0.076	SLC25A39
hsa-miR-873	-0.073	UTP15
hsa-miR-873	-0.063	XPO1
hsa-miR-873	-0.055	ACP1
hsa-miR-873	-0.052	ATIC

GO-ID	P-val	P-adj	Description	N genes in test set	Genes in test set
7049	2.11E-33	4.97E-30	cell cycle	89	MCM7, DSCC1, NCAPG2, CCNF, BUB1B, KIF11, MKI67, BRCA2, PPP1CC, CHAF1A, MYC, STMN1, NUSAP1, RCC1, KMT5A, KPNA2, POLE, MEN1, LIG1, DYNLT1, CKAP2, HAUS3, KIF23, ESCO2, KIF22, SMC1A, CDC25A, MSH6, SGO1, SGO2, ILF3, TFDP1, KIFC1, CCNE1, BIRC5, ANAPC5, MCM6, BLM, SEH1L, PSMD11, PSMD14, CDCA5, CUL2, CUL1, NCAPG, NOLC1, CDCA8, TTK, PKMYT1, CENPA, SKA1, PSMA7, PPM1G, RAD54B, AURKA, TBRG4, PSMB6, PPP2CA, PARD6B, CCNB1, RACGAP1, RAD21, RRS1, E2F3, BUB3, EIF4E, BUB1, E2F7, FANCI, NPM1, RCC2, PLK1, FANCA, CDC6, RAB11A, TPX2, ANLN, CENPF, STAG2, KRT18, CDK4, PSMC2, CDK1, TACC3, CDK2AP1, NCAPD2, TRIP13, MAD2L1, NUP37
22402	5.66E-32	6.64E-29	cell cycle process	75	DSCC1, NCAPG2, CCNF, BUB1B, KIF11, MKI67, BRCA2, MYC, STMN1, NUSAP1, RCC1, KMT5A, KPNA2, POLE, MEN1, DYNLT1, HAUS3, KIF23, KIF22, SMC1A, CDC25A, MSH6, SGO1, SGO2, ILF3, KIFC1, CCNE1, BIRC5, ANAPC5, BLM, SEH1L, PSMD11, PSMD14, CDCA5, CUL2, CUL1, NCAPG, NOLC1, CDCA8, TTK, PKMYT1, CENPA, SKA1, PSMA7, PPM1G, RAD54B, AURKA, TBRG4, PSMB6, PPP2CA, CCNB1, RACGAP1, RAD21, RRS1, BUB3, EIF4E, BUB1, NPM1, RCC2, PLK1, FANCA, CDC6, TPX2, ANLN, CENPF, STAG2, CDK4, PSMC2, CDK1, TACC3, CDK2AP1, NCAPD2, TRIP13, MAD2L1, NUP37
22403	1.40E-30	1.09E-27	cell cycle phase	64	DSCC1, NCAPG2, CCNF, BUB1B, KIF11, MKI67, BRCA2, STMN1, NUSAP1, RCC1, KMT5A, KPNA2, POLE, DYNLT1, HAUS3, KIF23, KIF22, SMC1A, CDC25A, MSH6, SGO1, SGO2, ILF3, KIFC1, CCNE1, BIRC5, ANAPC5, BLM, SEH1L, CDCA5, CUL2, CUL1, NCAPG, NOLC1, CDCA8, TTK, PKMYT1, SKA1, RAD54B, AURKA, TBRG4, PPP2CA, CCNB1, RAD21, RRS1, BUB3, EIF4E, BUB1, RCC2, PLK1, FANCA, CDC6, TPX2, ANLN, CENPF, STAG2, CDK4, CDK1, TACC3, CDK2AP1, NCAPD2, TRIP13, MAD2L1, NUP37
278	2.18E-30	1.28E-27	mitotic cell cycle	60	DSCC1, NCAPG2, CCNF, BUB1B, KIF11, STMN1, NUSAP1, RCC1, KMT5A, KPNA2, POLE, DYNLT1, HAUS3, KIF23, KIF22, SMC1A, CDC25A, SGO1, KIFC1, CCNE1, BIRC5, ANAPC5, BLM, SEH1L, PSMD11, PSMD14, CDCA5, CUL2, CUL1, NCAPG, NOLC1, CDCA8, TTK, PKMYT1, CENPA, SKA1, PSMA7, AURKA, TBRG4, PSMB6, CCNB1, RAD21, RRS1, BUB3, EIF4E, BUB1, RCC2, PLK1, CDC6, TPX2, ANLN, CENPF, STAG2, CDK4, PSMC2, CDK1, CDK2AP1, NCAPD2, MAD2L1, NUP37
279	1.08E-27	5.09E-25	M phase	55	DSCC1, NCAPG2, CCNF, BUB1B, KIF11, MKI67, BRCA2, STMN1, NUSAP1, RCC1, KMT5A, KPNA2, DYNLT1, HAUS3, KIF23, KIF22, SMC1A, CDC25A, MSH6, SGO1, SGO2, ILF3, KIFC1, BIRC5, ANAPC5, SEH1L, CDCA5, NCAPG, NOLC1, CDCA8, TTK, PKMYT1, SKA1, RAD54B, AURKA, PPP2CA, CCNB1, RAD21, RRS1, BUB3, BUB1, RCC2, PLK1, FANCA, CDC6, TPX2, ANLN, CENPF, STAG2, CDK1, TACC3, NCAPD2, TRIP13, MAD2L1, NUP37
280	7.85E-23	2.64E-20	nuclear division	41	SEH1L, CDCA5, DSCC1, NCAPG2, CCNF, NCAPG, NOLC1, CDCA8, BUB1B, KIF11, PKMYT1, SKA1, AURKA, CCNB1, RAD21, RRS1, NUSAP1, KMT5A, BUB3, BUB1, DYNLT1, RCC2, PLK1, HAUS3, KIF23, CDC6, KIF22, SMC1A, CDC25A, SGO1, TPX2, ANLN, CENPF, STAG2, KIFC1, CDK1, BIRC5, NCAPD2, ANAPC5, MAD2L1, NUP37
7067	7.85E-23	2.64E-20	mitosis	41	SEH1L, CDCA5, DSCC1, NCAPG2, CCNF, NCAPG, NOLC1, CDCA8, BUB1B, KIF11, PKMYT1, SKA1, AURKA, CCNB1, RAD21, RRS1, NUSAP1, KMT5A, BUB3, BUB1, DYNLT1, RCC2, PLK1, HAUS3, KIF23, CDC6, KIF22, SMC1A, CDC25A, SGO1, TPX2, ANLN, CENPF, STAG2, KIFC1, CDK1, BIRC5, NCAPD2, ANAPC5, MAD2L1, NUP37
90304	9.66E-23	2.84E-20	nucleic acid metabolic process	104	ATF1, POP7, POP1, DSCC1, RRP1, RRP9, KPNA2, MEN1, LIG1, PUS1, WRNIP1, ESCO2, CSNK1E, CDC25A, WDR77, MSH6, PRPF4, CLNS1A, GEMIN4, SRSF7, SNRPA, SNRPB, ZCCHC8, BLM, CBFB, DHX9, UTP23, NOLC1, RAD21, FANCI, CPSF6, CPSF1, NONO, FANCA, HMGA1, CDC6, PAN3, TDP2, HNRNPF, TDP1, AGO2, HNRNPD, GRSF1, FARSB, TOP2A, TRMU, FEN1, MOCS3, MCM7, HMGB2, HMGB3, BRCA2, PRPF19, USP39, MED17, CHAF1A, ZNF768, POLE, UTP15, PRMT5, KIF22, SMC1A, SENP2, RAD23B, PTBP3, SFPQ, POLR1B, MCM4, MCM6, PTMA, SF3B4, GTF3C2, TMF1, GTF3C5, SRRT, DDX21, TYMS, UNG, RAD54B, REPIN1, PPP2CA, PUF60, U2AF2, POLD2, IGF2BP1, E2F3, SRSF10, NOP56, POLQ, PPIL1, RRM2, NFYA, PTGES3, GINS3, SSRP1, TARBP1, VEGFA, CENPF, APEX1, TRMT6, CDK2AP1, TRIP13, POLR3K, HSPA1B
87	2.54E-22	6.64E-20	M phase of mitotic cell cycle	41	SEH1L, CDCA5, DSCC1, NCAPG2, CCNF, NCAPG, NOLC1, CDCA8, BUB1B, KIF11, PKMYT1, SKA1, AURKA, CCNB1, RAD21, RRS1, NUSAP1, KMT5A, BUB3, BUB1, DYNLT1, RCC2, PLK1, HAUS3, KIF23, CDC6, KIF22, SMC1A, CDC25A, SGO1, TPX2, ANLN, CENPF, STAG2, KIFC1, CDK1, BIRC5, NCAPD2, ANAPC5, MAD2L1, NUP37
48285	3.53E-22	8.29E-20	organelle fission	41	SEH1L, CDCA5, DSCC1, NCAPG2, CCNF, NCAPG, NOLC1, CDCA8, BUB1B, KIF11, PKMYT1, SKA1, AURKA, CCNB1, RAD21, RRS1, NUSAP1, KMT5A, BUB3, BUB1, DYNLT1, RCC2, PLK1, HAUS3, KIF23, CDC6, KIF22, SMC1A, CDC25A, SGO1, TPX2, ANLN, CENPF, STAG2, KIFC1, CDK1, BIRC5, NCAPD2, ANAPC5, MAD2L1, NUP37

51301	5.55E-22	1.18E-19	cell division	46	SEH1L, CDCA5, NCAPG2, CCNF, NCAPG, CDCA8, BUB1B, KIF11, BRCA2, SKA1, AURKA, PPP1CC, PARD6B, CCNB1, RACGAP1, RAD21, NUSAP1, RCC1, KMT5A, BUB3, BUB1, LIG1, DYNLT1, RCC2, PLK1, HAUS3, KIF23, CDC6, SMC1A, CDC25A, RAB11A, SGO1, TPX2, ANLN, SGO2, CENPF, STAG2, KIFC1, CDK4, CCNE1, CDK1, BIRC5, NCAPD2, ANAPC5, MAD2L1, NUP37
6139	3.48E-21	6.82E-19	nucleobase, nucleoside, nucleotide and nucleic acid metabolic process	114	ATF1, POP7, POP1, DSCC1, RRP1, RRP9, PPAT, KPNA2, MEN1, LIG1, PUS1, WRNIP1, ESCO2, CSNK1E, CDC25A, WDR77, MSH6, PRPF4, MTHFD1, CLNS1A, GEMIN4, SRSF7, SNRPA, SNRPB, ZCCHC8, BLM, CBFB, DHX9, UTP23, NOLC1, RAD21, FANCI, CPSF6, CPSF1, NONO, FANCA, HMGA1, CDC6, PAN3, TDP2, HNRNPF, TDP1, AGO2, HNRNPD, GRSF1, FARSB, TOP2A, TRMU, FEN1, MOCS3, MCM7, HMGB2, HMGB3, BRCA2, PRPF19, USP39, MED17, CHAF1A, ATIC, ZNF768, POLE, UTP15, PRMT5, ATP6V0B, KIF22, SMC1A, SENP2, RAD23B, PTBP3, NME1, SFPQ, POLR1B, MCM4, MCM6, UMPS, DCTPP1, PTMA, SLC29A2, SF3B4, GTF3C2, TMF1, GTF3C5, SRRT, DDX21, HMGCR, TYMS, UNG, RAD54B, REPIN1, PPP2CA, PUF60, U2AF2, POLD2, IGF2BP1, E2F3, SRSF10, NOP56, POLQ, PPIL1, RRM2, NFYA, PTGES3, GINS3, SSRP1, TARBP1, VEGFA, CENPF, VMA21, APEX1, TRMT6, CDK2AP1, TRIP13, POLR3K, HSPA1B
44260	4.02E-21	7.26E-19	cellular macromolecule metabolic process	173	ATF1, TOR2A, POP7, PGAP2, POP1, DSCC1, RRP1, CCNF, BUB1B, RRP9, PPP1CC, KPNA2, MAP3K4, MEN1, FKBPL, LIG1, PUS1, WRNIP1, ESCO2, CSNK1E, CDC25A, WDR77, MSH6, DPM2, PRPF4, CLNS1A, HMBS, GEMIN4, ANAPC5, MAPKAPK5, TRIB3, SRSF7, SNRPA, SNRPB, ZCCHC8, BLM, PSMD11, CBFB, PSMD14, DHX9, CUL2, UTP23, CUL1, NOLC1, FBXO45, PKMYT1, MRPL20, CCNB1, PRDX4, STK35, RAD21, PTPMT1, GRPEL2, FANCI, HSPA9, EIF2B4, TRAP1, CPSF6, HSPA5, CPSF1, EIF2AK1, NONO, PLK1, FANCA, HMGA1, CDC6, PAN3, EIF6, TDP2, CDK4, HNRNPF, TDP1, WNK2, AGO2, HNRNPD, CDK1, GRSF1, FARSB, CDK16, TOP2A, TRMU, FEN1, MOCS3, MCM7, HMGB2, HMGB3, BRCA2, PRPF19, USP39, MED17, CHAF1A, WDR5, ZNF768, ACP1, POLE, DSP, CCT3, UTP15, PRMT5, HSP90AA1, AHSA1, MRPS2, KIF22, SMC1A, SENP2, RAD23B, PTBP3, PDRG1, MRPL52, SFPQ, ADORA2B, PDIK1L, POLR1B, MCM4, PFDN2, MCM6, PTMA, OTUB1, SF3B4, GTF3C2, TMF1, GTF3C5, SRRT, DDX21, TTK, TYMS, PSMA7, CLN6, UNG, PPM1G, RAD54B, AURKA, PSMB6, REPIN1, PPP2CA, PUF60, U2AF2, POLD2, USP1, IGF2BP1, E2F3, BUB3, CCT7, SRSF10, DCAF12, BUB1, CCT4, NOP56, SUZ12, POLQ, PPIL1, RRM2, NFYA, GALNT3, PTGES3, GINS3, SSRP1, HSPE1, TARBP1, VEGFA, CENPF, APEX1, PSMC2, TRMT6, CDK2AP1, TRIP13, NAA15, POLR3K, HSPA1B, PTPN2, PTPN3, CDK5R1, MAD2L1
34641	3.14E-20	5.28E-18	cellular nitrogen compound metabolic process	123	ATF1, POP7, POP1, DSCC1, RRP1, RRP9, PPAT, KPNA2, MEN1, LIG1, PUS1, WRNIP1, ESCO2, CSNK1E, CDC25A, WDR77, MSH6, PRPF4, MTHFD1, CLNS1A, HMBS, GEMIN4, SRSF7, SNRPA, SNRPB, ZCCHC8, BLM, CBFB, DHX9, UTP23, NOLC1, RAD21, FANCI, CPSF6, CPSF1, NONO, FANCA, HMGA1, PYCR1, CDC6, PAN3, TDP2, HNRNPF, TDP1, AGO2, HNRNPD, GRSF1, FARSB, TOP2A, TRMU, FEN1, MOCS3, MCM7, ASNSD1, AMD1, HMGB2, HMGB3, BRCA2, PRPF19, USP39, MED17, CHAF1A, ATIC, ZNF768, POLE, UTP15, PRMT5, ATP6V0B, KIF22, SMC1A, SENP2, RAD23B, PTBP3, NME1, SLC7A5, SLC7A6, SFPQ, POLR1B, MCM4, MCM6, UMPS, DCTPP1, PTMA, SLC29A2, SF3B4, GTF3C2, TMF1, GTF3C5, SRRT, DDX21, HMGCR, TYMS, UNG, RAD54B, REPIN1, PPP2CA, PUF60, U2AF2, POLD2, IGF2BP1, E2F3, SRSF10, DTD1, NOP56, POLQ, PPIL1, RRM2, NFYA, PTGES3, GINS3, SSRP1, TARBP1, VEGFA, CENPF, SLC25A39, PSAT1, VMA21, APEX1, TRMT6, CDK2AP1, TRIP13, POLR3K, HSPA1B
6807	4.22E-20	6.60E-18	nitrogen compound metabolic process	127	ATF1, POP7, POP1, DSCC1, RRP1, RRP9, PPAT, KPNA2, MEN1, LIG1, PUS1, WRNIP1, ESCO2, CSNK1E, CDC25A, WDR77, MSH6, PRPF4, MTHFD1, MTHFD2, CLNS1A, HMBS, GEMIN4, SRSF7, SNRPA, SNRPB, ZCCHC8, BLM, CBFB, DHX9, UTP23, NOLC1, RAD21, FANCI, CPSF6, CPSF1, EIF2AK1, NONO, FANCA, HMGA1, PYCR1, CDC6, PAN3, TDP2, HNRNPF, TDP1, AGO2, HNRNPD, GRSF1, FARSB, TOP2A, TRMU, FEN1, MOCS3, MCM7, ASNSD1, AMD1, HMGB2, HMGB3, BRCA2, PRPF19, USP39, MED17, CHAF1A, ATIC, ZNF768, POLE, UTP15, PRMT5, ATP6V0B, KIF22, SMC1A, SENP2, RAD23B, PTBP3, NME1, SLC7A5, SLC7A6, SFPQ, POLR1B, MCM4, MCM6, UMPS, DCTPP1, PTMA, SLC29A2, SF3B4, GTF3C2, TMF1, GTF3C5, SRRT, DDX21, HMGCR, TYMS, CLN6, UNG, RAD54B, REPIN1, PPP2CA, PUF60, MTHFD1L, U2AF2, POLD2, IGF2BP1, E2F3, SRSF10, DTD1, NOP56, POLQ, PPIL1, RRM2, NFYA, PTGES3, GINS3, SSRP1, TARBP1, VEGFA, CENPF, SLC25A39, PSAT1, VMA21, APEX1, TRMT6, CDK2AP1, TRIP13, POLR3K, HSPA1B

9987	5.99E-20	8.63E-18	cellular process	319	ATF1, NUP107, POP7, PGAP2, POP1, RRP1, CCNF, ENO1, MKI67, RRP9, MYC, PPAT, STMN1, FDXR, RCC1, ESCO2, CSNK1E, MIF, BCS1L, SCAMP3, WDR77, MTHFD1, MTHFD2, CLNS1A, HMBS, TRIB3, ASF1B, NUP205, SEH1L, STXBP3, ANP32A, DHX9, CDCA5, NCAPG, NOLC1, CDCA8, SKA1, MRPL20, PTDSS1, PRDX4, RACGAP1, RAD21, PTPMT1, MYO6, GRPEL2, RRS1, SNX5, TRAP1, EIF2AK1, RCC2, PLK1, PYCR1, PILRB, CDC6, SQLE, TPX2, ANLN, STAG2, EIF6, TDP2, HNRNPF, TDP1, WNK2, AGO2, HNRNPD, SFXN1, FARSB, CDK16, TOP2A, TRMU, FEN1, DAZAP1, MOCS3, NCAPG2, KIF11, BRCA2, PRPF19, MED17, TUBA1B, CHAF1A, ATIC, SCML1, XPO1, CCT3, PRMT5, LYPLA1, MRPS26, ATP6V0B, SLC39A10, MRPS2, AEN, KIF23, BAZ1A, KIF22, PDRG1, NME1, MRPL52, SLC7A5, SLC7A6, KIFC1, PDIK1L, CLDN12, UMPS, PTMA, SLC29A2, SF3B4, TMF1, AHCY, SLC20A1, SRRT, TIMM13, TYMS, CENPA, PSMA7, UNG, RAD54B, PSMB6, PPP2CA, NRAS, MTHFD1L, PERP, USP1, CCT7, SRSF10, DTD1, CCT4, SUZ12, RANBP1, NPM1, PLEKHA1, NFYA, PTGES2, PTGES3, GINS3, MZT1, RAB11A, KTN1, TARBP1, VEGFA, CENPF, KRT18, TFAP4, VMA21, APEX1, SNX14, CAPZA1, PSMC2, TRMT6, TACC3, NCAPD2, TRIP13, HSPA1B, CDK5R1, MAD2L1, TOR2A, GOLT1B, NUP188, CSE1L, DSCC1, BUB1B, LCLAT1, TOMM20, PVR, PPP1CC, NUSAP1, KMT5A, KPNA2, MAP3K4, MEN1, FKBPL, LIG1, PUS1, WRNIP1, CDC25A, MSH6, SGO1, DPM2, SGO2, PRPF4, ILF3, SYPL1, CCNE1, NCL, GEMIN4, ANAPC5, MAPKAPK5, SRSF7, SNRPA, SNRPB, ZCCHC8, RTN3, BLM, PSMD11, CBFB, PSMD14, INSIG2, GLO1, CUL2, UTP23, CUL1, SPATA2, FBXO45, PKMYT1, LIN7C, ADIPOR2, CCNB1, STK35, PMAIP1, CYC1, NDUFV1, FANCI, HSPA9, EIF2B4, POU2F1, CPSF6, CBX4, HSPA5, CPSF1, HSPA4, CBX3, NONO, IDH2, FANCA, HMGA1, CRLS1, CNIH1, PAN3, CDK4, BAMBI, CDK1, CLPTM1L, GRSF1, SLC26A6, SLC25A1, MCM7, ASNSD1, AMD1, CHD7, HMGB2, HMGB3, TRIAP1, USP39, CHD1, YWHAQ, WDR5, ZNF768, SLC37A4, ACP1, POLE, YWHAG, DSP, UTP15, HSP90AA1, DYNLT1, VPS13A, SORD, CKAP2, HAUS3, AHSA1, SMC1A, SENP2, RAD23B, YWHAZ, PTBP3, SUPV3L1, RCN1, SFPQ, SLC25A17, TFDP1, ADORA2B, POLR1B, BIRC5, MCM4, PFDN2, MCM6, DCTPP1, OTUB1, NDUFB9, GTF3C2, GTF3C5, DDX21, TTK, SRI, HMGCR, CLN6, PPM1G, AURKA, TBRG4, REPIN1, PARD6B, PUF60, U2AF2, POLD2, IGF2BP1, E2F3, BUB3, SLC25A22, DCAF12, EIF4E, BUB1, E2F7, NOP56, POLQ, TIMM8A, PPIL1, RRM2, GALNT3, ZIC5, SSRP1, HSPE1, SLC25A39, PSAT1, SCD, CDK2AP1, NAA15, POLR3K, PTPN2, PTPN3, NUP37
44237	6.25E-20	8.63E-18	cellular metabolic process	214	ATF1, POP7, PGAP2, POP1, RRP1, CCNF, ENO1, RRP9, PPAT, FDXR, ESCO2, CSNK1E, MIF, WDR77, MTHFD1, MTHFD2, CLNS1A, HMBS, TRIB3, DHX9, NOLC1, MRPL20, PTDSS1, PRDX4, RAD21, PTPMT1, GRPEL2, TRAP1, EIF2AK1, PLK1, PYCR1, CDC6, SQLE, EIF6, TDP2, HNRNPF, TDP1, WNK2, AGO2, HNRNPD, FARSB, CDK16, TOP2A, TRMU, FEN1, MOCS3, BRCA2, PRPF19, MED17, CHAF1A, ATIC, CCT3, PRMT5, LYPLA1, MRPS26, ATP6V0B, MRPS2, KIF22, PDRG1, NME1, MRPL52, SLC7A5, SLC7A6, PDIK1L, UMPS, PTMA, SLC29A2, SF3B4, TMF1, AHCY, SLC20A1, SRRT, TYMS, PSMA7, UNG, RAD54B, PSMB6, PPP2CA, MTHFD1L, USP1, CCT7, SRSF10, DTD1, CCT4, SUZ12, NFYA, PTGES2, PTGES3, GINS3, TARBP1, VEGFA, CENPF, VMA21, APEX1, PSMC2, TRMT6, TRIP13, HSPA1B, CDK5R1, MAD2L1, TOR2A, DSCC1, BUB1B, LCLAT1, PPP1CC, KPNA2, MAP3K4, MEN1, FKBPL, LIG1, PUS1, WRNIP1, CDC25A, MSH6, DPM2, PRPF4, GEMIN4, ANAPC5, MAPKAPK5, SRSF7, SNRPA, SNRPB, ZCCHC8, BLM, PSMD11, CBFB, PSMD14, GLO1, CUL2, UTP23, CUL1, FBXO45, PKMYT1, ADIPOR2, CCNB1, STK35, CYC1, NDUFV1, FANCI, HSPA9, EIF2B4, CPSF6, HSPA5, CPSF1, NONO, IDH2, FANCA, HMGA1, CRLS1, PAN3, CDK4, CDK1, GRSF1, MCM7, ASNSD1, AMD1, HMGB2, HMGB3, USP39, WDR5, ZNF768, SLC37A4, ACP1, POLE, DSP, UTP15, HSP90AA1, SORD, AHSA1, SMC1A, SENP2, RAD23B, PTBP3, SFPQ, ADORA2B, POLR1B, MCM4, PFDN2, MCM6, DCTPP1, OTUB1, NDUFB9, GTF3C2, GTF3C5, DDX21, TTK, HMGCR, CLN6, PPM1G, AURKA, REPIN1, PUF60, U2AF2, POLD2, IGF2BP1, E2F3, BUB3, DCAF12, BUB1, NOP56, POLQ, PPIL1, RRM2, GALNT3, SSRP1, HSPE1, SLC25A39, PSAT1, SCD, CDK2AP1, NAA15, POLR3K, PTPN2, PTPN3

44238	7.15E-16	9.33E-14	primary metabolic process	212	ATF1, POP7, PGAP2, POP1, RRP1, CCNF, ENO1, RRP9, PPAT, FDXR, ESCO2, CSNK1E, MIF, WDR77, MTHFD1, CLNS1A, HMBS, TRIB3, DHX9, NOLC1, MRPL20, PTDSS1, PRDX4, RAD21, PTPMT1, GRPEL2, TRAP1, EIF2AK1, PLK1, PYCR1, CDC6, SQLE, EIF6, TDP2, HNRNPF, TDP1, WNK2, AGO2, HNRNPD, FARSB, CDK16, TOP2A, TRMU, FEN1, MOCS3, BRCA2, PRPF19, MED17, CHAF1A, ATIC, CCT3, PRMT5, LYPLA1, ATP6V0B, MRPS2, KIF22, PDRG1, NME1, MRPL52, SLC7A5, SLC7A6, PDIK1L, AGPS, UMPS, PTMA, SLC29A2, SF3B4, TMF1, SRRT, TYMS, PSMA7, UNG, RAD54B, PSMB6, PPP2CA, USP1, CCT7, SRSF10, DTD1, CCT4, SUZ12, NFYA, PTGES2, PTGES3, GINS3, TARBP1, VEGFA, CENPF, ERG28, VMA21, APEX1, PSMC2, TRMT6, TRIP13, HSPA1B, CDK5R1, MAD2L1, TOR2A, DSCC1, BUB1B, LCLAT1, PPP1CC, PMPCA, KPNA2, MAP3K4, MEN1, FKBPL, LIG1, PUS1, WRNIP1, CDC25A, MSH6, DPM2, PRPF4, NCL, GEMIN4, ANAPC5, MAPKAPK5, SRSF7, SNRPA, SNRPB, ZCCHC8, BLM, PSMD11, CBFB, PSMD14, INSIG2, GLO1, CUL2, UTP23, CUL1, FBXO45, PKMYT1, ADIPOR2, CCNB1, STK35, FANCI, HSPA9, EIF2B4, CPSF6, HSPA5, CPSF1, OSBPL3, NONO, IDH2, FANCA, HMGA1, CRLS1, PAN3, CDK4, CDK1, GRSF1, MCM7, ASNSD1, AMD1, HMGB2, HMGB3, USP39, WDR5, ZNF768, SLC37A4, ACP1, POLE, DSP, UTP15, HSP90AA1, SIGMAR1, SORD, AHSA1, SMC1A, SENP2, RAD23B, PTBP3, SFPQ, ADORA2B, POLR1B, MCM4, PFDN2, MCM6, DCTPP1, OTUB1, GTF3C2, GTF3C5, DDX21, TTK, HMGCR, CLN6, PPM1G, AURKA, REPIN1, PUF60, U2AF2, POLD2, IGF2BP1, E2F3, BUB3, DCAF12, BUB1, NOP56, POLQ, PPIL1, RRM2, GALNT3, SSRP1, HSPE1, PSAT1, SCD, CDK2AP1, NAA15, POLR3K, PTPN2, PTPN3
6974	1.08E-15	1.34E-13	response to DNA damage stimulus	43	TOP2A, BLM, FEN1, PGAP2, MCM7, HMGB2, FBXO45, TRIAP1, BRCA2, PRPF19, TYMS, UNG, RAD54B, CHAF1A, RAD21, MYO6, POLD2, POLE, MEN1, FANCI, POLQ, MRPS26, LIG1, NONO, PLK1, FANCA, AEN, WRNIP1, ESCO2, CSNK1E, KIF22, SSRP1, SMC1A, SENP2, RAD23B, MSH6, SFPQ, TFAP4, TDP2, TDP1, APEX1, CDK1, TRIP13
43170	1.45E-15	1.71E-13	macromolecule metabolic process	175	ATF1, TOR2A, POP7, PGAP2, POP1, DSCC1, RRP1, CCNF, BUB1B, RRP9, PPP1CC, PMPCA, KPNA2, MAP3K4, MEN1, FKBPL, LIG1, PUS1, WRNIP1, ESCO2, CSNK1E, CDC25A, WDR77, MSH6, DPM2, PRPF4, CLNS1A, NCL, HMBS, GEMIN4, ANAPC5, MAPKAPK5, TRIB3, SRSF7, SNRPA, SNRPB, ZCCHC8, BLM, PSMD11, CBFB, PSMD14, DHX9, CUL2, UTP23, CUL1, NOLC1, FBXO45, PKMYT1, MRPL20, CCNB1, PRDX4, STK35, RAD21, PTPMT1, GRPEL2, FANCI, HSPA9, EIF2B4, TRAP1, CPSF6, HSPA5, CPSF1, EIF2AK1, NONO, PLK1, FANCA, HMGA1, CDC6, PAN3, EIF6, TDP2, CDK4, HNRNPF, TDP1, WNK2, AGO2, HNRNPD, CDK1, GRSF1, FARSB, CDK16, TOP2A, TRMU, FEN1, MOCS3, MCM7, HMGB2, HMGB3, BRCA2, PRPF19, USP39, MED17, CHAF1A, WDR5, ZNF768, ACP1, POLE, DSP, CCT3, UTP15, PRMT5, HSP90AA1, AHSA1, MRPS2, KIF22, SMC1A, SENP2, RAD23B, PTBP3, PDRG1, MRPL52, SFPQ, ADORA2B, PDIK1L, POLR1B, MCM4, PFDN2, MCM6, PTMA, OTUB1, SF3B4, GTF3C2, TMF1, GTF3C5, SRRT, DDX21, TTK, TYMS, PSMA7, CLN6, UNG, PPM1G, RAD54B, AURKA, PSMB6, REPIN1, PPP2CA, PUF60, U2AF2, POLD2, USP1, IGF2BP1, E2F3, BUB3, CCT7, SRSF10, DCAF12, BUB1, CCT4, NOP56, SUZ12, POLQ, PPIL1, RRM2, NFYA, GALNT3, PTGES3, GINS3, SSRP1, HSPE1, TARBP1, VEGFA, CENPF, APEX1, PSMC2, TRMT6, CDK2AP1, TRIP13, NAA15, POLR3K, HSPA1B, PTPN2, PTPN3, CDK5R1, MAD2L1
6259	1.01E-14	1.12E-12	DNA metabolic process	48	TOP2A, BLM, FEN1, MCM7, DSCC1, HMGB2, HMGB3, BRCA2, PRPF19, TYMS, UNG, RAD54B, REPIN1, CHAF1A, RAD21, POLD2, KPNA2, POLE, MEN1, FANCI, POLQ, RRM2, LIG1, PTGES3, GINS3, NONO, FANCA, HMGA1, WRNIP1, CDC6, ESCO2, CSNK1E, KIF22, SSRP1, SMC1A, SENP2, RAD23B, CDC25A, MSH6, CENPF, SFPQ, TDP2, TDP1, APEX1, MCM4, CDK2AP1, MCM6, TRIP13
33554	1.05E-14	1.12E-12	cellular response to stress	53	TOP2A, FEN1, PGAP2, MCM7, HMGB2, TRIAP1, BRCA2, PRPF19, CHAF1A, POLE, MAP3K4, MEN1, MRPS26, LIG1, AEN, WRNIP1, ESCO2, CSNK1E, KIF22, SMC1A, SENP2, RAD23B, MSH6, SFPQ, ADORA2B, BLM, INSIG2, DHX9, FBXO45, TYMS, UNG, RAD54B, RAD21, MYO6, POLD2, FANCI, EIF2B4, TRAP1, POLQ, PLEKHA1, HSPA5, EIF2AK1, NONO, PLK1, FANCA, PYCR1, SSRP1, TFAP4, TDP2, TDP1, APEX1, CDK1, TRIP13
7059	2.04E-14	2.08E-12	chromosome segregation	20	TOP2A, SEH1L, CDCA5, DSCC1, NCAPG, SMC1A, SKA1, SGO1, SGO2, CENPF, CCNB1, STAG2, KIFC1, RAD21, RRS1, NUSAP1, BIRC5, NCAPD2, BUB3, NUP37

8152	4.62E-14	4.52E-12	metabolic process	225	ATF1, POP7, PGAP2, POP1, RRP1, CCNF, ENO1, RRP9, PPAT, FDXR, ESCO2, CSNK1E, MIF, WDR77, MTHFD1, MTHFD2, CLNS1A, HMBS, TRIB3, DHX9, NOLC1, MRPL20, PTDSS1, PRDX4, RAD21, PTPMT1, GRPEL2, TRAP1, EIF2AK1, PLK1, PYCR1, CDC6, SQLE, EIF6, TDP2, HNRNPF, TDP1, WNK2, AGO2, HNRNPD, FARSB, CDK16, TOP2A, TRMU, DHRS13, FEN1, MOCS3, BRCA2, PRPF19, MED17, CHAF1A, ATIC, CCT3, PRMT5, LYPLA1, MRPS26, ATP6V0B, MRPS2, KIF22, PDRG1, NME1, MRPL52, SLC7A5, SLC7A6, PDIK1L, AGPS, UMPS, PTMA, SLC29A2, SF3B4, TMF1, AHCY, SLC20A1, SRRT, TYMS, PSMA7, UNG, RAD54B, PSMB6, PPP2CA, MTHFD1L, USP1, CCT7, SRSF10, DTD1, CCT4, SUZ12, NFYA, PTGES2, PTGES3, GINS3, TARBP1, VEGFA, CENPF, ERG28, VMA21, APEX1, PSMC2, TRMT6, TRIP13, HSPA1B, CDK5R1, MAD2L1, TOR2A, DSCC1, BUB1B, LCLAT1, PPP1CC, PMPCA, KPNA2, MAP3K4, MEN1, FKBPL, LIG1, PUS1, WRNIP1, CDC25A, MSH6, DPM2, PRPF4, NCL, GEMIN4, ANAPC5, MAPKAPK5, SRSF7, SNRPA, SNRPB, ZCCHC8, BLM, PSMD11, CBFB, PSMD14, INSIG2, GLO1, CUL2, UTP23, CUL1, FBXO45, PKMYT1, ADIPOR2, CCNB1, STK35, CYC1, NDUFV1, FANCI, HSPA9, EIF2B4, CPSF6, HSPA5, CPSF1, OSBPL3, NONO, IDH2, FANCA, HMGA1, CRLS1, UCKL1, PAN3, CDK4, CDK1, GRSF1, NAA40, MCM7, ASNSD1, AMD1, HMGB2, HMGB3, USP39, WDR5, ZNF768, SLC37A4, ACP1, POLE, DSP, UTP15, HSP90AA1, SIGMAR1, SORD, AHSA1, SMC1A, SENP2, RAD23B, PTBP3, SFPQ, ADORA2B, POLR1B, MCM4, PFDN2, MCM6, DCTPP1, OTUB1, NDUFB9, GTF3C2, GTF3C5, NAA20, DDX21, TTK, HMGCR, CLN6, PPM1G, AURKA, REPIN1, PUF60, U2AF2, POLD2, IGF2BP1, E2F3, BUB3, DCAF12, BUB1, NOP56, POLQ, PPIL1, RRM2, GALNT3, SSRP1, HSPE1, SLC25A39, PSAT1, SCD, CDK2AP1, NAA15, POLR3K, PTPN2, PTPN3
6996	1.42E-13	1.34E-11	organelle organization	83	TOP2A, DSCC1, NCAPG2, CCNF, CHD7, HMGB2, BUB1B, KIF11, BRCA2, TOMM20, CHD1, TUBA1B, CHAF1A, STMN1, WDR5, NUSAP1, RCC1, KMT5A, MEN1, PRMT5, HSP90AA1, DYNLT1, HAUS3, KIF23, BAZ1A, MIF, KIF22, SMC1A, BCS1L, YWHAZ, CDC25A, SGO1, SGO2, KIFC1, NCL, POLR1B, BIRC5, ANAPC5, ASF1B, BLM, SEH1L, CDCA5, TIMM13, NCAPG, NOLC1, CDCA8, TTK, PKMYT1, CENPA, SKA1, CLN6, AURKA, NRAS, CCNB1, RACGAP1, RAD21, GRPEL2, RRS1, PMAIP1, BUB3, BUB1, SUZ12, TIMM8A, NPM1, CBX4, HSPA4, CBX3, RCC2, PTGES3, PLK1, HMGA1, CDC6, TPX2, ANLN, CENPF, STAG2, EIF6, CAPZA1, CDK1, TACC3, NCAPD2, MAD2L1, NUP37
6281	1.90E-12	1.72E-10	DNA repair	33	TOP2A, BLM, FEN1, HMGB2, BRCA2, PRPF19, TYMS, UNG, RAD54B, CHAF1A, RAD21, POLD2, POLE, MEN1, FANCI, POLQ, LIG1, NONO, FANCA, WRNIP1, ESCO2, CSNK1E, KIF22, SSRP1, SMC1A, SENP2, RAD23B, MSH6, SFPQ, TDP2, TDP1, APEX1, TRIP13